UNIVERSITAT DE BARCELONA

Exploring Three-State Opinion Dynamics: A Journey Through Single and Multilayer Network Topologies

Irene Ferri

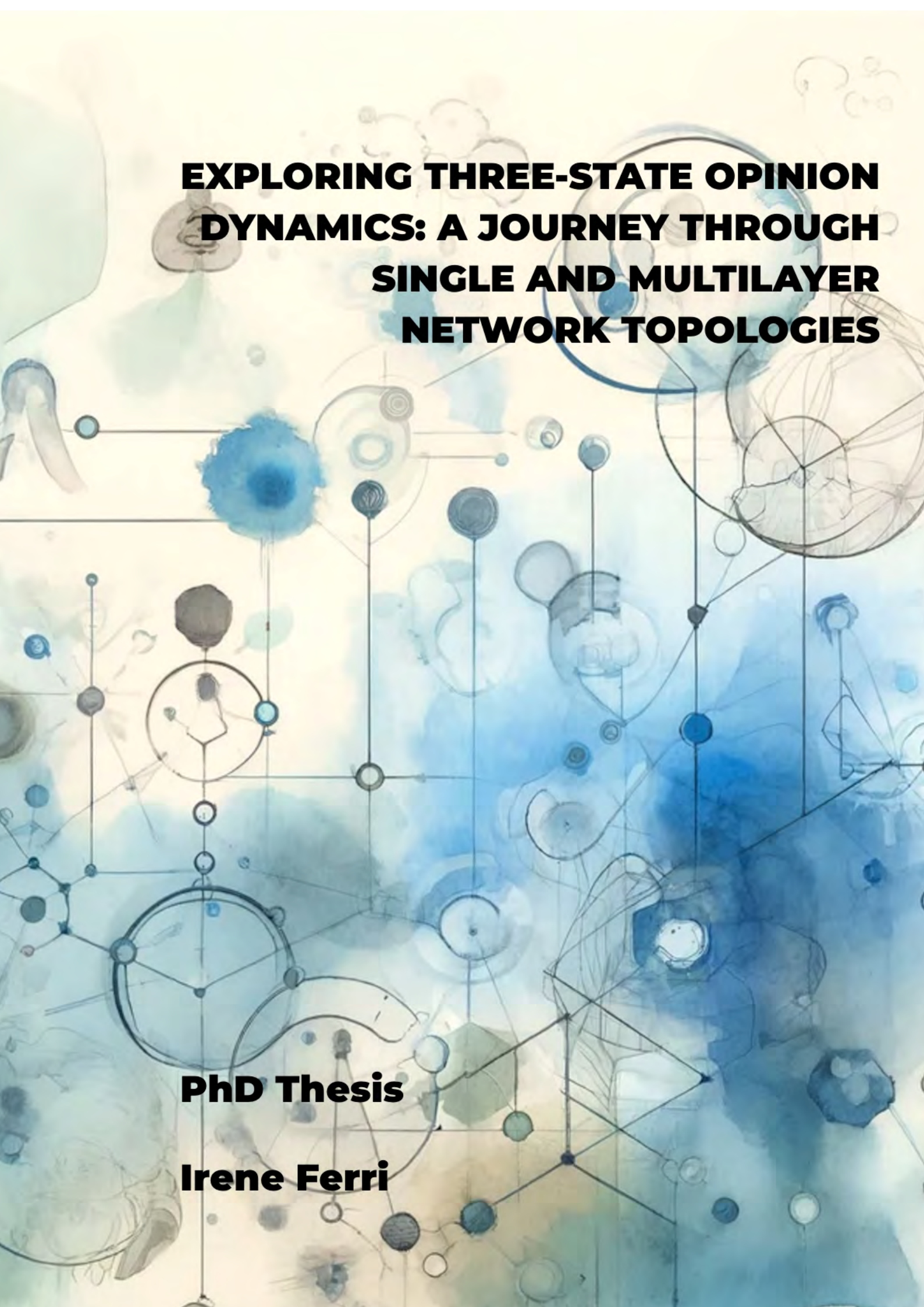

EXPLORING THREE-STATE OPINION DYNAMICS: A JOURNEY THROUGH SINGLE AND MULTILAYER NETWORK TOPOLOGIES

PhD Thesis

Irene Ferri

EXPLORING THREE-STATE OPINION DYNAMICS: A JOURNEY THROUGH SINGLE AND MULTILAYER NETWORK TOPOLOGIES

AUTHOR: **Irene Ferri**

DOCTORAL ADVISOR: **Albert Díaz-Guilera**

DOCTORAL THESIS

EXPLORING THREE-STATE OPINION DYNAMICS: A JOURNEY THROUGH SINGLE AND MULTILAYER NETWORK TOPOLOGIES

Memòria presentada per optar al grau de doctor

per la

Universitat de Barcelona

Programa de doctorat en Física

Autora:

Irene Ferri

Director: *Dr. Albert Díaz-Guilera*

Tutor: *Dr. Giancarlo Franzese*

UNIVERSITAT DE BARCELONA

Exploring Three-State Opinion Dynamics: A Journey Through Single and Multilayer Network Topologies

Irene Ferri
Institute of Complex Systems of the University of Barcelona (UBICS)
Universitat de Barcelona (UB)

PhD Thesis

Doctoral advisors: Dr. Albert Díaz-Guilera

For an updated version of this document, please visit https://www.tdx.cat or contact the author at irene.ferri@ub.edu.

Document typeset in *Latin Modern* using LaTeX 2_ε

I,

Albert Díaz-Guilera,
Professor of the Universitat de Barcelona,

DECLARE

that the thesis entitled "*Exploring Three-State Opinion Dynamics: A Journey Through Single and Multilayer Network Topologies*", submitted by Irene Ferri to the Department of Condensed Matter Physics of the Universitat de Barcelona in partial fulfillment of the requirements for the degree of Doctor in Physics, has been completed under my supervision and meets the requirements for the International Mention.

Barcelona, 2024.

Dr. Albert Díaz-Guilera	Irene Ferri
Advisor	Candidate

Contents

Abstract

THE word "emergence" refers to the formation of collective behaviors, actions not undertaken by the components of a system when isolated. On one hand, we have the components—particles or agents, ranging from water molecules to bees, birds, and humans. On the other hand, we see interactions, the capacity for these particles to perceive each other, through electrical energy, released and received substances, observation and movement coordination, or verbal communication.

Societies are intricate systems composed of multiple interacting layers. Grasping their mechanics enables us to enhance our analytical and strategic capabilities. For centuries, various disciplines have explored human behavior, primarily from qualitative and descriptive perspectives. Yet, in the digital era, fields such as physics and mathematics are increasingly contributing to this exploration, taking advantage of the growing amount of available data to provide fresh insights and enrich our understanding of these questions.

A significant breakthrough in twentieth-century science was the development of statistical physics, which bridges microscopic and macroscopic phenomena and provides an ideal framework for examining a system's emergent properties. Consequently, much of the sociophysics literature relies on physico-statistical models, initially devised to describe physical entities like gases and magnetic materials. These models were designed for specific media and therefore took into account the spatial properties appropriate for the context. For example, regular structures like lattices are often used when modeling solids. In complex systems, however, the connections among elements exhibit different types of patterns, with properties common across diverse fields, from ecology and genetic networks to neuroscience. Graph theory offers a mathematical framework to describe these topologies, and networks have been adopted as the substrate for physico-statistical models in complex system studies. This approach allows for the observation of novel behaviors within each model, based on network characteristics.

This thesis adapts a model, initially aimed at explaining the transition between two helium isotopes, to describe opinion dynamics. The model highlights a central faction's active role in opinion exchange and allows the modulation of neutral and extremist relative conviction levels, aiming to assess its impact. The system's evolution is influenced by the homophily principle or *peer pressure*— the inclination to align our opinions to those held by the people we interact with. Moreover, the model takes into account a certain probability that the agents will deviate from this principle. An increase in this probability is analogous to a rise in temperature in physical systems.

We propose an embedding of the model across various topologies, from less to more complicated. Its implementation in straightforward networks allows an accurate analytical treatment, laying a solid groundwork for examining more intricate structures aimed at capturing essential elements of human behavior. The goal is to integrate into the model, via topology, features such as the tendency to change our relationships to be surrounded by like-minded individuals or the phenomena of cognitive dissonance.

The introduction of the thesis provides an overview of network theory and social physics models and concludes with a description of the newly proposed model. The subsequent chapters are divided into two parts: one focused on single-layer topologies, and the other on spatiotemporal and multilayer topologies.

The first part establishes the foundations of dynamic and equilibrium studies in mean field theory before extending the model to various complex topologies. It starts with the application to entirely random networks, then incorporates a multi-level community structure in synthetic networks, and concludes with real networks derived from Twitter, offering a multi-resolution community structure analysis of the examined topologies.

The first chapter of the second part explores the coevolution of topology and opinion dynamics, blending active matter concepts with opinion models. The second chapter introduces another framework for individual opinion states, now depicted not by a singular variable but a belief network, governed by the three-state opinion model applied throughout the thesis.

In essence, the goal is to deepen our understanding of topological nuances within a discrete opinion model that has two extreme states and a neutral one — the latter not signifying indecision but a different option with various levels of engagement. When there is a dense connection pattern, with a homogeneous degree distribution, neutral agents can dominate the opinion dynamics, catalyzing neutral consensus, even when less committed than extremists. On the other hand, sparser topologies can prevent consensus and lead to echo chambers shaped by the network structure.

Finally, we use network descriptions to broaden the concept of opinion states, facilitating the study of consensus formation at multiple scales. This framework enables us to explain the presence of zealots as a result of a star-like internal topology in an agent's belief system. Sparse belief systems can lead to cognitive dissonance, which in some cases enhances global agreement. Furthermore, the intermixing of agents with diverse internal structures significantly affects individual and collective behavior, especially near critical transition points, which could be useful in understanding system-wide shifts in consensus.

Resum

La paraula emergència es refereix a l'existència o formació de comportaments col · lectius, allò que els constituents del conjunt no farien si estiguessin sols. Per un costat tenim les parts, les partícules, els agents, que poden ser qualssevol cosa: mol · lècules d'aigua, abelles, ocells, éssers humans. etc. Per l'altra banda tenim les interaccions, la capacitat d'aquestes partícules de sentir-se les unes a les altres, ja sigui a través d'una energia elèctrica, d'una substància que alliberen i que capten, d'una observació i coordinació amb el moviment d'aquells que els envolten o de paraules.

Les societats són sistemes complexos formats per moltes capes d'interacció. Entendre el seu funcionament ens permet millorar i actuar amb més capacitat d'anàlisi i estratègia. Moltes branques del coneixement han abordat l'estudi del comportament humà durant segles, principalment des d'una vessant qualitativa i descriptiva. En l'era de la informació, disciplines com la física i les matemàtiques s'estan sumant a la recerca, aprofitant l'augment del nombre de dades disponibles per oferir altres perspectives i enriquir la visió global.

Un dels avenços més importants de la ciència del segle XX va ser el desenvolupament de la física estadística, una teoría que conecta els fenòmens microscòpics amb els macroscòpics, oferint un marc perfecte per l'estudi de les propietats emergents d'un sistema. És per això que bona part de la literatura en sociofísica està basada en models fisico-estadístics, en un primer moment utilitzats per la descripció de sistemes físics com ara gasos, materials magnètics, etc. Els detalls del model i la topologia emprada per descriure la disposició de les partícules estava adaptada a aquests medis, i per tant es resolien els models considerant les propietats espaials adients, com per exemple, en el cas del sòlid, estructures regulars o "lattices" en varies dimensions. Tanmateix, els sistemes complexos no segueixen aquests patrons, sino que les seves connexions tenen propietats característiques i comunes a la majoria de camps d'estudi, desde l'ecologia a les xarxes genètiques, passant per la neurociència. La teoria de grafs ofereix el marc matemàtic per descriure aquestes topologies i, de manera natural, les xarxes van començar a ser

emprades com a sustrat dels models fisico-estadístics quan s'apliquen per estudiar sistemes complexos. A més, depenent de les característiques de cada xarxa, poden observar-se nous comportaments per a cada model.

Aquesta tesi adapta un model, originalment concebut per explicar la transició entre 2 isòtops d'heli, per descriure una dinàmica d'opinions. El model emfatitza l'existència d'una facció central que participa en l'intercanvi d'opinions de manera activa, i permet modular el seu grau de convicció respecte a les faccions extremistes per a estudiar-ne l'efecte. L'evolució del sistema està dominada pel principi d'homofília o pressió de grup, que assumeix la tendència a l'aliniament de les opinions pròpies amb les dels individus amb qui interaccionem. D'altra banda, el model també considera una certa probabilitat que aquesta tendència no es compleixi, per l'acumulació de diversos factors oposats a ella. L'increment d'aquesta probabilitat es relaciona amb el concepte de temperatura en els sistemes físics.

Es proposa l'aplicació del model a diferents topologies, de més senzilles a més elaborades. L'aplicació en xarxes senzilles perment un tractament analític acurat que serveix com a base sòlida per explorar estructures més complicades que busquin capturar alguns aspectes essencials del comportament humà, com ara la tendència a canviar de relacions per buscar connectar amb persones de pensaments afins, o el fenòmen de la dissonància cognitiva. L'objectiu és incorporar aquests trets al model a través de la topologia.

La introducció de la tesi consta d'un resum de la teoria de xarxes i els models de la física social que acaba amb una descripció del nou model proposat. La resta de capítols es divideixen en un primer bloc dedicat a topologies monocapa i un segon bloc amb topologies temporals i multicapa.

El primer bloc assenta les bases de l'estudi dinàmic i d'equilibri del model en camp mitjà i l'extén a diferents topologies complexes. En primer lloc aplica el model a xarxes purament al · leatòries, per després incorporar una estructura de comunitats de diversos nivells en xarxes sintètiques i acaba emprant xarxes reals extretes de Twitter. Com a resultat, s'arriba a una descripció multiresolutiva de l'estructura de comunitats de les topologies estudiades.

El primer capítol del segon bloc explora la coevolució de la topologia amb la dinàmica d'opinions, barrejant conecptes de matèria activa i models d'opinió. En el segon i últim capítol d'aquest bloc es proposa un nou marc per als estats d'opinió individuals, que ja no venen representats per una sola variable, sino per una xarxa de creences, governada pel mateix model d'opinó de 3 estats emprat en la resta de la tesi.

En conjunt es busca aprofundir en l'anàlisi de la casuística topològica en un model discret d'opinió amb dos estats extrems i un de neutre que no representa indecisió, sinó una tercera via amb diversos graus d'implicació. Quan hi ha un

patró de connexió dens i una distribució de graus homogènia, els agents neutres poden dominar la dinàmica, catalitzant un consens neutral, encara que estiguin menys compromesos que els extremistes. D'altra banda, les topologies més disperses poden impedir el consens i conduir a cambres de ressò conformades per l'estructura de la xarxa.

Finalment, utilitzem les descripcions en forma de xarxes per ampliar el concepte d'estats d'opinió, facilitant l'estudi de la formació de consens a diverses escales. Aquest marc ens permet explicar la presència de fanàtics com a resultat d'una topologia interna en forma d'estrella en el sistema de creences d'un agent. Els sistemes de creences amb poques connexions internes poden conduir a la dissonància cognitiva, que en alguns casos pot millorar el grau de consens social. A més, la barreja d'agents amb estructures internes diverses afecta significativament el comportament individual i col · lectiu, especialment a prop de punts de transició crítics, el que podria ser útil a l'hora d'entendre canvis en el consens global del sistema.

List of publications

- Irene Ferri, Albert Díaz-Guilera, and Matteo Palassini. Equilibrium and dynamics of a three-state opinion model. *arXiv preprint arXiv:2210.03054* (2022).
- Irene Ferri, Conrad Pérez-Vicente, Matteo Palassini, and Albert Díaz-Guilera. Three-State Opinion Model on Complex Topologies. *Entropy*, 24(11):1627, Nov 2022.
- I. Ferri, A. Gaya-Àvila, and A. Díaz-Guilera. Three-state opinion model with mobile agents. *Chaos: An Interdisciplinary Journal of Nonlinear Science* 33(9) (2023).
- I. Ferri, E. Cozzo, A. Nicolás-Olivé, A. Díaz-Guilera, and Luce Prignano. Asymmetric Opinion Formation Model of Agents Interacting Periodically *(In preparation).*
- I. Ferri, A. Díaz-Guilera, and H. Sayama. Equilibrium and dynamics of a three-state opinion model on a network of networks *(In preparation).*

Acknowledgements

MANY individuals have played a part, directly or indirectly, in making this thesis a reality. I wish to take a few lines here to express my gratitude openly.

First and foremost, I would like to extend my gratitude to my supervisor Albert Díaz Guilera, for guiding me in every step of this journey, and to my partners in research who have provided endless support and insightful dialogue. Your collaboration has been priceless.

I also want to acknowledge the support of the faculty personnel who have facilitated every step of this process with their assistance.

On a personal note, to my partner, whose love and patience have been invaluable, and to my son, who has been a source of joy and inspiration every day. To my parents and family, for instilling in me the values and drive that have carried me through this endeavor and helping me in every possible way. And to my friends, both old and new, who have provided laughter and relief when most needed.

Lastly, I thank the research community at large—those I've met at conferences, workshops, and summer schools. Your enthusiasm for knowledge and innovation has inspired and guided my work.

Introduction

CHAPTER 1

Introduction

This chapter introduces the dissertation topic and overviews the network theory concepts used in this thesis. After that, I discuss several commonly used opinion models before presenting the pivotal three-state opinion model at the heart of this work. The chapter concludes with some preliminary analyses of the model and an outline of the thesis.

1.1

Complex systems and opinion models

Complex systems theory is an interdisciplinary field that explores the emergent properties of systems formed by interacting components. Although the behavior of individual components might be easily reduced to a few analyzable parameters, the effects of their interactions lead to collective behaviors that are often rich, non-linear, or even chaotic and unpredictable. This phenomenon is ubiquitous across nature, highlighting the field's interdisciplinary relevance. Notable examples include the formation of spontaneous fields in ferromagnetic materials, insect swarming, birds flocking, neural activity in the brain, or the dynamics of power grids, among many others [(110; 87)].

The study of complex systems extends beyond these, touching on areas such as economic markets, where feedback loops and interaction patterns result in unpredictable behaviors. Prices, supply, and demand are not only determined by individual decisions but also by the overall market sentiment, policies, and external factors like political events or natural disasters. Emergent behaviors in economic markets can include bubbles, crashes, and long periods of stability

or volatility, all resulting from the interconnectedness of market participants' actions.

Healthcare systems comprise hospitals, insurance companies, patients, healthcare providers, and governmental bodies, among others. Conflicts of interest and policy issues, such as access to care or the cost of treatments, impact emergent behaviors such as epidemics, health disparities, and the varying effectiveness of health interventions. The unpredictability of human health and behavior adds another layer of complexity to the problem.

Political systems involve the interactions of various entities, including governments, political parties, interest groups, and the electorate. Policy-making, governance, and the balance of power are just a few examples of phenomena that emerge from the interactions within these systems. Understanding shifts in political ideology, changes in governance structures, and the rise of social movements, influenced by both internal dynamics and external pressures is one of the goals of social sciences.

Social networks, both online and offline, represent another example of a complex system, composed of individuals or groups connected by various types of relationships. Their structure and dynamics influence information spread, opinion formation, and the emergence of trends and social norms. Phenomena such as viral content [(128)], the rapid mobilization for social causes [(137)], or the formation of echo chambers [(153; 167; 14; 12)], where diverse opinions are minimized, illustrate the complex interplay of network effects.

Self-organization refers to the process by which structure or pattern emerges in an open system without a central authority, arising naturally from the interactions among the system's components. In the context of social sciences, this concept is applied to understand how individual behaviors, decisions, and interactions can lead to the emergence of complex social patterns, structures, and dynamics without a central control. Social norms and values are not just passively absorbed by individuals but are actively interpreted, internalized, and sometimes modified, leading to the evolution of these norms and values over time. For example, a social movement may begin with a small group of individuals but can rapidly grow and evolve as more people join, each bringing their own perspectives and motivations. The movement's goals and strategies may shift in response to its size, the reaction of external entities (such as governments or other organizations), and the social context, reflecting a cascade of self-organization where the movement's growth and direction are continually shaped by its participants, being the study of social complex systems itself just another expression of this mechanism.

Auguste Comte [(30)], who, in the 19th century, laid some of the foundational stones for what would become the scientific study of society. Comte aimed to establish sociology as a discipline capable of applying scientific methods to the

understanding of social life and exploring the mathematical underpinnings of social phenomena. Despite these intertwined beginnings, sociology and sociophysics followed different paths. For decades, sociology studied the qualitative and theoretical exploration of social structures, norms, and institutions, while the nascent field of sociophysics, lingering in a conceptual limbo, awaited the maturation of tools and methodologies that could quantify the dynamics of social interactions. The turn of the millennium marked a significant shift since the advent of digital technologies and the explosion of big data have provided access to large-scale social data sets, from online interactions to urban mobility patterns. Computational tools and methods, including network analysis, agent-based modeling, and machine learning, offer sophisticated means to analyze, model, and simulate the behaviors of complex social systems.

The application of models from statistical mechanics to the understanding of social phenomena can be traced back to figures like Lewis Fry Richardson (Arms and Insecurity (1949) [(134)], Statistics of Deadly Quarrels (1960) [(135)]) who applied techniques of weather forecasting to explore the origins of wars and strategies for their prevention. He proposed a system of equations to describe the dynamics of armament escalation between rival nations. According to his model, the rate at which a country increases its armament is directly proportional to its rival's armament level and the grievances held against this rival, and inversely proportional to its own arsenal size.

Other early approaches in the interdisciplinary field of sociophysics and complex systems include the Schelling model for cultural segregation [(140)], the Axelrod model for cultural dissemination [(8)], and the Watts and Strogatz model [(168)] for the formation of social networks.

The key idea in sociophysics is that the dynamics of opinion formation and propagation among individuals can be understood using the same principles that describe phase transitions in physical materials. Under certain conditions, a macroscopic order can emerge from the microscopic interactions among the components of a system, whether this order manifests as the transition from a liquid to a solid state or as the emergence of consensus within a population of individuals.

Various models have been developed to study these dynamics, being the most paradigmatic the voter model [(80)], which simplifies opinion exchange to discrete binary choices and examines how local interactions can lead to global consensus or coexistence of opinions. The voter model can be mapped to the Ising model, a spin model introduced by Ising in 1925 [(83)] to explain the formation of magnetic domains, which also has been applied to unravel voting patterns [(62)]. Another prominent model is the Sznajd model introduced by Sznajd-Weron (((159) Sznajd-Weron and Sznajd (2000))), which is based on the principle that a pair or

group of individuals holding the same opinion can influence their neighbors more effectively than a single individual, leading to larger clusters of consensus.

There is another branch of models that considers the opinion space as a continuum spectrum between two extremes. In 1964, Abelson proposed a time-differential equation to describe the opinion transition rates driven by the strength of persuasive communication and conformity pressure (1). Bounded confidence models, developed more recently, consider a continuous opinion space where individuals only interact with those who are placed close enough in the opinion space. [(41; 77; 40; 170)]. Such models usually predict the formation of opinion clusters in the stationary state, so their analysis leads us back to the idea of a discrete opinion space.

A study of a multibody bounded confidence model in its final stages is provided in Appendix B. A recent experiment showed that angry participants felt less trusting of pairs [(44)]. Another study concludes that anger can activate prejudice, revealing that angry participants were more prone to associate negative rather than positiive traits with members of an out-group [(42)]. In Appendix B, we propose a framework where the deviation threshold is determined by a decreasing function of the emotional arousal of the agents; the higher their emotional arousal, the smaller the deviation threshold. Additionally, by interacting, agents influence the timing of each other's activities. Our results highlight the importance of synchronization in shaping consensus formation. Furthermore, we demonstrate that varying confidence intervals alter the impact of parameters like step length in navigating the opinion space, leading to deviations from the predictions of the traditional Deffuant model.

By integrating sociological insights with physical models, opinion models in sociophysics provide a powerful tool for analyzing and interpreting social phenomena. They have applications in predicting social trends, designing more effective communication strategies, fostering social cohesion, mitigating the effects of misinformation and polarization, or understanding the effects of social network structures on public opinion. A more detailed explanation of discrete models closely related to this thesis is provided in Section 1.3.

1.2

Networks

The structure and pattern of connections among individuals significantly influence how ideas, beliefs, and norms are shared and evolve within a society. The study of these topological features provides insights into the mechanisms of opinion formation, the speed of information dissemination, and the emergence of

consensus or polarization. The geometry of social structures is crucial in opinion formation and other contemporary questions such as pandemic spreading, economics (151; 104; 146), and smart cities design (105; 5).

Mathematically speaking, a graph, or network is a pair $G = (V, E)$ where V is a set of nodes (also called vertices) that represent objects or entities and E is a set of links (or edges) $\{v_1, v_2\}$ that represent the connections or relationships between these objects. Different network topologies can lead to markedly different outcomes in opinion dynamics. For example, in highly clustered networks or those that exhibit a strong community structure, opinions can become localized, leading to a persistence of diverse viewpoints.

Embedding opinion models on complex topologies has expanded the knowledge about fundamental questions regarding critical behavior and transitions between states. At the same time, the study of the dynamics of these models on networks can also help in solving complex systems problems, for instance, community detection (75) or brain functioning [(172; 36; 131; 107)].

The adjacency matrix is a representation of a network that encloses all the information about the connections between nodes. For a network with n vertices, the adjacency matrix A is a square matrix of dimension $n \times n$ where the element a_{ij} represents the connection from vertex i to vertex j. Formally, the adjacency matrix for a network is defined as:

$$A = [a_{ij}] \quad \text{where} \quad a_{ij} = \begin{cases} \text{weight of the edge} & \text{if there is an edge between } i \text{ and } j, \\ 0 & \text{otherwise.} \end{cases} \tag{1.1}$$

The value of the element a_{ij} corresponds to the weight of the edge, and for signed networks, this weight can be positive or negative to reflect the nature of the relationship (friendly or antagonistic, in the context of social networks). The diagonal elements a_{ii} are often set to zero, indicating the absence of self-loops in the network. Symmetric adjacency matrices correspond to undirected networks, where the relationships are equivalent in both directions between any two connected nodes.

The adjacency matrix is a powerful tool for analyzing the structure and properties of a network, allowing the application of matrix theory to compute different properties. For instance, it can be used to compute the degree, or number of connections, for each node, which can be determined by summing the elements in the corresponding row or column of the matrix.; to calculate the number of connected components —subsets of vertices in which any two vertices are connected by a path, and no vertices outside the subset are linked to any vertex within it; or to determine the path length between nodes.

In the context of this work, we limit our consideration to symmetric, binary adjacency matrices, corresponding to undirected, unsigned, and unweighted networks, where an entry of one indicates the presence of an edge between nodes i and j, and zero indicates no edge. This simplification allows us to focus on the topology of the network without the added complexity of edge weights, directions, or signs.

A simple example of an adjacency matrix is the one corresponding to the fully connected (FC) graph, or complete network, where every node is directly connected to every other node. Each off-diagonal element is set to 1, indicating the presence of an edge between distinct nodes, while elements on the diagonal are zero.

1.2.1 Topological measures

In this section, I provide a brief overview of the key topological measures applied in this research. Note that the field of network science encompasses a broader array of significant metrics. Among these, various forms of centrality—such as degree, betweenness, closeness, eigenvector, and PageRank centralities—stand out as they provide deeper insights into the roles and influences of individual nodes within the network's overall connectivity and flow dynamics. For a thorough understanding of network topology measures, Newman's book "Networks: An Introduction" is a comprehensive guide to network theory and its applications across various fields (118).

Paths

A path in a network is a sequence of nodes in which each adjacent pair of vertices is connected by an edge. For a network represented as a graph $G = (V, E)$, a path P from vertex u to vertex v is a sequence of vertices $(v_1, v_2, \ldots, v_k)$ such that $v_1 = u$, $v_k = v$, and $\forall i, 1 \leq i < k, (v_i, v_{i+1}) \in E$. Paths are fundamental for understanding the structure of networks, allowing us to analyze connectivity and the flow of information or resources.

The average shortest path length is defined as the average length of the shortest paths between all pairs of vertices in the network and it can be expressed as:

$$L = \frac{1}{n(n-1)} \sum_{u,v \in V} d(u, v), \tag{1.2}$$

where n is the number of vertices in the network, $d(u, v)$ is the shortest path distance between vertices u and v, and the summation is over all pairs of vertices. A smaller average shortest path length implies that, on average, fewer steps are needed to get from one vertex to another, therefore indicating

a higher efficiency for the transmission of information or resources in the network.

Clustering Coefficient

The clustering coefficient quantifies the likelihood that two adjacent nodes of a given node are also connected, forming a triangle. There are two primary versions of the clustering coefficient: local and global. For a given node v, with degree k_v, the local clustering coefficient C_v is defined as:

$$C_v = \frac{2T(v)}{k_v(k_v - 1)}, \tag{1.3}$$

where $T(v)$ is the number of triangles passing through node v. This formula calculates the ratio of existing links connecting a node's neighbors to the total possible links between them.

The global clustering coefficient C is calculated by taking the ratio of the number of triangles in the network to the number of connected triples of nodes (subsets of three nodes where one node is connected to the other two), and it has a value of 1 in fully connected graphs. Alternatively, Watts and Strogatz measure the overall level of clustering in a network [(168)] as the average of the local clustering coefficients of all nodes, often referred to as transitivity.

This measure provides insights into the micro- and macro-structure of networks, revealing local grouping patterns and the overall tendency for the formation of cohesive groups. Networks with high clustering coefficients tend to be more robust against random link destruction, as the dense connections provide alternative paths for network flow. In social networks, a high clustering coefficient indicates a strong tendency for social groups to form tightly interconnected communities, while in biological networks, such as neural or genetic networks, a high clustering coefficient may indicate functional segregation into modular sub-networks.

Assortativity

Correlations measure the tendency of nodes to connect with other nodes that are similar (or dissimilar) in certain attributes. When considering attributes like age, race, or income, analyzing correlations offers insights into the underlying social structure and the extent of community segregation. In networks, the assortativity coefficient, r, quantifies the level of similarity between connected nodes in the network. It ranges from -1 to 1, where a value of 1 indicates perfect assortativity (high-degree nodes connect with high-degree nodes, and the other way around,), while 0 indicates no assortativity (node connections are random with respect to

degree), and -1 indicates perfect disassortativity (high degree nodes connect with low degree nodes). Mathematically, r is defined as:

$$r = \frac{\sum_{ij}(a_{ij} - k_i k_j/2m)k_i k_j}{\sum_{ij}(k_i\delta_{ij} - k_i k_j/2m)k_i k_j}, \tag{1.4}$$

where a_{ij} refers to the adjacency matrix of the network, k_i and k_j are the degrees of nodes i and j, m is the total number of edges in the network, and δ_{ij} is the Kronecker delta function.

In the context of social networks, this might refer to the tendency of individuals with similar social backgrounds to form connections and can influence, for instance, the threshold and dynamics of epidemic outbreaks. In technical networks, such as the Internet or neural networks, assortativity can describe how nodes of similar degrees (number of connections) preferentially connect to each other. Assortative networks, in which high-degree nodes are more likely to be connected, tend to be more robust against random link destruction, but more vulnerable to targeted attacks. A comprehensive understanding of these connection patterns can help in modeling the growth and evolution of networks, predicting how networks may develop over time based on their current structure.

Modularity

Modularity is a measure used to determine the strength of a partition of a network into communities (also called modules or clusters) [(117)]. These communities are groups of nodes that are densely connected internally and sparsely connected with the rest of the network. High modularity indicates a structure where there are clear divisions within the network.

Modularity (Q) for a given division of the network is defined as:

$$Q = \frac{1}{2m}\sum_{ij}\left[a_{ij} - \frac{k_i k_j}{2m}\right]\delta(c_i, c_j), \tag{1.5}$$

where m is the sum of all of the edge weights in the network, $\delta(c_i, c_j)$ is a delta function that equals 1 if nodes i and j are in the same community and 0 otherwise, and c_i denotes the community to which node i is assigned.

Modularity is crucial for understanding the underlying structure of networks, enabling the identification of community structures which can have significant implications in various domains such as biology (identifying functional modules within cellular networks), social sciences (discovering groups within social networks), and more [(60)].

Finding the optimal community structure in a network, as indicated by maximum modularity, is not a problem with a unique solution. This is due, among other reasons, to the resolution limit of modularity, which can make it difficult to detect smaller communities within large networks. As a result, multi-resolution algorithms that can adjust the scale at which the network is examined, are useful for the detection of community structures at various levels of granularity [(7)]. These algorithms work by modifying the modularity function or by applying different principles to explore the community structure across different scales, providing a more comprehensive understanding of the network's modular organization.

1.2.2 Real Networks: Twitter

Real networks, particularly social networks like Twitter, exhibit small-world properties, meaning that they have high clustering and small average path length. The small-world phenomenon facilitates efficient information transfer, enhancing the spread of opinions by allowing both local clustering of opinions and global dissemination.

Another well-known feature of real-world networks is that they exhibit scale-free properties, characterized by a power-law degree distribution of the form: $P(k) \sim k^{-\gamma}$, where $P(k)$ is the probability that a randomly selected node has degree k, and γ is a constant typically in the range $2 < \gamma < 3$ for many real-world networks. In such networks, a few nodes have a significantly higher number of connections than others. These hubs can act as influential spreaders of opinions, making the network more susceptible to rapid changes in the dominant opinion or the spread of information (or misinformation).

Twitter, a platform central to digital communication and social interaction, offers a rich dataset for analyzing real-world networks. These interactions form complex networks that provide insights into information dissemination, influence dynamics, and community structures. Networks are built by linking users (handles) when they re-share content from one another or mention them in their posts. The study of these networks can answer questions about the flow of information, the spread of ideas, and the viral nature of certain topics. They can be used to identify influential users, understanding how information travels through social groups, and map the diffusion of news, rumors, or misinformation.

1.2.3 Generative Models

Generative network models offer frameworks for understanding the underlying mechanisms that drive network formation and evolution. These models aim to reproduce some structural characteristics observed in real-world networks, such as scale-free degree distributions, small-world properties, and community

structures. [(118)]. By simulating the process through which networks grow and develop, generative models help to analyze the fundamental principles governing network dynamics across various domains, including social, biological, and technological systems. This section explores some of the classical network models, although many extensions, variants, and other important models have been proposed in the past years. Some of these extensions, like the Holme-Kim model [(81)], have successfully explained all features in Table 1.1).

Model	$\langle L \rangle$	$\langle C \rangle$	$P(k)$
Erdös-Rényi (ER)	$\sim \ln N / \ln \langle k \rangle$	$\langle k \rangle / N$	Poisson
Barabási-Albert (BA)	$\sim \ln N / \ln (\ln N)$	$\sim (\ln N)^2 / N$	$\sim k^{-3}$
Watts-Strogatz (WS) (p intermediate)	$\sim \ln N$	$\mathcal{O}\left(N^0\right)$	$\sim$ Poisson

Table 1.1: Dependencies of generative network models on the number of nodes N, for the average shortest path length $\langle L \rangle$, the average clustering coefficient $\langle C \rangle$, and the degree distribution $P(k)$. Cells are colored green if the model successfully reproduces properties of real networks, and red otherwise.

Erdös-Rényi Graphs

Erdös-Rényi (ER) graphs, named after Paul Erdös and Alfréd Rényi, are one of the simplest yet most studied models of synthetic random graphs [(47)]. There are two versions of the model, denoted as $G(n, p)$ and $G(n, M)$, where n indicates the number of nodes in the network:

- In the $G(n, p)$ model, a graph is constructed by connecting nodes randomly. Each pair of distinct nodes is connected with probability p, independent of every other pair.
- In the $G(n, M)$ model, a graph is formed by selecting exactly M out of the possible $n(n-1)/2$ edges, uniformly at random.

A phenomenon of particular interest within these models is the existence of a critical probability, $p_c = \frac{1}{n}$, which marks a phase transition in the graph's structure from a collection of small disconnected subgraphs to a phase where a giant component emerges (21). In $G(n, p)$ graphs, the degree distribution follows a binomial distribution, which approximates a Poisson distribution for large n and small p.

In real-world networks, the average clustering coefficient decreases with an increase in the average node degree and is independent of the system size, but in ER networks $\langle C \rangle$ increases with $\langle k \rangle$ and decreases with N. Despite their limitations, ER graphs can reproduce the small average shortest path observed in real networks although they fail to capture scale-free degree distributions.

(see Table 1.1).

Watts-Strogatz

The Watts-Strogatz (WS) model, introduced by Duncan J. Watts and Steven Strogatz in 1998, is a simple and influential network model that captures the small-world phenomenon, producing networks that exhibit both high clustering and short average path lengths.

The model starts with a regular lattice network where each node is connected to k nearest neighbors in a ring topology. Then, with a probability p, each edge is rewired to a randomly chosen node, introducing a transition from a highly ordered state to a random one.

For small values of p, the network maintains a high clustering coefficient, however, the average shortest path length is large. As p increases, the average path length between nodes quickly decreases, entering a range with small-world properties where any node can be reached from any other in a small number of steps and the clustering coefficient is still high (see Figure 1.1).

Barabási-Albert Graphs

The Barabási-Albert (BA) graph, introduced by Albert-László Barabási and Réka Albert in 1999, is a model that reproduces the scale-free properties observed in real-world networks, via two mechanisms: growth and preferential attachment[(11)].

The generation process of a BA graph starts with a small number (m_0) of fully connected nodes. New nodes are added to the network one at a time, each connecting to $m(\leq m_0)$ existing nodes with a probability $p_i = k_i / \sum_j k_j$ proportional to the number of links that the aforementioned nodes already have. This "rich-get-richer" mechanism ensures that nodes with higher degrees have a higher chance of receiving new links, leading to the emergence of hubs or highly connected nodes. This process not only reproduces some key properties of real-world networks at a macro scale but also mimics micro-mechanisms of real-world network formation (4).

The degree distribution of BA graphs follows a power law with $\gamma = 3$ and they have small average path lengths. However, although their average clustering coefficient is higher than that of ER graphs, it is still smaller than what is observed in real networks (see Table 1.1).

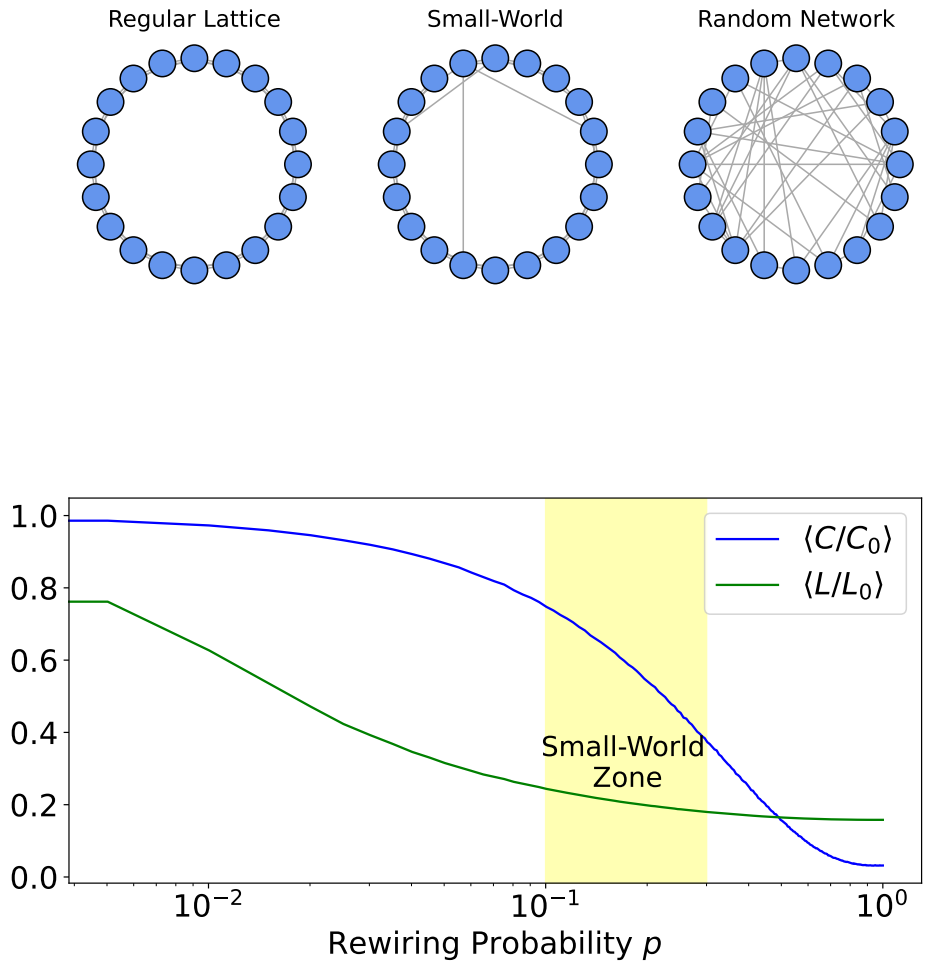

Figure 1.1: Transition from a regular lattice to a random network via the Watts-Strogatz model. The relationship between rewiring probability p and network metrics, average clustering coefficient $\langle C \rangle$, and average shortest path length $\langle L \rangle$ with the small-world regime highlighted. Adapted from (168)

Girvan-Newman communities

A widely recognized benchmark in community detection is a graph structure proposed by Girvan and Newman [(120)], consisting of 128 vertices divided into four groups of 32. Each vertex has an average degree of 16, and the internal group connectivity is adjusted by a parameter z_{in}, which represents the average number

of edges each vertex has within its own group. When z_{in} is close to 16, the graph exhibits a clear community structure, as most connections are within the same group, making the communities distinct. When $z_{in} \leq 8$ edges predominantly link vertices across different groups, blurring the community boundaries.

The effectiveness of a given community detection method is tested by comparing the algorithm's groupings to the graph's known partition into four "natural" groups. A vertex is considered correctly classified if it shares a cluster with at least 16 of its original group members. If an algorithm merges two or more of the natural groups into a single cluster, all vertices in that cluster are considered incorrectly classified. Algorithms generally perform well when z_{in} is high but struggle as z_{in} decreases toward 8 (116; 58), which in turn suggests that the randomness introduced in the rewiring process challenges the assumption that the initial four-group partition represents the true structure of the graph.

Random Geometric graphs

In Random Geometric Graphs (RGGs) nodes occupy a physical space and edges represent proximity-based interactions. RGG's are generated by randomly placing their vertices within a given space, forming links between nodes within a certain distance threshold. The foundational work by Penrose [(126)] provides a comprehensive mathematical framework for RGGs, emphasizing their application in modeling and analyzing spatially structured networks.

RGGs have a critical percolation threshold that marks the transition from a disconnected network to one where a giant connected component emerges, spanning a significant portion of the network. This point is related to the density of nodes and the radius within which nodes are considered neighbors by: $(N_{init} - 1)\pi d_c^2/L^2 \approx 4.51$ (141). Dall et al. (2002) discussed graphs with vertices assigned random coordinates in a geometric space, focusing on the critical connectivity found numerically by examining the size of the largest cluster [(33)].

This model is especially suitable for networks which connectivity is dictated by spatial positioning, like wireless communication networks [(147; 88)], brain networks [(127)], and social interactions that have a spatial component [(22)].

1.2.4 Graph Product Multilayer Networks

Traditional network analysis assumes all interactions are similar, which overlooks the varied nature of real-world connections. For instance, human relationships can be categorized as personal or professional, flight routes as commercial or cargo, and relationships in an ecosystem as mutualistic, predatory, or parasitic. Multilayer networks allow for the examination of different types of links within the same framework. This approach includes multiplex networks, where different

layers represent various kinds of interactions among the same nodes; hypergraphs, which include connections among more than two nodes to capture higher-order interactions; and interdependent networks, which reveal how different scales or domains are interconnected, influencing each other's functionality. These interdependencies often highlight critical points of vulnerability and resilience within interconnected systems.

Another structure that can be englobed in the multilayer framework is the networks of networks, in which each node is a network itself, and inner nodes are connected to other inner nodes via the external nodes' connections. This kind of graph can be mathematically represented as graph products, offering a rich framework to model complex systems spanning multiple scales [(139)]. Such representations are crucial for understanding the emergent behavior in systems ranging from biological entities to technological and social systems, where different layers of interaction play a relevant role in determining the system's overall dynamics.

Graph Product Multilayer Networks (GPMNs) represent a framework for constructing complex network structures through the application of graph product operators. Originating from graph theory, these operators facilitate the combination of simpler factor networks into a comprehensive product network, particularly useful for modeling multilayer networks where different types of interactions coexist across multiple layers. This subsection provides a brief description of the three principal graph product operators: Cartesian, direct (tensor), and strong products (see Figure 1.2).

Cartesian Product

The Cartesian product of two graphs G and H, denoted as $G\square H$, constructs a graph whose vertices correspond to all possible pairs (g, h) for $g \in G$ and $h \in H$. Edges between vertices (g_1, h_1) and (g_2, h_2) exist if:

- $g_1 = g_2$ and h_1 is adjacent to h_2 in H, or
- $h_1 = h_2$ and g_1 is adjacent to g_2 in G.

This means that if one component of the pair is identical and the other is adjacent in its respective graph, then the pairs are connected in the product graph. This product can be used to model networks where connectivity in one layer operates independently of another. The adjacency matrix of the Cartesian product $G\square H$ is given by: $A_{G\square H} = A_G \oplus A_H = A_G \otimes I_{|V_H|} + I_{|V_G|} \otimes A_H$ $\oplus$ denotes the Kronecker sum, and $\otimes$ denotes the Kronecker product. $I_{|V_H|}$ and $I_{|V_G|}$ are identity matrices of sizes corresponding to the number of vertices in H and G, respectively.

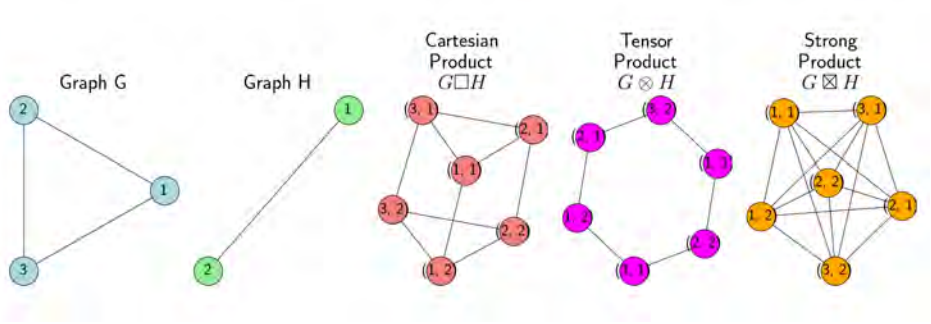

Figure 1.2: Visual Representation of Graph Products in Network Analysis – This series of diagrams illustrates different graph products derived from a simple triangle graph G and a line graph H. From left to right: Graph G as a triangle, Graph H as a line, their Cartesian Product $G\square H$ showing possible connections based on matching vertices, the Tensor Product $G \otimes H$ emphasizing direct connectivity, and the Strong Product $G \boxtimes H$ combining properties of both Cartesian and Tensor products. Each graph product helps in exploring complex network structures and their properties, demonstrating how different layers and connectivity patterns can be analyzed in multilayer networks.

Direct (Tensor) Product

The direct or tensor product of two graphs G and H, denoted as $G \otimes H$, creates a graph whose vertices are all possible pairs (g, h) for g in G and h in H. In this graph, an edge connects vertices (g_1, h_1) and (g_2, h_2) if and only if g_1 is adjacent to g_2 in G and h_1 is adjacent to h_2 in H. This condition means that connections in the product network depend on simultaneous connections in both of the original or factor networks, highlighting the necessity for coordinated adjacency in both dimensions. Such a model is particularly useful for scenarios where interactions within the combined network are dependent on the presence of corresponding connections in each of the separate networks.

The adjacency matrix of the tensor product $G \otimes H$ is given by:

$$A_{G \otimes H} = A_G \otimes A_H$$

where $\otimes$ denotes the Kronecker product. Unlike the Cartesian product, which combines the identities and adjacency matrices in a form representing independent connectivity across layers, the tensor product uses a straightforward Kronecker product, creating a matrix that represents direct pairwise connections across both graphs.

Strong Product

The strong product, denoted by $G \boxtimes H$, merges the properties of both the cartesian and direct products, thereby providing a rich structure for network analysis. The vertices of the strong product are formed by pairs (g, h) for every g in G and h in H. An edge between two vertices (g_1, h_1) and (g_2, h_2) in $G \boxtimes H$ is established under any of the following conditions:

- $g_1 = g_2$ and h_1 is adjacent to h_2 in H, reflecting the connectivity pattern of the Cartesian product;
- $h_1 = h_2$ and g_1 is adjacent to g_2 in G, also reflecting the Cartesian product structure;
- g_1 is adjacent to g_2 in G and h_1 is adjacent to h_2 in H, reflecting the tensor product's connectivity requirements.

The strong product can highlight pathways for redundancy and multiple connectivity routes, thereby providing insights into how network architecture can influence overall system stability and functionality. This makes the strong product particularly useful in scenarios where network resilience and robustness against failures are studied.

1.3

Opinion Models

Instead of creating a universal model to explain human behavior comprehensively, it is more effective to construct specific models that focus on distinct aspects of behavior. These models isolate and analyze the key characteristics useful for the particular research question at hand. By examining and synthesizing the main findings of these models, one can establish connections that may facilitate the development of a more complete theory for describing human behavior. (63; 64; 97).

Opinion models in sociophysics allow for the study of the mechanisms underlying opinion formation and the conditions leading to various societal outcomes. These models employ variables to represent individual opinions, which evolve according to specified rules. The aim is to capture the complex interplay of factors that drive consensus formation, polarization, fragmentation and other social large scale phenomena. Recent advancements in the field of sociophysics have led to refined models targeting specific aspects of societal interactions, such as the formation of echo chambers [(14; 12)], polarization [(145; 176; 90; 91)], opinion expression (61), information spreading [(113; 106; 24)] or gerrymandering

[(84; 154; 17)]. This section offers a description of a few examples of discrete opinion models, which represent opinions as discrete values, as they are more relevant to the present work. For a more extensive review of opinion models in sociophysics, the reader can refer to [(26; 144)].

Despite the differences in the details of each model, the questions they aim to answer are primarily related to the distribution of opinions in the population. A common goal in many of these works is to understand the transition from an initial disordered state, where opinions are random and uncorrelated, to a state where agents exhibit some form of local or global consensus.

1.3.1 The voter model

The first opinion model in the field of sociophysics is often credited to the voter model. Introduced in the early 1970s by Thomas M. Liggett and Richard A. Holley (80), the voter model is a binary simple time-discrete agent-based model that describes the dynamics of opinion formation through a stochastic Markovian (memoryless) process of imitation.

Each agent is assumed to have a discrete opinion, typically represented as $+1$ or -1, and at each time step, an agent is randomly selected and adopts the opinion of one of its neighbors, also chosen at random. The global state of the system at any time can be represented by a configuration $\{\sigma\}$, where $\sigma_i \in \{+1, -1\}$ denotes the opinion of the i^{th} agent. The evolution of the system over time can be treated analytically via the master equation (which form will depend on the agents' connection pattern) or numerically, through Monte Carlo simulations.

In the absence of external influences or additional rules, a finite system will always reach consensus, however, the network structure on which the voter model is applied (e.g., lattice, random graph, scale-free network) significantly affects the time to reach consensus. For instance, in highly connected networks, consensus is typically reached faster than in sparsely connected networks due to the increased interaction opportunities between differing opinions. The process of reaching consensus in the voter model can be mathematically described as a random walk, especially in one-dimensional or two-dimensional systems, an analogy that helps in analyzing the model's behavior.

Several extensions have been developed to capture more realistic social mechanisms and scenarios. One notable variant is the majority rule voter model, where the update rule is modified to ensure that the state of a chosen agent is determined by the predominant opinion among all its neighbors within a certain local neighborhood or interaction range. From a social perspective, this variant simulates social conformity under peer pressure, a mechanism that drives individuals to adopt the most common opinion or behavior observed in their social circle.

The role of "zealots", stubborn agents who never change their opinion, has been explored in many studies. Mobilia et al. (2003) find that the effectiveness of "zealots" in influencing the entire system varies with the system's dimensionality (111). Yildiz et al. (2013) (178) study how the density fluctuations of "zealots" and their position impact the process of consensus formation. Granovsky et al. introduce noise by allowing agents to randomly flip their opinions (73) and Galam et al. (2007) investigate the role of opinion inertia (65). The model has also been embedded on a wide variety of topologies (156; 96).

Classical Voter Model Dynamics

Step 1: *Agent Selection*

Randomly select one agent, denoted as i, from among the N agents in the system.

Step 2: *Random Neighbor Selection*

Randomly select one neighbor of agent i, denoted as j, from its immediate local neighborhood or defined interaction range.

Step 3: *Opinion Adoption*

Agent i adopts the opinion of the selected neighbor j, effectively mirroring j's state.

1.3.2 The Ising model

In the attempt to model basic human behavior, the complex systems community realized very soon that the analogies with well-known physical models could be exploited. For instance, the tendency to align one's opinion with those of their neighbors is a property that ferromagnetic materials exhibit as well (98; 169; 62; 94; 66; 102).

The first and simplest choice was the Ising model, a statistical physics model originally developed to describe the behavior of magnets [(83)]. Atomic spins can take two orientations $\sigma_i = -1, +1$ and interact with their nearest neighbors via a potential energy that is a function of the spins' alignment:

$$H = -J \sum_{\langle i,j \rangle} \sigma_i \sigma_j - h \sum_i \sigma_i, \tag{1.6}$$

where J is a positive constant representing the coupling strength between neighboring spins, h is an external magnetic field, and the summation runs over nearest neighbors. The external field term can be associated to an external influence or propaganda that attempts to sway the general population's opinion in a particular direction. It models how external pressures or information campaigns can shift the overall sentiment of a population towards a specific viewpoint. The pairwise term accounts for the agents' tendency to align their opinions. The system evolves to minimize this energy, subject to temperature fluctuations. The key phenomenon described by the Ising model is the second-order (continuous) phase transition from a disordered state at high temperatures to an ordered state (all spins aligned) as the temperature decreases below a critical point.

While there is no energy function explicitly defined in the voter model, there exists a mapping between these two models that becomes apparent when considering the Ising model at zero temperature and in the absence of an external magnetic field. Despite their microscopic rules being different, under these conditions, both models exhibit the same macroscopic behavior and can be considered part of the same equivalence class. An equivalence class in this context, is a set of models that are equivalent in terms of their long-term dynamics, although sometimes this concept is used in a more relaxed form to refer to models which order parameters show the same behavior near their critical points (171; 71),. This equivalence highlights the universality of certain statistical properties across models, allowing us to understand the common properties of collective phenomena, transcending the specific details of individual models, and predicting the behavior of complex systems using simpler or more well-studied models.

Although the Ising model is an equilibrium model, it can be dynamically simulated—similarly to the voter model—through a Markov chain, and sample from its equilibrium distribution once it reaches a stationary state. This approach is interesting from a social perspective, as understanding the system's temporal evolution in this context can offer valuable insights. The sequences below describe one elementary move for the two most commonly used dynamical algorithms: the Glauber dynamics and the Metropolis dynamics.

Metropolis dynamics

Step 1: Pick one agent i at random with uniform probability among the N agents.

Step 2: Propose a random opinion change with probability 1/2 for the agent i and calculate the energy difference ΔH between the new and old configuration.

Step 3: Accept the change with probability $\min\{1, e^{-\beta\Delta H}\}$, otherwise remain in the current state.

Glauber dynamics

Step 1: Pick one agent i at random with uniform probability among the N agents.

Step 2: Calculate the energy differences ΔH_1 and ΔH_2 between the new and old configuration, for the two possible opinion changes for the agent i.

Step 3: Accept either of the two possible changes with probability $P_k = w_k/(1+w_1+w_2)$, where $w_k = e^{-\beta\Delta H_k}$ for $k = 1, 2$, or remain in the current state with probability $1 - P_1 - P_2$.

Just as in physical systems where particles settle into states of minimum energy, opinions in a social network evolve towards stable configurations that can be viewed as attractors. A basin of attraction in this framework can be understood as the set of initial configurations that lead the system to a particular stationary state, and their shape and size will depend on the network topology and the dynamics governing opinion/spin changes.

Various studies have compared these dynamics and those of the voter Model. for instance, Paula *et al.* analyzed the Glauber and Metropolis master equations in one and two-dimensional lattices, revealing that neglecting spin correlations can lead to discrepancies between predictions and simulation results [(124)]. Castellano textitet al. examined Glauber and voter dynamics on complex networks with varying degrees of heterogeneity in their distribution. They discovered that,

unlike voter dynamics, Glauber dynamics at zero temperature gets trapped into metastable states without ever achieving an ordered state, even in finite systems [(26)]. More recent studies explore how Glauber and Metropolis can lead to different between basins of attraction and the influence of long-range interactions on coarsening processes (66; 86).

By modeling voters as spins and their social interactions as links among these spins, we can effectively simulate how localized interactions give rise to large-scale phenomena, such as political consensus or polarization, analogous to phase transitions observed in physical systems [(19; 57; 102; 12)]. These investigations into binary opinion dynamics motivate the exploration of the model on complex topologies, including synthetic graphs, real networks, coevolving networks, and multilayer networks [(78; 121; 37; 29; 82)]. The results of these studies indicate that the topology influences the universality class of the model.

1.3.3 The Potts Model

The Ising and voter models are well-suited for analyzing polarized scenarios characterized by clear bipartisanship. However, in more complex situations, adopting a model that accommodates a broader range of opinions provides a more realistic representation of the opinion space.

The Potts model (130) generalizes the Ising model to take into account three or more opinions. In the Potts model, each agent can be in one of $\sigma_i \in \{1, q\}$ distinct independent states, with no inherent ordering or notion of distance between them. The expression for the Potts Hamiltonian, which gives the system's total energy, is:

$$H = -J \sum_{\langle i,j \rangle} \delta(\sigma_i, \sigma_j), \tag{1.7}$$

where σ_i is the state of the spin at site i, $J > 0$ is the interaction strength, and δ is the Kronecker delta. The global energy is minimized when adjacent spins are in the same state, thus promoting domain formation where contiguous sites preferentially align in the same state.

Many results observed in the Ising model context can be easily generalized (148). For instance, the Potts model also exhibits phase transitions, undergoing a change in behavior from disordered to ordered states at certain critical temperatures. The nature and universality class of these transitions depend on the number of states q and the connections pattern. For instance, in two-dimensional lattices, the model has a second-order (continuous) phase transition for $q \leq 4$ and a first-order (discontinuous transition) for $q > 4$ (173). Bray provides a review in phase ordering kinetics, including a study of the coarsening dynamics in the Potts model after a quench from a high to a low temperature, highlighting the scaling laws and the universality of the domain growth process. (25).

This model offers a robust framework to simulate how individuals with diverse states or opinions might spontaneously organize into communities sharing similar attributes or ideologies. In the realm of community detection, having multiple states facilitates the identification of clusters, especially in real-world networks, where community ties are not strictly binary but display a wide range of interactions (132; 58; 101)

The model has also been embedded in random graphs (46; 51) and more recently on complex signed networks finding that the nature of relationships (positive or negative) can significantly affect the propagation of opinions. For instance, antagonistic ties might hinder consensus or lead to the formation of polarized opinion clusters (103).

Schulze (2005) used the Potts model with temperature to study the formation of ghettos in cities, modeled as two-dimensional lattices (142). Bordogna et al. applied the Potts model to model social behavior shedding light on the conditions under which a social system might reach a consensus or become divided, considering factors such as the strength of interpersonal influence and the structure of the social network (23).

Another work studies the effect of quenched disorder caused by the presence of "zealots" (111; 112), which introduction in the system disrupts the conservation of magnetization in lattices. In dimensions $d \leq 2$, a single zealot can influence the entire system, inducing a general consensus in alignment with its own stance. In higher dimensions, while a consensus may not be achieved, the stationary state in the zealot's vicinity is biased toward its opinion.

1.3.4 Three-state models

A compelling scenario in social dynamics is the three-party system, encompassing extremists on both ends of the opinion spectrum and a neutral group in the middle. The inclusion of an intermediate or neutral state is not merely theoretical but finds grounding in real-world phenomena. This setup, reflecting a significant portion of social debates, underscores the relevance of neutral agents in facilitating or obstructing consensus within diverse groups (162; 177; 52). The Catalan independence consultation in 2014 and language competition in multilingual societies are prime examples where three distinct choices or states naturally emerge, requiring models that can accommodate this nuance (27).

In contrast with the Potts model, where all states are equivalent, models adapted to this context often interpret neutral agents as mediators in the interaction between opposing extremists, effectively serving as a bridge for opinion exchange. Vazquez et al. (2003) propose a three-party Ising-like model where extremists are incompatible and do not affect each other, thus the only opinion changes allowed are those involving neutral agents, which often leads to situations

with a mixture of extremists (162). One year later they studied a stochastic kinetic model in the mean-field approximation, finding that the final configuration depends strongly on the initial proportion of agents in each state (163). Along similar lines, Svenkeson et al. (2015) incorporated temperature and find a phase transition analogous to the one exhibited by the Ising model (157).

1.3.5 - The Blume-Emery-Griffiths model

The Blume-Emery-Griffiths model [(20)], introduced in 1971, incorporates interactions between pairs of spins as well as a single-ion anisotropy term and a term that models the interaction between spins and a non-magnetic impurity or a lattice distortion. In its general form is described by the Hamiltonian :

$$H^{BEG} = -J \sum_{\langle i,j \rangle} \sigma_i \sigma_j - K \sum_{\langle i,j \rangle} \sigma_i^2 \sigma_j^2 + \sum_i \Delta_i \sigma_i^2 + C \,. \tag{1.8}$$

Although the direct application of the BEG model in sociophysics is less common compared to the Ising or Potts models, its potential for capturing the nuances of multi-state social dynamics is significant. The biquadratic interaction term in the Hamiltonian can be thought of as representing the societal pressure for individuals to adopt a strong (extremist) stance, rather than remaining neutral. The single-ion anisotropy term penalizes non-zero spins, making it energetically favorable for spins to be in the neutral state. In social terms, this might represent an inherent individual or societal bias towards neutrality or indecision. The nearest-neighbor exchange contribution, analogous to the Ising model, favors the alignment of extremist agents only. The contribution from the coupling of two neutral neighbors is equal to zero, the same as if they hold different opinions.

Yang (2010) applied the BEG model in the context of social networks, showing that the probability distribution function of opinion time series under Glauber dynamics exhibits a Gaussian-like shape (177). The same year Gauvin et al. mapped the zero-temperature BEG model with kinetic constraints onto the Schelling model of spatial segregation (140; 67), investigating the role of neutral agents (interpreted as vacancy density) on the system's phase diagram. Their findings reveal that the interfaces between clusters of differing agent types, as shaped by the dynamics, can lead to segregation distinct from that observed in Schelling's original formulation.

1.3.6 - The Blume-Capel model

The Blume-Capel model, developed in the 1960s, is a particular case of the BEG model which hamiltonian includes only the nearest-neighbor exchange term and single-ion anisotropy term with a global parameter D:

$$H^{BC} = -J \sum_{\langle i,j \rangle} \sigma_i \sigma_j + \Delta \sum_i \sigma_i^2 \,. \tag{1.9}$$

Hohnish et al. (2005) successfully applied the model to replicate large fluctuations observed in time series obtained from German business-climate data (79). Fernandez et al. (2016) explored the model on random graphs, Watts-Strogatz networks, and networks following Newman's models from a social perspective (52). They showed that the network topology on the system's macrostate behavior, in particular low connectivity may hinder global consensus. Naskar (2021) conducted a study investigating the lifetime of metastable states using Metropolis simulations, applied to both the Ising and Blume-Capel models, which were extended to include additional discrete states (115).

1.4

A vectorial three-state opinion model

In many real-world social systems, there is a significant proportion of individuals who hold a neutral or centrist opinion, and their behavior can have a crucial impact on the overall dynamics of opinion formation.

The model is inspired by magnetic spin-like models and aims to emphasize the role of the relative degree of conviction between neutral agents and extremists. It considers three possible states for the agents: two extreme opposite states and a neutral one. The third opinion is placed symmetrically between the two polarized ones, and we quantify the probability transition to this central state using a neutrality parameter denoted by α.

Model description

In our model, agents live on the nodes of an undirected and unweighted graph of size N, and their opinions are represented by two-dimensional vectors $\mathbf{S}_i$ that can take three orientations:

- $\mathbf{S}_i = (1, 0)$; positive opinion / rightist
- $\mathbf{S}_i = (0, \alpha)$; neutral opinion / centrist
- $\mathbf{S}_i = (-1, 0)$; negative opinion / leftist

where α is a dimensionless parameter. We assume that the agents prefer to agree with their neighbors so as to minimize, in the absence of social agitation or

temperature T, the following cost function, or Hamiltonian:

$$H = -J \sum_{\langle i,j \rangle} \mathbf{S}_i \cdot \mathbf{S}_j, \tag{1.10}$$

where $J > 0$ and the sum runs over all the edges of the graph.

The possible values of the interaction energy between two agents, $-J\mathbf{S}_i \cdot \mathbf{S}_j$ are shown in Figure 1.3. The quantity $J(\alpha^2 - 1)$ thus measures the reward of the presence of connected neutral pairs of nodes, we called it the neutrality parameter.

Although the model considers the tendency to align agents opinions with those of their neighbors as the main opinion change mechanism, we also consider the possibility that an agent adopts a state that does not minimize the sum of opinion products with their neighbors with a certain probability. This probability is governed by a parameter that we call temperature, by its analogy with physical systems in contact with a thermal bath T. It is the same parameter used in the conventional Metropolis dynamics, and accounts for a coarse-graining of all sources of noise that may lead an agent to take a stand against their neighbors as, for instance, social agitation. For simplicity, we use dimensionless units for the energy and temperature such that $J = 1$.

The order parameters of the model are the Ising-like magnetization $m = \sum_i \langle \sigma_i \rangle / N$, namely the difference between the fractions of rightists and leftists, and the fraction of neutral agents, $n_0 = 1 - \sum_i \langle \sigma_i^2 \rangle / N$. Here, $\langle \ldots \rangle$ denotes either the theoretical expectation with respect to the Boltzmann distribution, or the average over the different repetitions of the simulations.

Mapping to the BEG model

An equivalent way to express the model Hamiltonian is to replace the state vectors with scalar variables taking the values $\sigma_i \in \{1, 0, -1\}$, which gives

$$H = -J \sum_{\langle i,j \rangle} \left[\sigma_i \sigma_j + \alpha^2 (\sigma_i^2 - 1)(\sigma_j^2 - 1) \right] . \tag{1.11}$$

In this form, the model can be seen as a special case of the BEG model (20), which In fact, we recover Eq.(1.11) by setting

$$K = J\alpha^2, \quad \Delta_i = k_i K, \quad C = -NzK \,/\, 2, \tag{1.12}$$

where k_i is degree of node i, i.e. the number of nodes connected to it, and $z = \sum_i k_i / N$ is the average degree of the graph. Note that the standard BEG model has a unique value $\Delta_i = \Delta$ for all i. Therefore, for graphs with constant degree $k_i = z$, we can obtain the phase diagram of our model by projecting that of

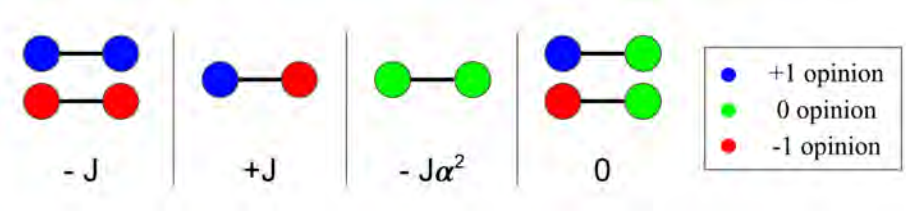

Figure 1.3: Contribution of a pair of interacting agents to the energy of the system.

the BEG model, which is defined in the three-dimensional parameter space (K/J, Δ/J, T/J), onto the two-dimensional semiplane $(\alpha, T/J)$ defined by Eq.(1.12).

In contrast with the Blume-Capel (BC) model, whose Hamiltonian rewards the presence of neutrals within the system, the model introduced here specifically rewards the alignment of opinions among neutral neighbors. This distinction underlines that, in the context of our model, a neutral opinion is not simply indicative of indecision; rather, it represents a deliberate choice within the spectrum of possible opinions, which is spread among agents similarly to extremist views.

1.5

Preliminar analysis and open questions

For $\alpha = 0$, the model can be thought of as an Ising model with vacancies. Hence, in the thermodynamic limit it will generically display a continuous phase transition in the Ising universality class at a critical temperature $T_c^0 > 0$, between a low-temperature polarized (ferromagnetic) phase, characterized by $m \neq 0$, and a high-temperature disordered (paramagnetic) phase, in which $m = 0$.

We can anticipate some general features of the equilibrium phase diagram in the plane (α, T). For $\alpha < 1$, the ground state is ferromagnetic, namely the agents achieve a global consensus either in the positive or in the negative state ($m = \pm 1, n_0 = 0$). For $\alpha > 1$, all agents assume the neutral opinion ($m = 0, n_0 = 1$) in the ground state. Hence, moving along the zero-temperature axis we encounter a discontinuous phase transition at $\alpha = 1$.

We thus generally expect a phase boundary in the plane (α, T) connecting the two points $(\alpha = 0, T = T_c^0)$ and $(\alpha = 1, T = 0)$. Since the transition is discontinuous at one end of the boundary and continuous at the other, we also expect a tricritical point (α_{tc}, T_{tc}) at some point along the boundary, separating a line of continuous transitions at $T = T_c(\alpha)$ for $0 \leq \alpha \leq \alpha_{tc}$ from a line of discontinuous transitions at $T = T_d(\alpha)$ for $\alpha_{tc} < \alpha \leq 1$. Such a phase boundary

was indeed observed for a different projection of the BEG model, the Blume-Capel model, on various types of random graphs, including some cases in which the phase boundary is reentrant (99). Exceptions to this scenario are represented by 1D system, in which $T_c^0 = 0$, since no long-range order can survive at finite temperature, and by graphs with a degree distribution falling more slowly than k^{-3} for large k, in which the system is known to remain ferromagnetic at all temperatures for $\alpha = 0$ (99) (we expect this to remain true for all $\alpha < 1$.)

When embedded in different networks, we expect changes in the energy landscape, with local minima appearing and/or disappearing. The population's macrostate, determined by the system's order parameters, may transition from consensus to polarization or vice versa as a result of topological variations, even while maintaining the same temperature and neutrality parameter values. Our goal is to determine which network features are most influential. Starting from the baseline of a fully connected network, which can be solved analytically, we will explore more complex topologies, varying average degrees and modular structures. We will assess global features of both synthetic and real networks and identify which synthetic networks yield outcomes most similar to those observed in real networks.

Changing one's opinion is not the only way to align with neighboring agents; people can also decide to change their connections by breaking old relationships and forming new ones. Allowing the coevolution of opinion dynamics and network structure enables us to understand the interplay between these two mechanisms. When studying in-person interactions, link formation and breaking can be connected to movement patterns in a physical space. Moreover, since these processes generally occur at different time scales, it is interesting to examine how the adjustment of these time scales affects not only the system's outcome but also the time it takes to achieve it.

Finally, we can expand the opinion space in a topology-oriented fashion by maintaining the same model and constructing networks that represent people's belief systems. This approach not only provides interpretability to the structure of the studied topology beyond the existence of mere community structures but also allows for the study of cognitive dissonance phenomena and its interplay with social consensus formation. By focusing on the structure of internal connections among beliefs, we can analyze its potential to reinforce or alter outcomes observed when considering a single belief per agent and interpret how it may impact on both individual and population-wide behavior.

1.6

Organization of this thesis

The thesis is divided into two main parts:

- A first part including:
  - Chapter 2, providing a detailed analysis of the mean-field approximation (MFA), exploring the equilibrium phase diagram of the model through different analytical approaches and Monte Carlo (MC) simulations at zero and finite temperatures.
  - Chapter 3, discussing the model embedding Erdös-Rényi graphs. Chapters 2 and 3 present the results derived in the article [(54)]
  - Chapter 4, exploring the model on modular networks. We use both synthetic and real networks and examine their community structure and their interplay with the model. This Chapter exposes the findings of the article [(55)]
- A second part, presenting a branch of the research focused on the study of spatiotemporal and multilayer topologies:
  - In Chapter 5, addressing the implications of considering movement in a two-dimensional plane and coevolving opinion-structure dynamics. We combine an active matter framework with the three-state opinion model to incorporate new behaviors to the study. This chapter corresponds to the results published in [(53)].
  - Chapter 6, analyzing the role of belief systems in consensus formation. We apply the description of beliefs as networks offers a more nuanced representation of agents and has been used in many recent studies in psychology.

Finally, Chapter 7 closes the thesis and discusses possible future directions.

Single Layer Complex Networks

CHAPTER 2

Fully-Connected Graph

In this chapter, we provide an analysis of the equilibrium and dynamic behavior of the model described in Section 1.4. in the fully connected graph. We analyze the equilibrium order parameters' behavior as a function of both the neutrality parameter α and the temperature T. We discuss the dynamic basins of attraction at $T = 0$ for different values of α and analyze the distribution of the magnetization near the tricritical point.

2.1

Introduction

The mean-field approximation (MFA) provides an initial understanding of the equilibrium behavior of the model and is exact for the fully connected graph as $N \to \infty$. There exist different ways to carry out the approximation, yielding identical results. This section, along with Chapter 6, adopts the Weiss molecular field theory approach (71) (the Bragg-Williams derivation can be found in (54)), focusing on a single agent a, with state $\bar{s}_a$ and $k_i \equiv z$ neighbors in a network with a uniform degree distribution $P(k) = z$. One foundational assumption of mean-field theory is to argue that the chosen agent's is representative, hence its expected value must be identical to the magnetization, thus establishing a self-consistency condition $m = \langle s_a \rangle$.

We define the monoparticular hamiltonian $\bar{s}_a$:

$$h = \frac{H}{z} = -\frac{J}{z^2} \sum_{i \neq j}^{N} \bar{s_i} \bar{s_j} = -J(\frac{1}{z} \sum_{i}^{N} \bar{s_i}) \cdot (\frac{1}{z} \sum_{j}^{N} \bar{s_j}), \tag{2.1}$$

$$h_{\bar{s}_a} = -\bar{s}_a \cdot J(\frac{1}{z}\sum_j^N s_{j_m}, \frac{1}{z}\sum_j^N s_{j_{n_0}}) \tag{2.2}$$

where the sum extends over agent a neighbors. If we decompose the neighbors spins into their mean value and fluctuations, $s_j = m + (s_j - m)$, and then we set the fluctuations to zero, $(s_j - m) = (s_j - \langle s_j \rangle) \to 0$, the hamiltonian reads:

$$h_{\bar{s}_a} = -\frac{J}{N}\bar{s}_a(m, \alpha n_0) = -\bar{s}_a \bar{m}. \tag{2.3}$$

The mean-field analysis allows for the study of the system's equilibrium properties. We explore zero-temperature dynamics by analyzing the order-parameter fluxes within in the Metropolis dynamics, while finite-temperature behavior is investigated through Monte Carlo simulations employing both Metropolis and Glauber algorithms.

2.2

The Mean-field solution

The computation of the order parameters' expected values via the canonical ensemble yields the following system of self-consistent equations (SCE):

$$m = \frac{2e^{\beta z \alpha^2 (n-1)} \sinh(\beta z m)}{1 + 2e^{\beta z \alpha^2 (n-1)} \cosh(\beta z m)}, \tag{2.4}$$

$$n = \frac{2e^{\beta z \alpha^2 (n-1)} \cosh(\beta z m)}{1 + 2e^{\beta z \alpha^2 (n-1)} \cosh(\beta z m)}, \tag{2.5}$$

where $n = 1 - n_0$ and $J = 1$. By expanding them for small m, we find a line of continuous transitions between the disordered phase and the polarized phase, at an inverse critical temperature $\beta_c(\alpha)$ given by

$$\alpha^2 = \frac{1}{\beta_c(\alpha) z - 1} \ln\left[2(\beta_c(\alpha) z - 1)\right] . \tag{2.6}$$

In particular, we have $\beta_c(0)^{-1} = 2z/3$, which is below the critical temperature $T_c = z$ of the Ising model in the mean-field approximation. This is because, even if at $\alpha = 0$ the neutral state does not contribute to the energy, it brings an additional entropy that destabilizes the polarized phase. The line of critical points, shown in Fig. 2.1, ends at a tricritical point $(\alpha_{tc}, \beta_{tc})$ determined by the condition

$$\ln[2(\beta_{tc} z - 1)] = \frac{3 - \beta_{tc} z}{2} \tag{2.7}$$

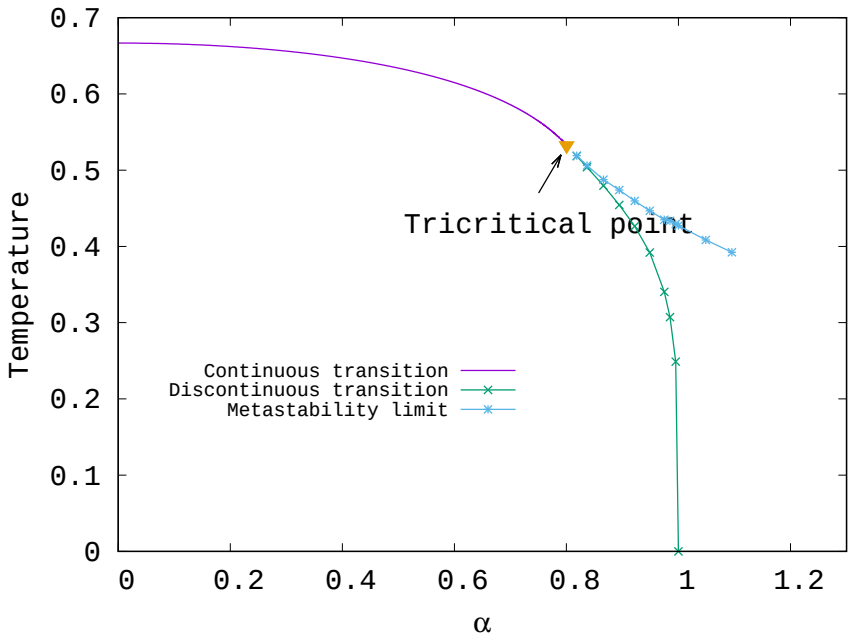

Figure 2.1: Mean-field phase diagram. The line of continuous transitions $T = \beta_c(\alpha)^{-1}$ for $\alpha < \alpha_{tc}$ is given by Eq.(2.6). For $\alpha > \alpha_{tc}$, the points are obtained numerically as explained in the text, the lines being only a guide to the eye.

By solving this numerically we obtain $\beta_{tc}^{-1} = 0.532573$, and substituting this value into Eq.(2.6) gives $\alpha_{tc} = 0.800354$.

For $\alpha > \alpha_{tc}$, the phase diagram displays a line of discontinuous transitions at inverse temperature $\beta_d(\alpha)$, which we locate by finding numerically the values of m, n, β that satisfy simultaneously Eqs.(2.4) and (2.5), together with the condition of equality between the free energies of the ferromagnetic and paramagnetic phases. The resulting phase boundary is shown in Fig. 2.1. Also shown in the figure Figure 2.1 is the limit of metastability of the ferromagnetic phase, namely the value of T above which the SCEs no longer admit a solution with $m \neq 0$.

The equilibrium values $\langle m \rangle$ and $\langle n_0 \rangle = 1 - \langle n \rangle$, obtained by solving numerically Eqs.(2.4) and (2.5), are shown in Fig. 2.2 as a function of temperature. For $\alpha < \alpha_{tc}$, the magnetization vanishes continuously at the critical temperature and is described by the usual mean-field critical and tricritical exponents as $T \to T_c(\alpha)^-$, namely $\langle m \rangle \sim (T_c(\alpha) - T)^{1/2}$ for $\alpha < \alpha_{tc}$ and $\langle m \rangle \sim (T_{tc} - T)^{1/4}$ for $\alpha = \alpha_{tc}$. The fraction of neutral agents $\langle n_0 \rangle$ increases with T up to the critical point $T_c(\alpha)$, then it decreases monotonically towards $\langle n_0 \rangle = 1/3$ in the $T \to \infty$ limit, in which the three states become equiprobable. We note that at $T = T_c(\alpha)$ we have $\langle n_0 \rangle = 1 - T_c(\alpha)$.

For $\alpha_{tc} < \alpha < 1$, $\langle m \rangle$ decreases monotonically with T and jumps to zero at $T = T_d(\alpha)$, while $\langle n_0 \rangle$ has a strongly non-monotonic temperature dependence: starting from $\langle n_0 \rangle = 0$ at $T = 0$, it increases slowly with T, then it jumps to a large value at the discontinuous transition, before decreasing monotonically towards 1/3.

Finally, for $\alpha \geq 1$, we have $\langle m \rangle = 0$ at all temperatures, and $\langle n_0 \rangle$ decreases monotonically with T, starting from $\langle n_0 \rangle = 1$ at $T = 0$, since in the ground state all agents are in the neutral state.

From a social point of view, we see that agents agree on one of the polarized opinions when coupling dominates over temperature, and above the discontinuous transition they have a neutral preference at intermediate levels of upheaval.

The qualitative features of the phase diagram and of the behavior of $\langle m \rangle$ and $\langle n_0 \rangle$ described above will hold in a large class of graphs. In particular, for d-dimensional regular lattices we expect the same qualitative phase diagram when $d \geq 2$ (no finite-temperature phase transition can exist for $d = 1$), with mean-field critical exponents for $d > 4$ and non-mean-field exponents of the Ising universality class for $d = 2, 3$.

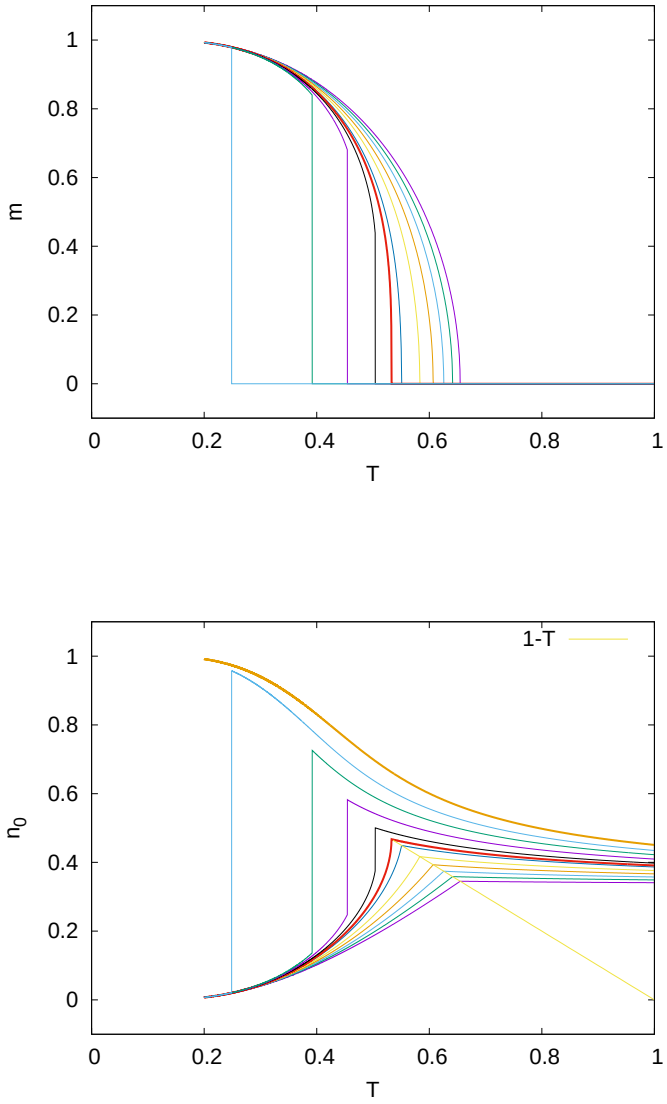

Figure 2.2: Mean-field results for the equilibrium values of the magnetization (a) and the fraction of neutral sites (b), as a function of the temperature and for different values of α. The thick red line corresponds to $\alpha = \alpha_{tc}$, separating the continuous transition from the discontinuous transition. In b) the thick green curve corresponds to $\alpha = 1.2$, and the other curves are as in a).

2.3

Zero-temperature dynamics

Next, we discuss the stochastic dynamics of the model on the FC graph, in which each agent interacts with all other agents. In this case, in order for the Hamiltonian to be extensive (i.e. proportional to N), we must replace in Eq.(1.10) the coupling constant J by J/N. Since the degree is $z = N - 1$, for large N we have $zJ/N = J$, which is equivalent to setting $z = 1$ in the mean-field solution. The Hamiltonian can then be written, up to terms of order $1/N$ and setting again $J = 1$, as

$$H = -\frac{N}{2}(m^2 + \alpha^2 n_0^2)\,. \tag{2.8}$$

The dynamics can then be represented as the evolution of a point (m, n_0) inside the triangle of vertices $(1, 0), (-1, 0), (0, 1)$ shown in Fig. 2.3. We will refer to this as the macrostate of the system, to distinguish it from the microscopic configuration of the N agents.

If we sample the initial configuration of the N agents independently and uniformly at random among the three states, the distribution of the initial macrostate is

$$p(m, n_0) = 3^{-N} \frac{N!}{(Nn_+)!\,(Nn_-)!(Nn_0)!}, \tag{2.9}$$

where $n_\pm = (1 - n_0 \pm m)/2$ is the fraction of agents in the positive and negative state, respectively. For large N, one has $p(m, n_0) \sim \exp[Nf(m, n_0)]$, where $f(m, n_0)$ is a large-deviation function that has a maximum at $m = 0, n_0 = 1/3$, which corresponds to equal fractions of the three opinions and is shown by the red point in Fig. 2.3. The probability of any macrostate different than this point decreases exponentially with N.

It is nevertheless interesting to analyze the fate of the system prepared in an arbitrary macrostate (m, n_0), even if exponentially rare, as it might be relevant from a social viewpoint. At zero temperature, with both the Glauber and the Metropolis dynamics the system can only evolve from any given configuration by moves that do not increase H. In the following we will focus on the Metropolis dynamics, in which an elementary move consists in choosing an agent at random and proposing to change its state with probability $1/2$ to either of the two states different from the current one, and accepting the proposal if the energy change ΔH is negative or zero, in which case a new macrostate $(m', n_0') = (m + \Delta m, n_0 + \Delta n_0)$ is reached.

Since there are two possible proposals starting from each of the three opinion states, there are six possible moves, except at the edges of the triangle where

some transitions are forbidden, and at the vertices where they are all forbidden. The six moves are listed in Table 2.1 together with their proposal probability w_r ($r = 1, \ldots, 6$), the displacement vector $(\Delta m^r, \Delta n_0^r)$ multiplied by N, and the energy change ΔH_r (up to terms of order $1/N$) upon accepting the move r. For example, move $r = 1$ consists in picking at random an agent i that is currently in the state $\sigma_i = -1$ and proposing to change its state to $\sigma_i = +1$. The probability to propose this move is $n_-/2$ (since the fraction of agents with $\sigma_i = -1$ is n_- and we can choose to go to $\sigma_i = 1$ or 0 with probability 1/2). The total magnetization changes by $+2$, the number of neutral sites remains unchanged, and the energy changes by $-[(M+2)^2 - M^2]/(2N) = -(2m + 2/N)$.

All macrostates are unstable with respect to downhill moves (i.e. moves with $\Delta H_r < 0$) except the vertices of the triangle, which are absorbing states. The lines $m = \pm\alpha^2 n_0$ are the separatrices of the basins of attractions of the absorbing states, as they discriminate between different sets of allowed moves. In fact, for $m > 0$ (the case $m < 0$ follows by symmetry), the only downhill moves are moves 1, 3, and 5 below the separatrix, and moves 1, 3, and 4 above it. This is illustrated in Fig. 2.3.

A full analysis of the master equation associated to the stochastic dynamics would allow to determine the probability to end up in each of the absorbing states for a given initial macrostate, but is beyond the scope of the paper. In Fig. 2.3 we display instead the flux lines corresponding to the average displacement, $(\langle \Delta m \rangle, \langle \Delta n_0 \rangle)$, given by

$$\langle \Delta m \rangle = \sum_{r=1}^{6} w_r \Delta m_r \theta(-\Delta H_r)\,, \tag{2.10}$$

and similarly for $\langle \Delta n_0 \rangle$, where θ is a Heaviside function ensuring that only downwill moves contribute. One can observe that below the separatrices, the average flux flows to the polarized $m = \pm 1$ states, and above the separatices it flows to $n_0 = 1$.

In detail, if $\alpha < 1$, all the allowed moves from a point below the separatrix (moves 1, 3, and 5 for $m > 0$) displace the point further away from it. Thus all the points below the separatix belong to the basin of attraction of the $m = 1$ absorbing state and have zero probability to flow to $n_0 = 1$. In contrast, a point above the separatrix can move away from the separatrix with probability $n_+/2$ (move 4) or move towards it with total probability n_- (the sum of the probabilities of moves 1 and 3). If $n_0 < 1 - 3m$, the former probability is smaller than the latter, thus the preferred direction is towards the separatrix. Therefore, a starting point in the triangle defined by $m/\alpha^2 < n_0 < 1 - 3m, m > 0$ will have a non-zero probability to end up in the "wrong" absorbing state $m = 1$.

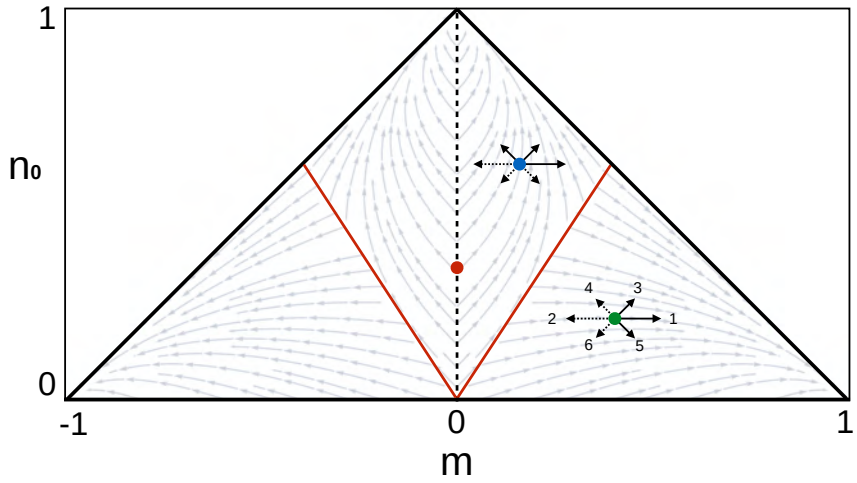

Figure 2.3: Evolution of the Metropolis dynamics on the FC graph. The red lines are the separatrices $m = \pm n_0\alpha^2$ of the three basins of attraction (shown here for $\alpha = 0.8$). The red point shows the equiprobable macrostate $m = 0, n_0 = 1/3$. The solid black arrows represent the allowed moves ($\Delta H \leq 0$) from a macrostate below (green point) and above (blue point) the separatrix for $m > 0$. The dashed arrows represent the forbidden moves ($\Delta H > 0$). The light grey lines show the average direction of the evolution at each point.

However, since there are many more paths towards $n_0 = 1$ than towards $m = 1$, this probability will in fact decrease exponentially with N.

We verified the above predictions by performing repeated MC simulations with the Metropolis dynamics at $T = 0$ and estimating, for every possible initial macrostate, the probability to reach each of the three aborbing states. In Fig. 2.4 (left column) we display our results for $\alpha = 0.8$. Indeed, points below the separatrices end up in the $m = \pm 1$ absorbing states, while above the separatrices we observe regions of "mixed fate" points, which we define as those with a probability larger than 1.5% to end up in a state different than their "natural" absorbing state (for example, points displayed in green can end up in $m = 1$ instead of $n_0 = 1$). The width of the mixed fate regions decreases with N, approximately as

r	Transition	w_r	$N(\Delta m^r, \Delta n_0^r)$	ΔH_r
1	$- \longrightarrow +$	$n_-/2$	$(2, 0)$	$-2m$
2	$+ \longrightarrow -$	$n_+/2$	$(-2, 0)$	$2m$
3	$- \longrightarrow 0$	$n_-/2$	$(1, 1)$	$-m - \alpha^2 n_0$
4	$+ \longrightarrow 0$	$n_+/2$	$(-1, 1)$	$m - \alpha^2 n_0$
5	$0 \longrightarrow +$	$n_0/2$	$(1, -1)$	$-m + \alpha^2 n_0$
6	$0 \longrightarrow -$	$n_0/2$	$(-1, -1)$	$m + \alpha^2 n_0$

Table 2.1: Allowed transitions for the Metropolis algorithm. The second column shows the transition between two spin values. w_r is the probability of proposing the transition, $N\Delta m^r$, $N\Delta n_0^r$, ΔH_r are the changes in total magnetization, number of neutral spins, and Hamiltonian upon executing the transition r.

$1/N$ as implied by the previous argument. We also verified that the probability of a point above the separatrix to end up in $m = 1$ decreases exponentially with its distance from the separatrix (not shown).

An analogous analysis for the Glauber dynamics shows that, since there are fewer allowed downhill moves, the probability to cross the separatrix is even smaller and thus the mixed-fate region is thinner, as confirmed numerically in Fig. 2.4 (right column).

It is also interesting to observe that a deterministic downhill dynamics that follows the direction opposite to the gradient of H, $-\nabla H = N(m, \alpha^2 n_0)$, also has the same separatrices.

From a social perspective, the above results show that for $\alpha < 1$, when we start from equiprobable opinions ($m = 0, n_0 = 1/3$), the population evolves towards neutrality ($n_0 = 1$), despite the optimal configurations are the polarized states. As we show below, social agitation is necessary in order to overcome the energy barrier and reach optimality.

2.4

Finite-temperature dynamics

We performed MC simulations at $T > 0$ with the Glauber dynamics with $N = 500$ agents, again starting from a random configuration. When $\alpha < \alpha_{tc}$ or $\alpha > 1$, the system is able to equilibrate at all temperatures $T > 0.1$ in less than 10^3 Monte Carlo steps (MCS), where 1 MCS = N elementary moves. Our MC estimates for

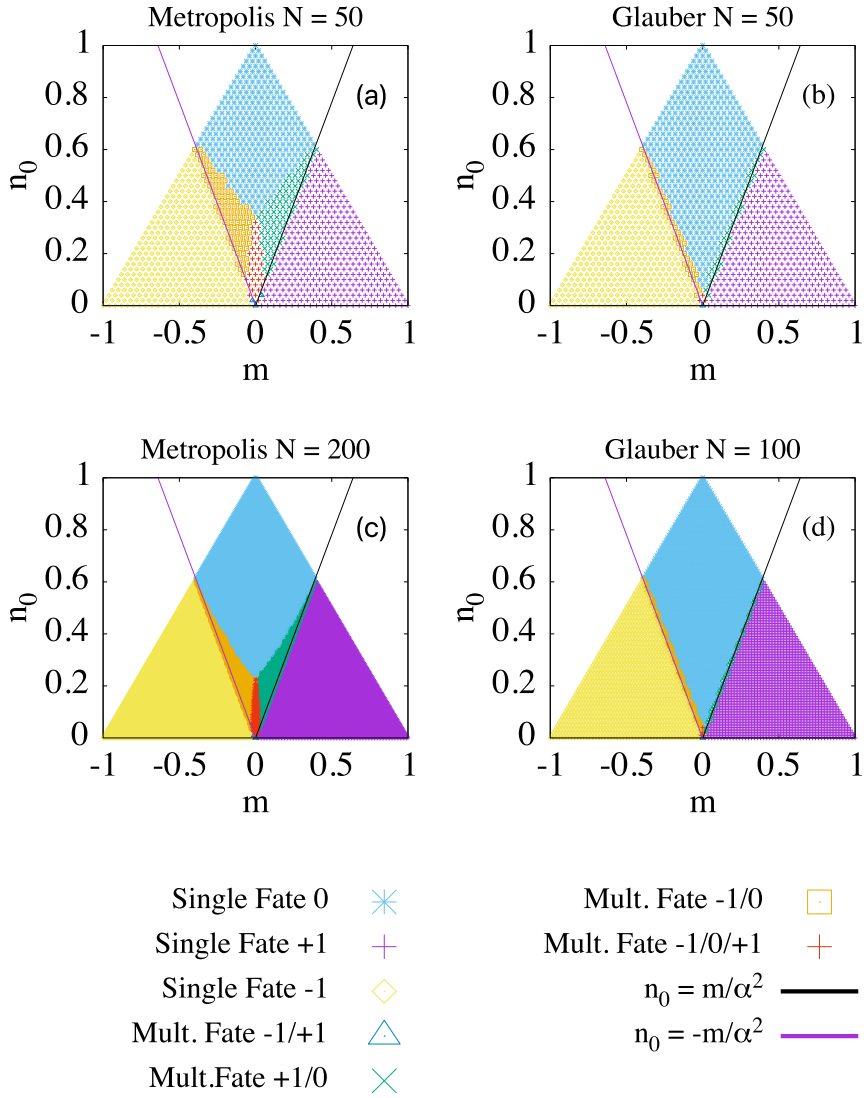

Figure 2.4: Basins of attraction at $T = 0$ and $\alpha = 0.8$ on the FC graph. (a) $N = 50$, Metropolis dynamics; (b) $N = 50$, Glauber dynamics; (c) $N = 200$, Metropolis dynamics; (d) $N = 100$, Glauber dynamics. The lines are separatrices. Symbols at each point indicate the fate of the system starting from that point. Results are obtained with 1000 MC runs for each point above the separatrix, and 40 for each point below it.

$\langle m \rangle$ and $\langle n_0 \rangle$ agree with the exact mean-field results displayed in Fig. 2.2, with negligible finite-size effects.

For $\alpha_{tc} < \alpha < 1$, at temperatures below the phase boundary (see Fig. 2.1), we expect metastability effects due to the discontinuous transition: starting from a random configuration, the system gets trapped in a region of the configuration space with $m \simeq 0$ for a time that diverges exponentially with N and with $1/T$.

This is confirmed by inspecting the probability distribution of the magnetization obtained from many MC runs, shown in Fig. 2.5. The right column shows results for $\alpha = 0.9$, which is well into the discontinuous region and for which the transition temperature is $T_d = 0.47$. We see that for $T = 0.4$, after 10^3 MCS the distribution is bimodal, with one peak at the mean-field equilibrium magnetization $\langle m \rangle = 0.83$, and the other near $m = 0$, corresponding to runs stuck in the metastable state. After 10^6 MCS, the system is able to overcome the free energy barrier and the peak at $m = 0$ disappears. In contrast, for $T \leq 0.3$ even after 10^6 MCS the distribution remains peaked around $m = 0$, while the equilibrium value is close to $m = 1$. This shows that almost all agents remain in the neutral state (similarly to the $T = 0$ case analyzed in the subsection 2.3), and social agitation is not enough to overcome the free energy barrier towards polarized consensus.

This contrasts with the results for $\alpha = 0.75$, shown in the left column of Fig. 2.5, at which the continuous transition takes place at $T_c = 0.56$. We now see that for $T \geq 0.3$, already after 10^3 MCS the distribution is peaked around the mean-field equilibrium value ($\langle m \rangle = 0.95, 0.85, 0.63$ for $T = 0.3, 0.4, 0.5$ respectively), which shows that in this case thermal fluctuations are able to bring the system towards consensus. On the other hand, for $T = 0.1$ there is only a small peak near the equilibrium value $\langle m \rangle \simeq 1$, and a large peak at $m \simeq 0$, which hardly changes from 10^3 to 10^6 MCS. At such low temperature, the system remains in a metastable configuration because the probability to flip a polarized agent surrounded by agents of opposite sign is exponentially small.

2.5

Conclusions

At high temperatures, the agents do not feel the influence of their peers and evolve quickly towards a disordered state, that can be interpreted as social unrest. At low temperature, for $\alpha > 1$ the system reaches a configuration dominated by neutral agents on all networks, while for $\alpha < 1$ we observe different behaviors depending on the network type, and on the value of α, as we summarize below.

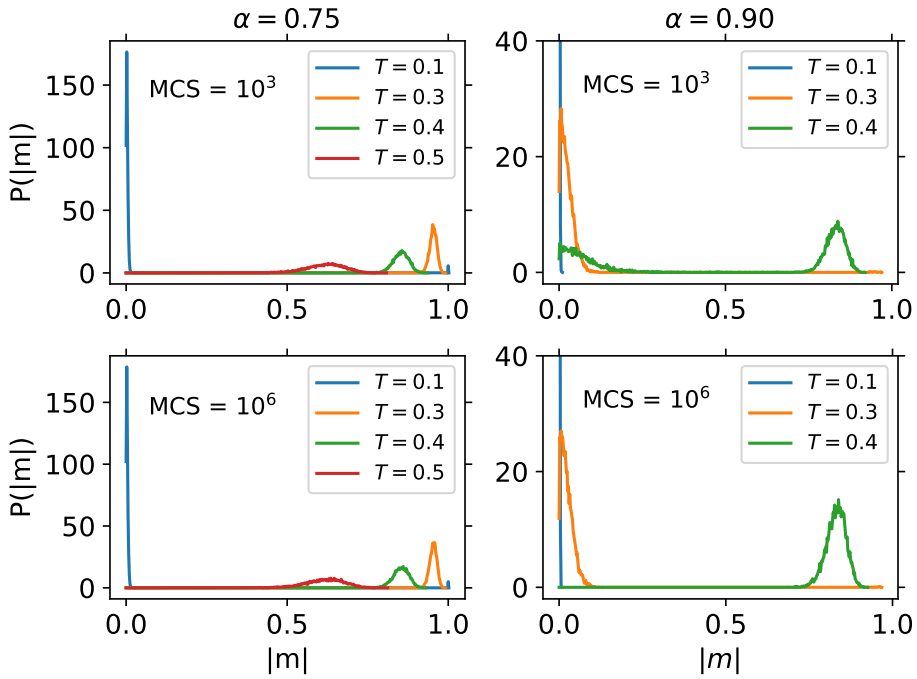

Figure 2.5: Probability distribution of the magnetization for two values of α below (left) and above (right) the tricritical point for different temperatures obtained with Glauber MC simulations with $N = 500$ agents and 10^4 repetitions. The first row show results for a computational time of 10^3 MCS and the second row for 10^6 MCS.

The equilibrium phase diagram of the model exhibits a phase boundary for $\alpha < 1$ between a low-temperature phase, in which one of the polarized opinions prevail, and the high temperature disordered phase. At temperatures just above the transition, we observe a majority of neutral agents and equal-sized minorities of extremists of both signs. Upon crossing the phase boundary by decreasing the temperature, the fraction of polarized agents increases continuously from zero when α is below the tricritical value α_{tc}, while it jumps discontinuously to a non-zero value when $\alpha_{tc} < \alpha < 1$. We also found that in the absence of social agitation, starting from a random configuration, the population is exponentially more likely to get stuck in neutral consensus than to reach the optimal polarized consensus. Moderate social agitation allows the system to reach polarized consensus for $\alpha < \alpha_{tc}$, while for $\alpha < \alpha_{tc} < 1$ the barriers to achieve equilibrium are much higher due to metastability.

It is interesting to compare our results with those of other three-state models. Vazquez and Redner (164) studied a kinetic model in which pairs of agents interact stochastically. Their model exhibits the same three absorbing states, but the largest basin of attraction is that of an absorbing boundary on the bottom line of the triangle (see Fig.2.3), representing frozen mixtures of oppositely polarized agents. A large bipolarized region was also found by Balenzuela et al.(10), who proposed a kinetic model in which agents hold a continuous spectrum of convictions, which is partitioned in three states according to some thresholds. The pair interaction is such that oppositely polarized agents tends to increase their polarization, leading to a phase transition from a neutral to either a bipolarized or a polarized population. Svenkeson and Swami (158) considered a pair dynamics, in which polarized agents can become neutral and viceversa, with a temperature coupled to the instantaneous magnetization. They find a transition of the Ising type without a tricritical point.

CHAPTER 3

Erdös-Rényi Networks

In this Chapter we embed the model on Erdös-Rényi (ER) random graphs with different mean degrees. We apply the annealed mean-field approximations and use Monte-Carlo simulations to examine the changes in critical temperature in comparison with the fully connected graph, and we study the metastable states at zero temperature.

3.1

Introduction

Although the Erdös-Rényi (ER) random graph ensemble is not representative of real-world structures, it is frequently used as a baseline model to study complex networks (120), providing insightful results into how phenomena such as consensus or polarization may develop in such topologically simplified settings.

Sood and Redner applied the voter model to ER graphs and highlighted the role of fluctuations in reaching consensus, demonstrating that the consensus time scales logarithmically with system size in dense graphs [(150)].

Xie et al. explored the effects of zealotry in an Ising-like system on ER graphs, comparing the results with those obtained for the complete graph. They found that a larger number of "zealots" is necessary to cause a drop in the consensus time is longer for sparser networks. However, once this threshold is reached, the average time to achieve consensus decreases with the average degree [(175)].

Benjamini et al. study the basins of attraction of the majority voter model (Section 1.3) in ER graphs with random initial conditions and found that the

state with the initial majority gets global consensus when the average degree is sufficiently large [(16)].

For random graphs, the mean-field approximation is not exact and various other theoretical approaches have been developed to study the equilibrium properties of spin models. For the Ising model, it was found, using the replica method, that if the degree distribution falls off as $k^{-\gamma}$ for large k with $\gamma > 5$ (which includes the case of random-regular and ER graphs), a continuous transition with mean-field exponents takes place. On the other hand, for $\gamma \leq 5$ different scenarios depending on γ are observed [(99)]. In the Blume-Capel model, a tricritical point was found using an annealed mean-field approximation (see Section 3.2) [(39)].

3.2

Annealed mean-field approximation

In the case of non-uniform degrees k_i, in principle one could solve numerically the $2N$ local SCEs. Alternatively, one can make the additional approximation consisting in treating the graph in an "annealed' fashion, by replacing the adjacency matrix $\epsilon_{i,j}$ (which is one if i, j are connected and zero otherwise) by $k_i k_j / zN$, where $z = \langle k_i \rangle$ (18; 43). If we introduce the weighted order parameters

$$m_w = \frac{1}{zN} \sum_j k_j m_j, \quad n_w = \frac{1}{zN} \sum_j k_j n_j, \tag{3.1}$$

we have

$$\sum_{j \in V(i)} m_j = \sum_{j \neq i} \epsilon_{i,j} m_j = \frac{1}{zN} \sum_{j \neq i} k_i k_j m_j = k_i m_w, \tag{3.2}$$

and similarly $\sum_{j \in V(i)} n_j = k_i n_w$. Multiplying the local SCEs by $k_i/(zN)$ and summing over i we thus obtain two SCEs for the weighted order parameters

$$m_w = \frac{1}{zN} \sum_i k_i \frac{2e^{\beta\alpha^2 k_i (n_w - 1)} \sinh(\beta k_i m_w)}{1 + 2e^{\beta\alpha^2 k_i (n_w - 1)} \cosh(\beta k_i m_w)}, \tag{3.3}$$

$$n_w = \frac{1}{zN} \sum_i k_i \frac{2e^{\beta\alpha^2 k_i (n_w - 1)} \cosh(\beta k_i m_w)}{1 + 2e^{\beta\alpha^2 k_i (n_w - 1)} \cosh(\beta k_i m_w)} \tag{3.4}$$

For large N we can replace the sum over i with a sum over all possible degrees,

$$m_w = \frac{1}{z} \sum_k k P(k) \frac{2e^{\beta\alpha^2 k (n_w - 1)} \sinh(\beta k m_w)}{1 + 2e^{\beta\alpha^2 k (n_w - 1)} \cosh(\beta k m_w)}, \tag{3.5}$$

$$n_w = \frac{1}{z} \sum_k k P(k) \frac{2e^{\beta\alpha^2 k (n_w - 1)} \cosh(\beta k m_w)}{1 + 2e^{\beta\alpha^2 k (n_w - 1)} \cosh(\beta k m_w)}. \tag{3.6}$$

Finally, after solving the above equations we can obtain the average order parameters as

$$m = \frac{1}{N}\sum_i m_i = \sum_k P(k)\frac{2e^{\beta\alpha^2 k(n_w-1)}\sinh(\beta k m_w)}{1+2e^{\beta\alpha^2 k(n_w-1)}\cosh(\beta k m_w)}, \tag{3.7}$$

$$n = \frac{1}{N}\sum_i n_i = \sum_k P(k)\frac{2e^{\beta\alpha^2 k(n_w-1)}\cosh(\beta k m_w)}{1+2e^{\beta\alpha^2 k(n_w-1)}\cosh(\beta k m_w)}., \tag{3.8}$$

3.3

Phase transition

In this case, one also expects a tricritical point separating a line of continuous transitions for low α from a line of discontinuous transitions at large α, as in the Blume-Capel model on ER graphs [(100)]. We determined the location of the continuous transition by solving numerically the SCEs using a Broyden first Jacobian approximation from the optimize root of SciPy. Fig. 3.1 shows the comparison between the numerical solution and MC simulations for $\alpha = 0$ and 0.4. For low connectivity (panel (a)), we find a significant discrepancy between the annealed approximation and the simulations, while for high connectivity (panel (b)) we obtain a better agreement.

Fig. 3.2 shows that the critical temperature, normalized by z, converges asymptotically for large z to that of the FC graph. The critical temperature decreases with α for any $\langle k\rangle$, as in the mean-field solution.

The presumed tricritical point and the discontinuous transition can, in principle, be located from a Taylor expansion in m of the annealed SCEs. We have not attempted this, and note that it is a more complicated task than in the Blume-Capel model (100), in which the SCE m decouples from n.

3.4

Zero-temperature dynamics

We performed MC simulations with the Metropolis and Glauber dynamics at $T = 0$. starting from a random configuration as in the FC graph. We consider graphs with only one connected component, created by generating ER graphs with the Python *networkx* library and then randomly adding and/or subtracting agents and links until the desired N and $z = \langle k\rangle$ are reached, preserving the degree distribution of the original graph.

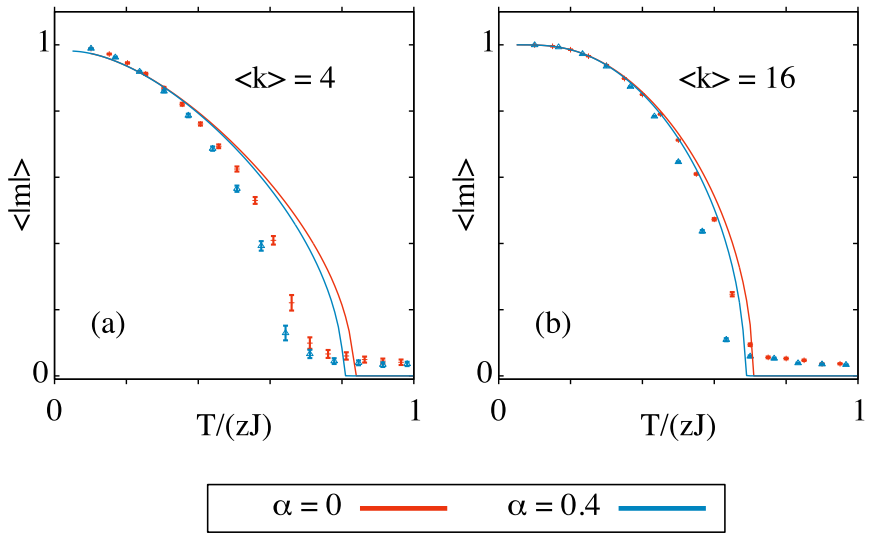

Figure 3.1: Magnetization vs. temperature on ER graphs of average degree $z = 4$ (a) and $z = 16$ (b) for $\alpha = 0$ and $\alpha = 0.4$. The lines corresponds to the numerical solution in the annealed approximation, while the bars are the results of MC simulations with 10^4 MCS, averaged on 100 realizations of different ER graphs with $N = 1000$ agents.

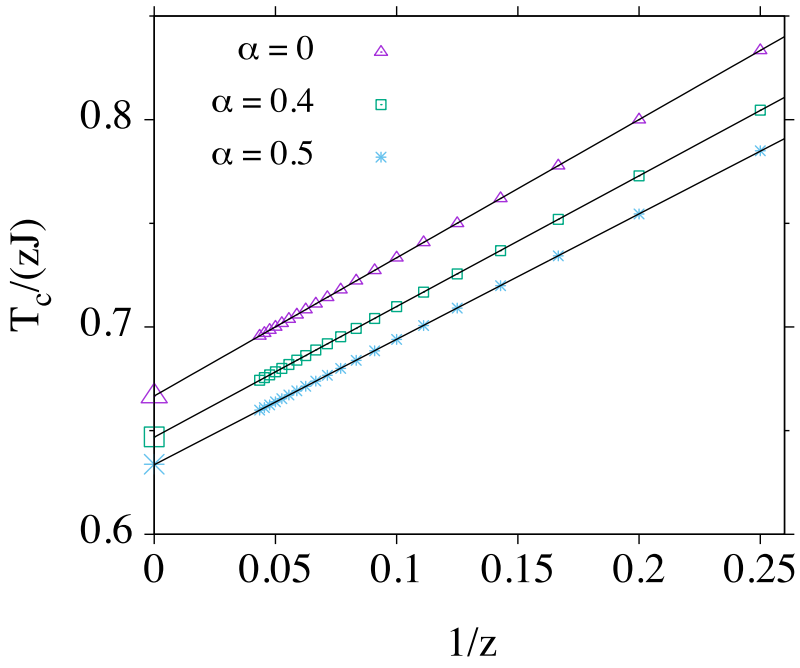

Figure 3.2: Critical temperature vs. $1/z$ for different values of α, calculated by solving numerically the system of equations (3.7), (3.8). Mean-field results are represented by bigger points at $z \to \infty$.

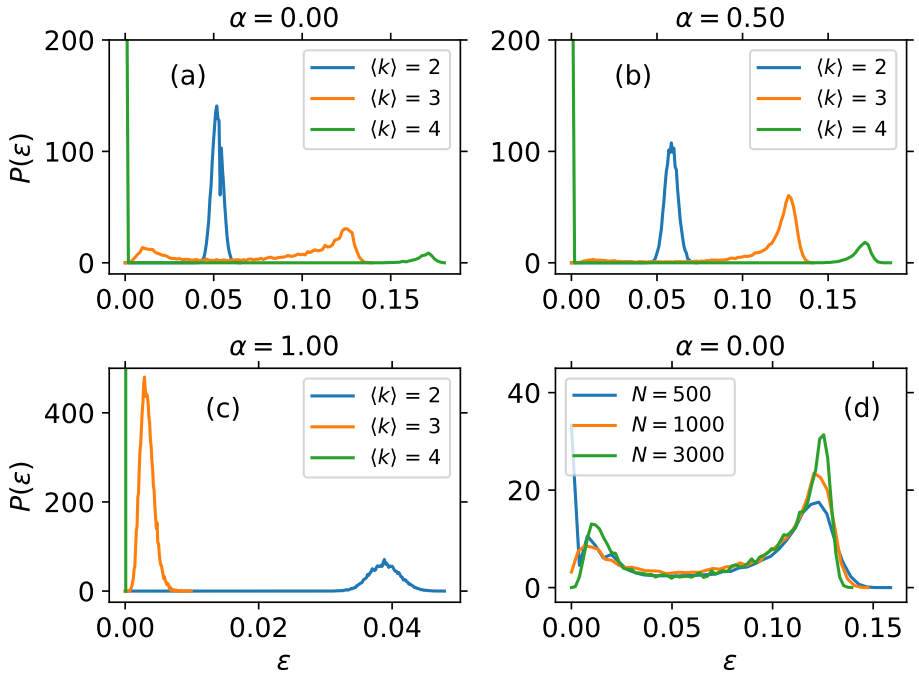

Figure 3.3: Probability distribution function of the residual energy ϵ, for the steady state reached through Glauber dynamics on a ER graph with $N = 3000$ and $z = \langle k \rangle = 2, 3, 4$ for (a) $\alpha = 0$, (b) $\alpha = 0.5$, and (c) $\alpha = 1$. (d) Comparison of the probability distribution function for $\langle k \rangle = 3$ and different values of N. Data are obtained from 10^5 different random initial conditions on a single realization of the network for $N = 500$ and $2 \cdot 10^4$ different random initial conditions for $N = 1000, 3000$.

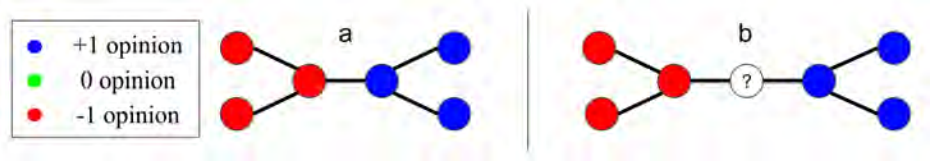

Figure 3.4: Example of subgraphs with a stuck spin configuration, despite not being compatible with the ground state.

We perform many runs for each graph, letting the system relax until it reaches a steady state in which the energy no longer changes. In this way we collect the probability distribution $P(\epsilon)$ of the residual energy, defined as the normalized difference between the energy of the steady state reached in a given run and the ground-state energy of the graph, $\epsilon = (E_{steady} - E_0)/Nz$. Fig. 3.3 shows the results obtained with the Glauber dynamics for $z \leq 4$ and different values of α. For $z = 2$, in all cases $P(\epsilon)$ has a single peak at $\epsilon > 0$, indicating that the system never reaches the ground state as it gets stuck in a manifold of excited isoenergetic configurations, the energy of which changes from run to run. The same behavior persists for $\alpha > 1$ (see Appendix E for $N = 500$).

A similar behavior has been observed before for the Ising model (9), and Häggström (123) showed rigorously that it stems from the existence of an extensive number of subgraphs in which some nodes are frozen (i.e. they cannot change state without increasing the energy) in an excited configuration. In addition, some nodes are *blinkers*, namely they can change state forever without changing the energy, thus the system gets trapped in a manifold of configurations at constant energy above the ground state. As an illustration, the two central nodes of Fig. 3.4-a) are frozen, while the middle node in Fig. 3.4-b) is a blinker.

For $z = 3$, there are fewer dynamical traps, as the number of frozen nodes and blinkers decreases upon increasing z. As shown in Fig.3.3, in this case upon increasing α the distribution is first bimodal with both peaks at $\epsilon > 0$ for $\alpha \leq 0.75$ (the ground state is never reached), then the peak closer to $\epsilon = 0$ disappears for $0.85 \leq \alpha \leq 0.95$, and finally it becomes unimodal with a finite weigth at $\epsilon = 0$ for $\alpha > 1$ (see Appendix E). Note that these dynamical traps are not a finite-size effect: as shown in Fig. 3.3d) for $z = 3$ and $\alpha = 0$, the peak near $\epsilon = 0$ decreases with the system size, and the one at larger ϵ grows.

For $z = 4$, we observe a large probability $P(0)$ to reach the ground state for all values of α. For $\alpha < 1$ there is still a peak at $\epsilon > 0$, which is largest for $0.85 \leq \alpha \leq 0.95$, but significantly smaller than that for $z = 3$. It is an interesing question whether the increase of the trapping probability in a range before $\alpha = 1$

is related to the possible discontinuous nature of the phase transition between the polarized and disordered phases.

Finally, we observed that the Metropolis dynamics gives very similar results to the ones just discussed. A comparison between the two dynamics for several values of α, z and N is shown [(54)].

These results show that the relaxational $T = 0$ dynamics on ER graphs, is quite different from the FC case in which, as shown in Chapter 2, for large N the system prepared in a random configuration always reaches the ground state if $\alpha > 1$ (namely the absorbing state $n_0 = 1$), and never reaches it if $\alpha < 1$. In ER graphs, instead, except for small values of z, the system is able to reach the ground state for all α.

3.5

Conclusions

ER random graphs, which are somewhat closer to a real population where agents have a finite number of contacts, exhibit a finite-temperature transition to a polarized phase that mirrors the behavior seen in the FC graph. This indicates that despite the randomness of connections, some properties presented in the complete graph remain preserved.

However, differences dependent on the connectivity pattern arise in the dynamical process. For graphs with a high average degree, our simulations show that the system achieves the polarized instead of the neutral state consensus when starting from a random configuration at low temperatures. For graphs with lower connectivity, the system gets stuck in dynamical traps due to the presence of frozen nodes, locked in states that do not change, impeding the system's progression to the ground state. We find that the residual energy distribution shows different characteristics based on the average degree and the value of the neutrality parameter α. These findings have significant implications for understanding the dynamics of opinion formation and consensus in social networks, where connectivity can vary widely. The insights gained from the ER graphs can help designing strategies to mitigate the effects of structural traps and enhance consensus formation.

In summary, the results on ER random graphs extend the understanding of the model, shedding light on how network topology influences collective phenomena.

CHAPTER 4

Modular Networks

In Chapter 4, we apply the model to networks characterized by a well-defined community structure. We start with a synthetic benchmark choosing one and two levels of community structure and conclude with an embedding in Twitter networks (55). We find that the opinion groups identified across different values of the neutrality parameter, α, help reveal the community structure within these networks at different resolutions.

4.1

Introduction

Many complex networks, and social networks in particular, have been shown to have a clear community (modular) structure (59). Community detection has been intensely studied, and many different methods have been suggested (35). At the same time, benchmarks for testing the efficiency of these methods have also appeared in the literature. For instance, in a system of coupled oscillators, modular structures corresponding to well-defined communities of nodes, ordered in a hierarchical way, emerge at different time scales during the synchronization process (6).

Our purpose now is to assess the role of community structure in the opinion dynamics of our model. In the limit of low temperatures, the homophilic term that drives the agents to agree with their neighbors is expected to dominate over the social agitation. Therefore, we put the focus on the achievement of a polarized or a neutral consensus, or on the contrary the arising of bipartidism or tripartidism at low levels of temperature. We explore the outcomes for different levels of the neutrality parameter α.

Models based on magnetic-like interactions, as the Ising or the Potts model, have been used previously for community detection (149; 28; 101; 180). In our case, it turns out that the correlations of the final opinion state of the nodes are sensitive to the value of α. Actually, for small α, only the smaller clusters arrive to local consensus; however, larger values of α enable consensus in a larger scale. We can take advantage of this feature and reveal the different levels of structure by tuning the parameter α, like other multiresolution methods (7) have done before. In this way, we can study at the same time the opinion dynamics on a particular network and learn about its community structure.

In practice, we define a matrix $\hat{C}_{ij}$, where each element represents the number of times nodes i and j conclude a Metropolis Monte Carlo (MMC) simulation with identical opinions. We run a large number of simulations N_{reps} and normalize this correlation value as $C_{ij} = \hat{C}_{ij}/N_{reps}$. Given that our Hamiltonian, as specified in equation (1.10), only contains positive interactions among nodes (i.e., it lacks a repulsive term which could lead to divergent opinions among neighboring nodes at lower temperatures), we expect a correlation value of $C_{ij} = 0$ for node pairs belonging to separated, well-defined communities. In order to compare graphs with different average connectivity $\langle k \rangle = z$ in a meaningful way, we always consider the rescaled reduced temperatures $T^* = T/z$. For a description of the algorithms we use to find the correlation between nodes and to identify the community structure of the networks see Appendix A .

4.2

Girvan-Newman

One of the most commonly used benchmarks for community detection was the one proposed by Newman and Girvan (119). There, the authors construct a set of networks with different community structures, as explained in detail in Section 1.2 . Each network has 128 nodes divided into four communities of 32 nodes each. In the original model, links are established independently at random between nodes with probability p_{in} if both nodes belong to the same community and p_{out} otherwise, with $z = 16$. Here, we work with a slightly different version in which we fix the number of links a node has to nodes in the same community, k_{in}, and to other communities, $k_{out} = 16 - k_{in}$. In this way, we can tune the relevance of the community structure, which is evaluated in terms of modularity (see Figure 4.1)).

In Figure 4.2 (a), we can see the average of the absolute value of the magnetization as a function of the number of intra-community links at a very low

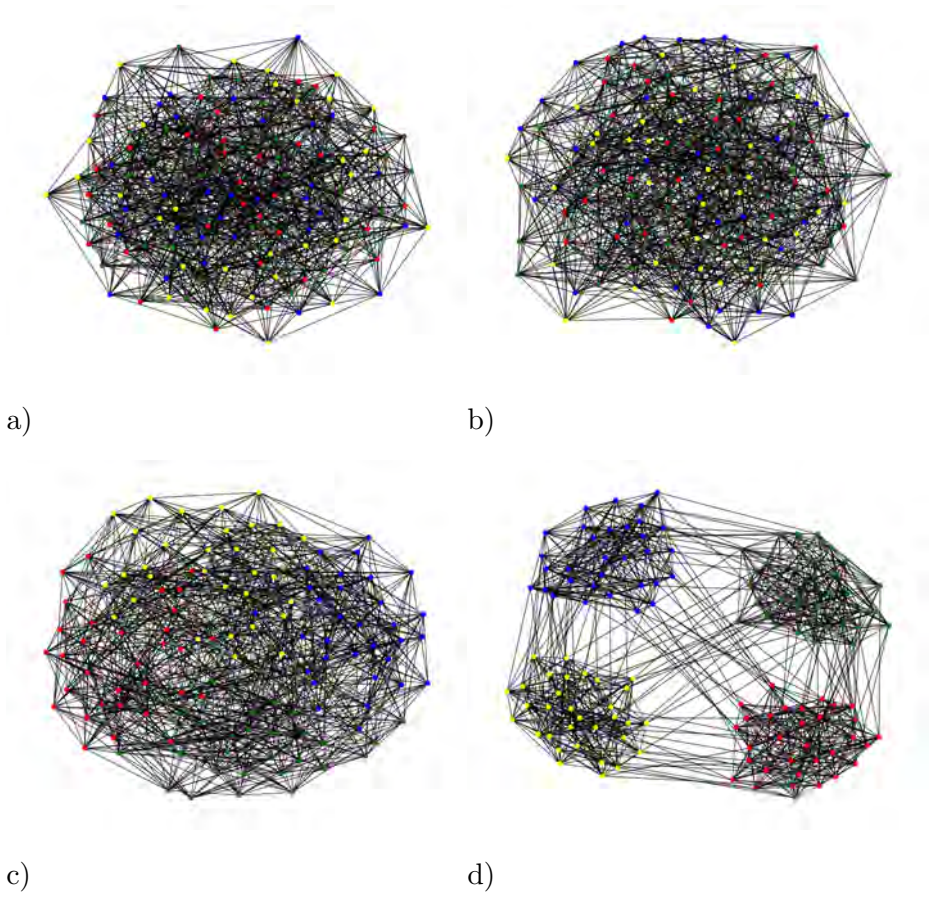

Figure 4.1: (**a**) $k_{\text{out}} = 1$, all links distributed at random; (**b**) $k_{\text{out}} = 6$, communities are still not well-defined; (**c**) $k_{\text{out}} = 9$, it is possible to distinguish communities. (**d**) $k_{\text{out}} = 14$, community structure is clear. Colors are assigned to different communities to distinguish them and do not represent opinion states in this case.

temperature for different values of α. The green line corresponds to the modularity of the best partition. There is a clear change in behavior around $k_{in} = 8$ that can be understood by examining the probability of acceptance for a given flip proposal in the dynamics. In particular, if we consider two communities of agents, each holding +1 and -1 opinion, respectively, we have that, for $\alpha = 0$, the probability of an agent in the positive community accepts to change their opinion to state $\sigma_i = -1$ (in two steps, i.e., passing through the neutral opinion) is equal to $P_{acc} = \min\left[\exp((16 - 2 \cdot k_{in})/T^*), 1\right]$, where k_{in} denotes the number of intra-community links. Therefore, when $k_{in} \leq 8$, we have $P_{acc} = 1\ \forall T$.

For low values of α, these networks are not able to achieve global consensus when the number of intra-community links exceeds 8 (however, the modules reach internal consensus in all cases; see Figure 4.3(a)). When $\alpha = 0.75$, we observe that $\langle |m| \rangle \neq 1$ even for $k_{in} \leq 8$. We speculate that these results are related to a putative first order transition analogous to that of the fully-connected graph (54), which may occur at alpha around the interval $\alpha \in (0.8, 1)$. In this range, the dynamics end up in consensus, but this consensus occurs in a polarized opinion for roughly half of the simulations, and in a neutral opinion the other half. For $k_{in} > 8$, we observe a decay in $\langle |m| \rangle$, similar to the one presented for $\alpha = 0$. Finally, for $\alpha \geq 1$, when the neutral consensus becomes an absolute energy minimum, we observe clear preference for the neutral consensus for all k_{in}. Nevertheless, some polarized clusters can appear for $\alpha = 1$, especially for the largest values of intra-community links.

Figure 4.2 (b) shows the average value of the magnetization as a function of temperature for several values of intracommunity links k_{in} and $\alpha = 0$. For values $k_{in} > 8$, we observe a peak which indicates that the greatest majority in a polarized opinion occurs at $T > 0$. As we mentioned above, the different communities arrive at a local consensus in the steady state, but, in general, the modules do not share all the same opinion. Figure 4.2 (c) shows the position of this peak for every value of k_{in}. Above $k_{in} = 8$, the system still reaches $|m| \sim 1$ at a temperature that increases with the number of intra-community links until $k_{in} = 11$; above this value, the maximum value of $\langle |m| \rangle$ starts decreasing.

The case $k_{in} = 15$, with very well-defined communities in the limit of low temperatures, is examined in Figure 4.3. The left panel shows an example of a final configuration for this network at $T^* = 0.1$ and $\alpha = 0.75$. This is just one of the possible final outcomes for this network, in which magnetization and fraction of neutral agents turn out to be $|m| = 0$ and $n_0 = 0.5$, respectively. The right panel shows the possible final values for $|m|$ and n_0 for 30 MMC repetitions, starting from random initial conditions. These results show that the final configurations correspond to situations of consensus within communities but, in general, the system does not reach a global consensus. Notice that neutral communities do

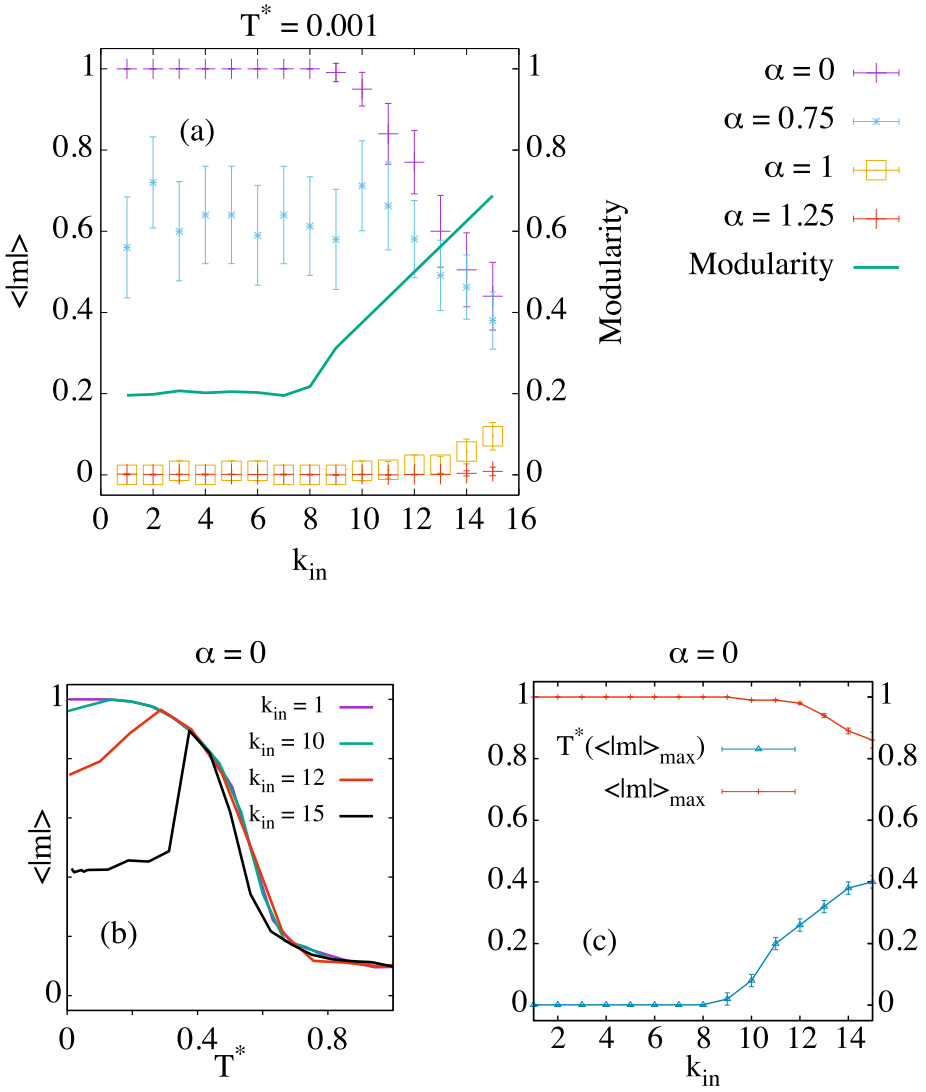

Figure 4.2: (**a**) Absolute value of the magnetization in the stationary state as a function of the number of intracommunity links at $T^* = 0.001$, for different values of α; (**b**) absolute value of the magnetization versus temperature for several values of the number of intracommunity links and $\alpha = 0$ (for clarity, errorbars have been removed); (**c**) position of the magnetization peak as a function of the number of intracommunity links. Results are averaged over 100 simulations, except those for $k_{in} = 15$ in panel (**b**), which are averaged over 500 simulations because of large fluctuations.

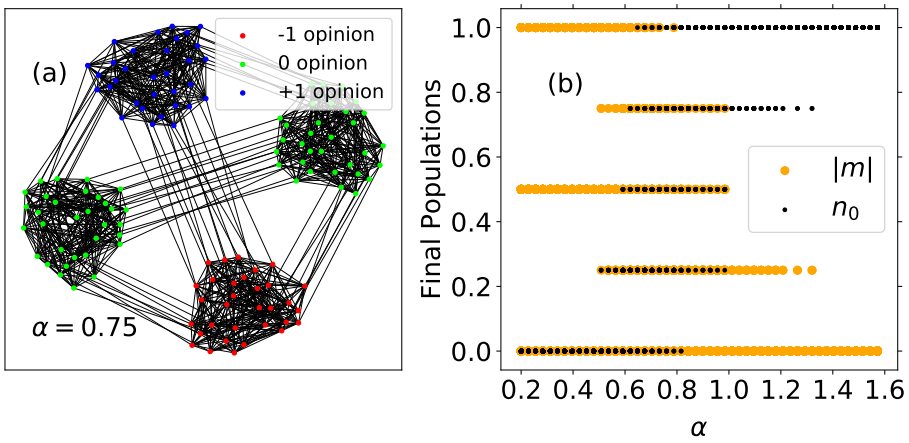

Figure 4.3: (**a**) Example of a stationary configuration for the $k_{in} = 15$ network at $T^* = 0.1$ and $\alpha = 0.75$, corresponding to $m = 0$ and $n_0 = 0.5$; (**b**) final values of $|m|$ (orange dots) and n_0 (black dots) for the $k_{in} = 15$ network at $T^* = 0.1$ versus α. Outcomes of 30 independent simulations with 10^4 MC steps for several values of α between 0.2 and 1.6. A dot is plotted when at least one of the simulations ends up at these values of $|m|$ and n_0.

not have representation for $\alpha \lesssim 0.5$; therefore, in this range, the final n_0 is always 0, and the magnetization can take three possible values:

- $|m| = 0$, corresponding to a system divided into two communities, each one holding a different extremist opinion.
- $|m| = 0.5$ that is obtained when three communities hold the same polarized opinion and the fourth holds the opposite one.
- $|m| = 1$, if by chance the system reaches the global consensus.

When $0.5 \lesssim \alpha \lesssim 1.0$, the number of possible final configurations is larger because they include all combinations with communities in any of the three opinion states. For $\alpha \gtrsim 1$, the contribution of the neutral nodes to the energy becomes larger than the contribution of polarized agents and most often the system reaches neutral consensus, characterized by $|m| = 0$ and $n_0 = 1$. However, in some cases, the magnetization takes the value $|m| = 0.25$ and the fraction of neutral agents is $n_0 = 0.75$, indicating that one extremist community appears in the final state while the other three are neutral. Finally, for values of $\alpha \gtrsim 1.4$, we always obtain neutral consensus as the final macrostate.

4.3

Two-level modular networks

We have also considered synthetic modular networks with a hierarchical community structure formed by more than one cluster level. These networks have been used in previous studies regarding community detection, (6), in this case using the Kuramoto model, as they are specifically constructed to highlight the nodes correlations between the final states of a specific dynamics.

In Figure 4.4, we can see a network with two community levels generated as follows: a set of 256 nodes is divided into 16 clusters that will represent the first community level. The second organizational level of the network is formed by four compartments, each one containing four different clusters of the first level. Here, node colors do not represent opinions but are just to clarify the network topology. The results for $\alpha = 0$ show clearly the first level, corresponding to the smallest subgraphs that appear with correlation $C_{ij} = 1$ in 16x16 boxes in the main diagonal (Figure 4.4 (b)) (We expect that, for $\alpha = 0$, the results would resemble those obtained by using the Ising model). The second level is not so evident, but, when we use $\alpha = 0.75$, we can distinguish it better, as the correlations within the four big compartments are stronger. This property, which is caused by the fact that a higher value of the neutrality parameter increases opinion diffusion, can also be used to detect asymmetries in the link distribution between nodes. For example, in Figure 4.5, we can see a network formed by four compartments which are in turn divided in two subgroups, but connections are not perfectly symmetric, unlike in the case shown in Figure 4.4. In particular, we can see one node, marked with a circle in Figure 4.5 (a) that has more out-community links outside its compartment (on the second level of community structure) than the rest of the vertices. This feature is not visible when we perform simulations with $\alpha = 0$, but it becomes noticeable when we use $\alpha = 0.75$.

4.4

Twitter networks

We started applying the model on well-known topologies that have been used for benchmarking reasons (35). Let us now analyze its behavior when embedded on real social networks. In particular, we study interaction networks of Twitter handles around a given topic, i.e., hashtag. Each vertex in the network represents a Twitter handle and a link represents an interaction (retweet or mention) between two handles in a tweet containing the selected hashtag. Multiple edges and

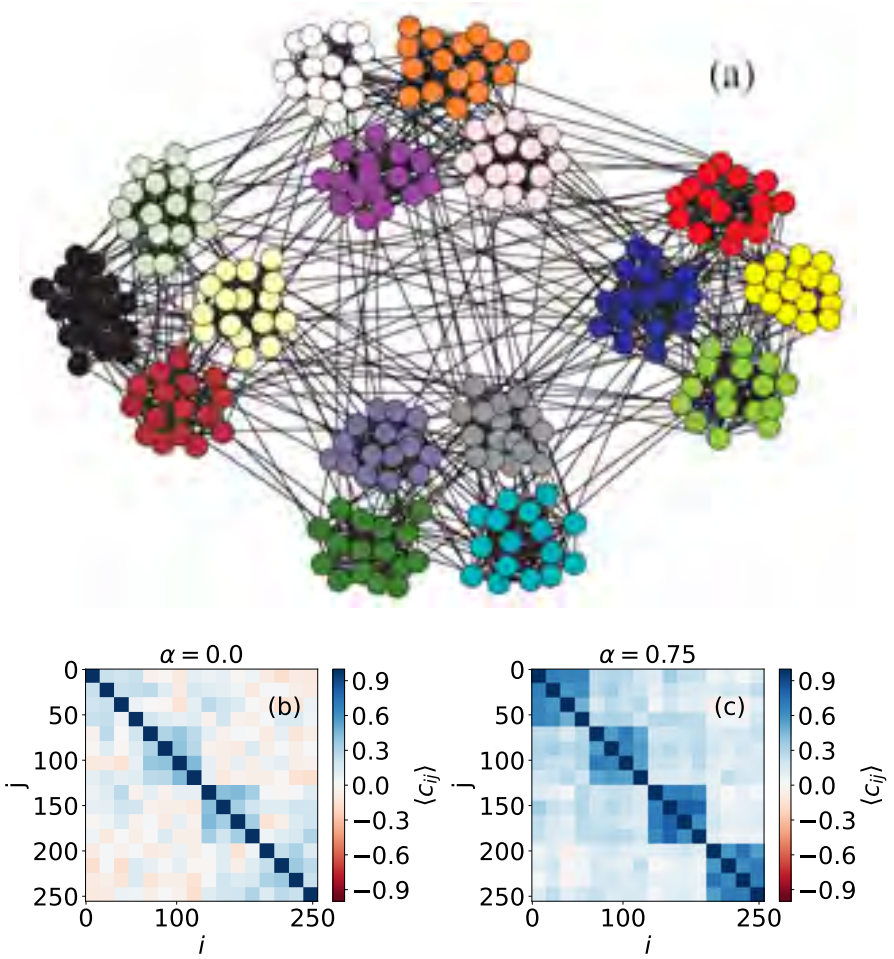

Figure 4.4: (**a**) Representation of a two-level synthetic network formed by $N = 256$ nodes. Colors are just here to visualize the community levels; (**b**) correlation values for every pair of nodes, obtained using $\alpha = 0$; (**c**) correlation values for every pair of nodes, obtained using $\alpha = 0.75$. Results are obtained using 5000 MMC steps, and are averaged over 200 repetitions.

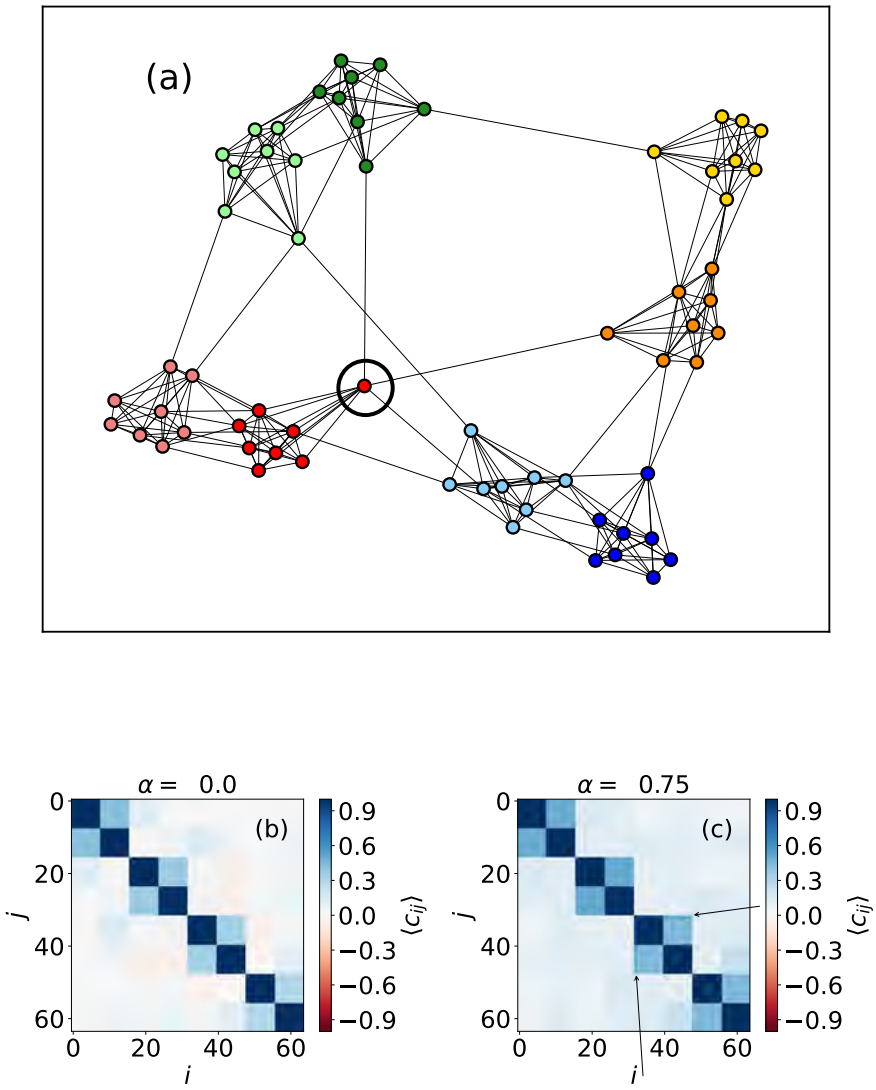

Figure 4.5: (**a**) Representation of an heterogeneous two-level synthetic network formed by $N = 64$ nodes. Colors are just here to visualize the community levels; (**b**) correlation values for every pair of nodes, obtained using $\alpha = 0$; (**c**) correlation values for every pair of nodes, obtained using $\alpha = 0.75$. Results are obtained using 5000 MMC steps, and are averaged over 1000 repetitions.

self-edges have been removed from the network, as well as small non-connected components.

Data (provided by Associació Heurística) were collected through the Twitter Standard Search API, which returns a collection of Tweets matching a specified query, namely a hashtag or a set of keywords. The network was built by adding an edge between two Twitter users whenever a user retweets or mentions another one. The fact that they are built from retweets/mentions instead of "follows" is the reason for the low clustering coefficient of these networks, dominated by star-like structures.

Twitter networks are directed, since one can follow a user that does not follow you back; however, we have considered links as undirected, for simplicity. The graph is not used for a realistic embedding but rather as a proxy for social networks of information diffusion. Another hard assumption is the achievement of a stationary state; surely, many observable states are transient, since social systems are often perturbed by supervening events, but this is beyond the scope of the present work.

The networks we chose correspond to the hashtags #yotambiensoynazi (which in English means I am also a Nazi, and we shorten as #yotambien), #nochebuena (in English Christmas Eve) and #martarovira (the name of a Catalan politician). (The first one is a small network that does not have to be confused with the feminist movement since it actually corresponds to an altercation occurred in Zaragoza (Spain), in the context of the Catalan independence process. The second one came in the wake of a speech that the Spanish King delivered against the aforementioned process on 3 October 2017. This official communication was sarcastically criticized by pro-independence supporters, making fun of it by using a comparison with the King's yearly Christmas Eve speech. The third one is associated with the Spain government legal actions against the politician Marta Rovira, again in the context of the independence process in Catalonia.)

Some properties of these networks are displayed in Table 4.1. The table shows that the absolute value of the magnetization at very low T is inversely proportional to the modularity value of the best partition.

Despite not considering transient regimes and directed or weighted links, we would expect to be able to observe some well known social phenomena regarding opinion spreading. According to simulations, all of these systems are unable to reach consensus at low temperatures, as we see in Figure 4.6. The behavior resembles the one found in BA networks with $\langle k \rangle = 2$, indicating that the dynamics are mainly driven by the existence of highly connected vertices which lead to the formation of opinion bubbles (Figure 4.7) because the opinion of the hubs is harder to change. The attractors of the dynamics at low temperature are metastable configurations that depend on the particular initial configuration,

Table 4.1: Network global coefficients for the explored topologies and average value of the magnetization at low T and $\alpha = 0.5$, denoted by $\langle |m|_\circ \rangle$. C is for the clustering, L for the average shortest path length, A for the assortativity, and $\mathcal{M}$ for the best partition modularity.

	ER z4	**#yotambien**	**#martarovira**	**#nochebuena**	**#BA z2**
N	2000	2408	29110	20022	BA z2
z	4	2.8	3.67	2.45	2
C	0	0.12	0.08	0.01	0
L	5.58	3.1	4.04	4.14	8.04
A	0	-0.28	-0.27	-0.33	-0.13
$\mathcal{M}$	0.52	0.62	0.65	0.76	0.94
$\langle \|m\|_\circ \rangle$	1.0	0.70	0.47	0.32	0.19

which is set at random for every repetition; therefore, we observe a large dispersion in the results. Blinkers, which are present for instance in random networks with low connectivity (see Section 3.4), appear in the final configurations reached by the MMC simulations for these networks as well.

In order to infer which topological property is related to the lack of consensus at $T \to 0$, we have compared different network coefficients and the value of $\langle |m| \rangle$ at $T = 0$ for $\alpha = 0.5$ (see Table 4.1) for the three real networks, the BA graph with $\langle k \rangle = 2$ and the ER network with $\langle k \rangle = 4$ (included as a null model). The comparison suggests that that the maximum value of the magnetization that the system is capable of reaching is related to the modularity value of the best partition for each network.

Note that the strong modular structure prevents the system from reaching zero-magnetization at $T \to 0$, even for $\alpha = 1.25$, where the energy has a unique global minimum at the macrostate of neutral consensus. As in some networks analyzed in the previous section, once opinion bubbles are formed, changes between different microstates become too costly, not only between extremists but also when the change occurs from or towards the neutral opinion.

The highest value for the magnetization at low temperatures is found at α around 0.5; $\alpha = 0.75$ in the case of BA graphs with $\langle k \rangle = 2$. When the magnetization reaches its maximum value the fraction of neutral agents n_0 is zero. From a social point of view, this means that the system gets divided into communities formed by positive or negative agents, but there is a stronger majority in one polarized opinion than for other values of α. Neutral communities are found at higher values of α, destabilizing the polarized majority. The fact that a moder-

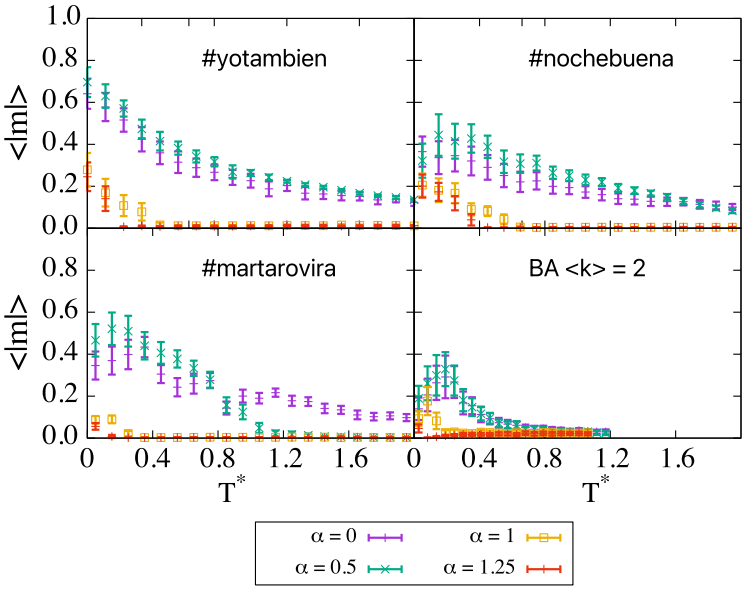

Figure 4.6: Comparison of the magnetization curves for three real networks and the BA network with $\langle k \rangle = 2$, all of them presenting frozen configurations at low temperatures, dominated by the presence of big hubs in the network. Results are averaged over 100 repetitions, except for #martarovira, whose results are averaged over 20 repetitions.

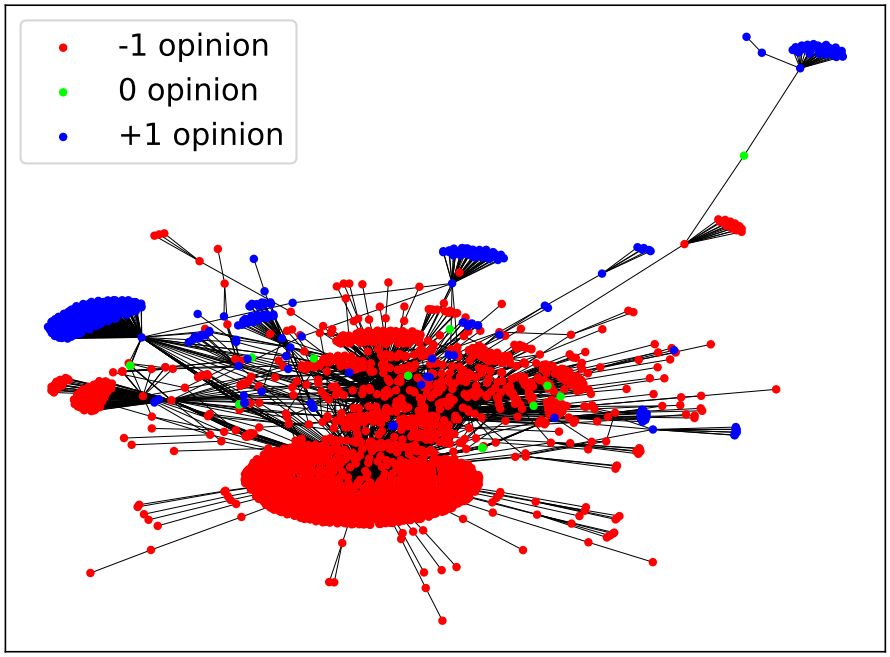

Figure 4.7: Example of a stationary configuration for #yotambien network at $T = 0.05$ and $\alpha = 0$, reached after 10^4 MMC steps.

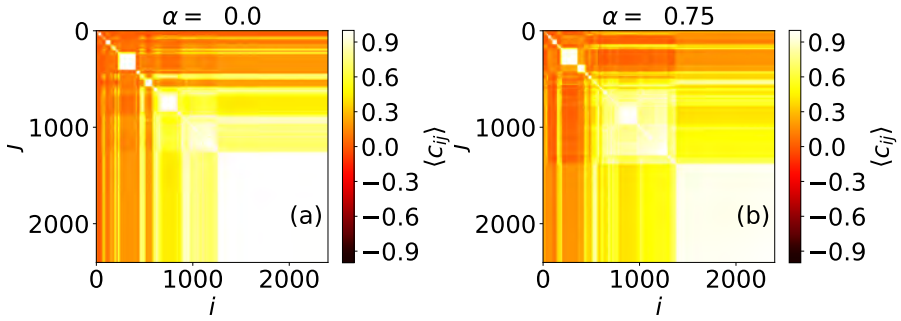

Figure 4.8: Correlation values for every pair of nodes of the Twitter network #yotambien, obtained using (**a**) $\alpha = 0$ and (**b**) $\alpha = 0.75$. Results are obtained using 10^4 MMC steps, and are averaged over 1000 repetitions.

ate neutral intensity catalyzes the majority in one polarized opinion adds to the conclusions presented in (158).

The networks #martarovira and #nochebuena exhibit a non-monotonic behavior of $\langle |m| \rangle$ with T for $\alpha = \{0, 0.5\}$. This is caused by the fact that the model presents a very complex energy landscape with multiple local minima when embedded in these topologies. This landscape is sensitive to the neutrality parameter α, since it changes the energy difference between the local neutral consensus and local polarized consensus. When the temperature increases, some energetic barriers can be easily overcome, so the attractors of the dynamics change. In some cases, this can enhance the dominance of one polarized opinion over the other one, which corresponds to higher average absolute magnetization; in others, it is the other way around.

The community structure of real networks can be easily visualized using the method described in the Appendix A. In Figure 4.8, we observe a large community containing approximately half of the nodes and a few smaller clusters. Simulations using $\alpha = 0$ and $\alpha = 0.75$ show just some minor differences in this network; for instance, the biggest community is slightly smaller. The network does not appear to have more than one level of community structure.

4.5

Conclusions

Here, we apply the three-state model t to modular networks, both synthetic and real.

At low temperatures, homophilic behavior dominates, and the system reaches either global or local consensus. At very high temperatures, the entropic term becomes dominant and agents change constantly their opinion regardless of their neighbors' states. This disordered state could be associated with conflict or riots. Although it may seem counterintuitive, moderate levels of social agitation can also help to catalyze consensus in modular graphs. On some networks, the system is unable to reach consensus at $T \to 0$, but it can do so when there is enough energy available in the form of upheaval. This energy is used by agents to transition between states until the system reaches a globally ordered state (consensus), which is more difficult to destabilize since it corresponds to a lower energy minimum.

When the modularity value of the best partition of a given network is $M \gtrsim 0.6$ indicates that the graph has a well-defined community structure, with multiple attractors that exhibit partial order. When this happens, the steady state at low temperatures is not consensus but a population fragmented into opinion clusters, which are different depending on the initial conditions. Some "blinker" agents may appear at the domain walls in some topologies; these nodes freely change their opinion, since they are connected to two or more clusters aligned in different directions.

The opinion fragmentation into clusters, known as echo chambers or opinion bubbles' formation, is mainly related to the network topology, but the contribution of neutral agents to the energy of the system is also relevant. Within a certain range of the neutrality parameter value, that depends on the specific network and is always below $\alpha = 1$, the neutral state becomes a bridge between polarized states. This behavior enhances polarized consensus, since agents do not remain in the neutral state, they just use it to transition between opposite opinions. Nonetheless, beyond a certain threshold, approximately $\alpha \gtrsim 0.5$—using the Newman–Girvan network with $k_{in} = 15$ as a benchmark—neutral clusters emerge at low temperatures. At higher levels of social agitation, agents can overcome some energetic barriers between domains, which, for $\alpha < 1$, increases the magnetization and hence drives the system closer to a polarized consensus. In this situation, any neutral clusters present at low temperatures tend to disappear as T rises.

On the other hand, when the best partition of the network has a modularity value $M \lesssim 0.6$, there is not a strong community structure in the system. In these cases, the population of agents already reaches the most possible ordered state at $T \to 0$, and its dominant order parameter (either $|m|$ for low α or n_0 for high α) decreases at intermediate temperatures by the effect of thermal fluctuations.

Opinion formation appears to be strongly determined by the action of influential nodes and modularity. Social media networks exhibit tree-like diffusion properties, which naturally lead to bipartisan or tripartisan configurations in our model, depending on the strength of the neutral opinion α. When the modularity of the best partition is sufficiently low, a moderate level of noise allows agents to partially align. Results from real networks indicate that intermediate levels of individual thinking, meaning a moderate disregard for peer pressure, (i.e., the existence of a finite temperature that does not exceed the critical point) can foster a closer approach to consensus than pure imitation of linked agents' ideologies ($T \to 0$).

Spatio-Temporal and Multilayer Networks

CHAPTER 5

Mobile agents

ANOTHER area of research, originally detached from traditional sociophysical models, focuses on the collective dynamics of agents moving within a plane. A prominent example of this category is the Vicsek model [(165)], where agents are represented as particles moving on a two-dimensional plane, with interactions governed by an alignment rule. Each agent adjusts its movement direction to align with the average vector of motion observed among its nearest neighbors. These models are used to analyze collective motion and flocking behavior in systems of self-propelled entities, ranging from biological organisms to synthetic systems. [(133; 31; 122)].

5.1

Introduction

The recent access to massive mobile phone data allows a deeper study of human mobility patterns [(13; 138)]. It has been found that in some cities there exist gender gaps, for instance, in (68) they show that in Santiago de Chile men tend to visit more diverse places than women, and women tend to spend less time at each location compared to men. Other demographic factors, including age, socio-economic status, and race can also be linked to heterogeneous mobility patterns (174; 155), contributing to the persistence of social segregation.

Faras et al. combined the Potts model with spatial motion in a recent work (50), finding similarities with systems having long-range interactions, even though the interactions are short-ranged. We follow a similar approach in this chapter to explore the interplay between the opinion dynamics studied in this work and mobility (50). We allow the agents to move on a plane according to a random

walk, with their velocities taken as a parameter of the system, and interact only with neighbors placed within a given distance. The agents' opinions are updated in parallel with their movement, using a Markov Chain Monte Carlo algorithm (Metropolis et al.; 69). The transition probability for an agent to change its opinion depends on the relative number of agents with different opinions in its neighborhood. By coupling the movement of the two-dimensional spatial structure and the opinion changes, we study their interplay and its impact on phenomena such as the formation of the global consensus or the appearance of spatial clusters of agents with similar opinions.

By varying the parameters of the model, we find that the mobility patterns and the role of neutral agents in the opinion updating rules affect the emergent patterns of opinion formation, leading to non-trivial outcomes. We compare our results with those obtained in (54; 55) for static networks, showing that, in general, velocity enhances the appearance of consensus and diminishes the neutral basins of attraction. However, it is shown that the amount of time necessary to reach a consensus is much shorter when it occurs in the neutral state. Our findings have implications for understanding the mechanisms that drive the dynamics of opinion formation in some real-world social phenomena, such as the spread of misinformation on social media, the polarization of political opinions, and the emergence of extremist groups, and will contribute to the ongoing dialogue between the fields of sociology and physics.

Our model not only considers opinion dynamics, but also incorporates movement rules that reflect a co-evolving process between homophily (i.e., the tendency to align opinions with those around us) and the capacity of agents to change their connections and the people they discuss a topic with. In their book (74), Gross and Sayama provide a review of previous studies on the interplay between dynamics and network structure. Here we analyze the behavior of the system for different movement rules, starting from the static case, where $v_i = 0$ for all agents, following with the case with constant finite velocity $v_i = v$, with two subcases: return to the initial position after every movement and subsequent opinion update and advance to the next position with no return. In the following sections, we introduce an acceleration term for the extremists, influenced by the proportion of neighbors sharing the same opinion state. This concept is grounded in the understanding that extremists exhibit a stronger confirmation bias, leading them to actively seek like-minded neighborhoods instead of opting for places with diverse opinions to evade discussions. Conversely, neutrals may demonstrate greater open-mindedness and be content in any kind of neighborhood [(114)].

We explore three different scenarios for the accelerated case, taking into account diverse intensities in the extremists' reactions to their neighbors: total halting, non-accumulative acceleration, and accumulative acceleration. In the total halting scenario, extremists come to a complete stop when surrounded by

like-minded agents, while neutrals maintain the constant initial velocity v. In the non-accumulative acceleration scenario, the initial velocity of extremists is doubled when surrounded by agents holding opposing opinions, but it is halved when the majority of their neighbors share their own opinion. Centrists continue to move at a constant velocity v throughout the simulation. In the accumulative acceleration scenario, extremists experience a doubling of their velocity at each time step when they are surrounded by agents with opposing opinions. In the last variant, centrists retain the velocity they acquired in previous time steps if they were extremists at those times.

We will consider low temperature for this context and Agents evolve until either they reach a stability condition that will depend on the particular case of study, or they have completed a fixed number of steps. In this case, along with the order parameters, we also measure the number of steps required to achieve the stability condition, when it is reached, and the size of the biggest cluster, in case the system ends up fragmented into several connected components with different opinions.

5.2

Static case

In this section, we assume that all agents remain immobile, i.e., $v_i = 0$; $\forall i$, so we only consider the opinion updating dynamics. To create the network displayed in Fig. 5.1(a), we randomly place $N_{init} = 155$ agents in a square with side length $L = 1$. We then connect all pairs of nodes that are separated by a distance less than or equal to $R = (1 + \epsilon)d_c$, where d_c is the critical distance and is defined by the following relation: $(N_{init} - 1)\pi d_c^2/L^2 \approx 4.51$ (141). Finally, we remove all connected components with a size N_C less than $0.2N_0$.

The critical distance d_c separates the system's regime below percolation, in which it is divided into several small connected components, from the regime above percolation, in which a giant connected component appears. For this case, we choose $\epsilon = 10^{-5}$, which places us slightly above the critical distance and enables us to take only the nodes belonging to the giant connected component.

As mentioned in the previous section, we already analyzed this model in (54; 55) for a wide variety of graphs, including the complete graph, the one-dimensional chain, Erdos-Renyi graphs, Barabási-Albert networks, the Girvan-Newman communities (70), and other synthetic modular graphs, as well as three particular cases of hashtags and mentions networks extracted from Twitter. In general, we found that networks with a well-defined community structure are

unable to reach the global consensus and that the local consensus within communities is the stationary state at low temperatures.

When randomly scattering nodes on a plane and connecting them based on a maximum Euclidean distance between first neighbors, we obtain a random geometric graph. When this distance is close to the percolation threshold the giant connected component of the graph exhibits a strong community structure (34). We expect that the opinion dynamics we propose will never lead to the global consensus in such networks. Panels (b) and (d) in Fig. 5.1 were obtained by running 1000 Monte Carlo simulations on the graph shown in panel (a), starting from different initial opinions each time. The correlation value C_{ij} between any pair of nodes i and j takes the value 1 if the nodes belonging to that pair always finish the simulations in the same opinion state, and -1 if they always finish in different states. We identify pairs of nodes with $C_{ij} = 1$ as belonging to the same community, since their opinions at the end of the simulation are totally correlated, while nodes with $C_{ij} \leq 0$ denote pairs of nodes in different communities whose opinions are totally uncorrelated. Intermediate values $0 < C_{ij} < 1$ indicate more levels of community structure, in other words, partitions of the network that achieve local consensus with a certain probability proportional to C_{ij} (see Appendix A).

For $\alpha = 0$, we observe mainly one level of community structure, corresponding to the small groups with $C_{ij} = 1$ that appear in the diagonal. When α increases, the transition between extremist opinions and the neutral one becomes easier, leading to two consequences. Firstly, a second level of community structure emerges, as a consequence, we observe that small communities in the diagonal appear surrounded by nodes with correlation values $C_{ij} > 0$, indicating bigger communities that achieve local consensus in a partial number of simulations. Secondly, the number of attractors of the dynamics increases, causing the fragmentation of the first level of community. For instance, the nodes that occupy the positions $\{12, \ldots, 28\}$ in Fig. 5.1 b) form a single community with a correlation value equal to one for $\alpha = 0$. However, they rearrange into smaller communities for $\alpha = 0.75$, as the neutral state can now also form a stable local consensus. In fact, panel c) shows that the fraction of neutral agents n_0 becomes non-zero for $\alpha \approx 0.8$, indicating the appearance of neutral communities above this value of the neutrality parameter. Below this value, the system becomes fragmented only into extremist communities. We would expect them to be evenly distributed, with an average magnetization $\langle |m| \rangle$ close to zero, by symmetry reasons. However, we observe a non-zero $\langle |m| \rangle$ due to finite-size effects. For higher values of α, the number of neutral communities rapidly increases until the global consensus at the neutral opinion is guaranteed for $\alpha > 1.5$.

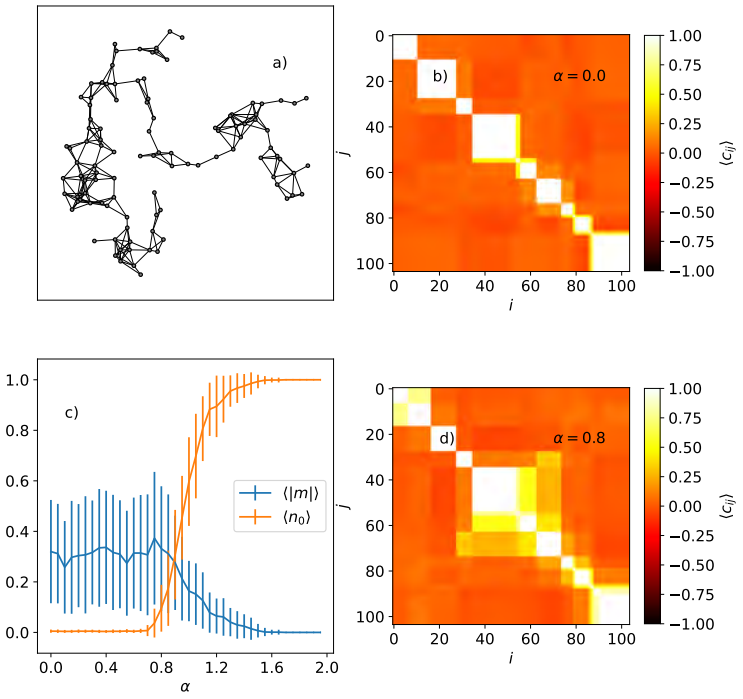

Figure 5.1: (a) Random geometric graph with $N = 104$ nodes and an average degree $\langle k \rangle = 4.87$. (b) Opinion correlation matrix for $\alpha = 0.0$, obtained from simulations on the graph represented in (a) 1000 with different initial opinions. (c) Absolute value of the magnetization and fraction of neutrals as a function of the neutrality parameter α, with their standard deviations. Results are averaged over simulations with 100 different initial opinions. (d) Opinion correlation matrix for $\alpha = 0.75$, obtained from simulations with 1000 different initial opinions.

5.3

Constant velocity. Elastic

In this section, we continue our study of the same graph analyzed in the previous section, but now incorporating movement. At each time step, agents are allowed to move in a random direction with a constant velocity $v_i = v$. They update their opinions in the new position and return to their original position afterward, indicating that agents have a preferred location, akin to a home, to which they periodically return. This movement can be understood as oscillations around the initial positions, with short amplitudes for low velocities. Therefore, for $v \to 0$, the results are similar to those obtained for the static case, since the agents are not able to change their neighbors.

As we increase the velocity, opinions can be transmitted to different neighbors at each time step, which makes the global consensus more likely to emerge, since it creates connections between more pairs of agents. The emergence of the global consensus is related to the saturation value of the aggregated reachability (see 5.2 a), defined as the accumulated proportion of links between any pair of agents holding different opinions that have been present in the system up to a given moment, in the absence of opinion updates. At the initial instant, the aggregated reachability is equal to the ratio between the number of links connecting agents with different opinions in Fig. 5.1(a) and the total number of pairs of agents that have different opinions. This number will monotonically increase until it reaches its maximum value, which depends on the velocity. Notice that since we impose periodical boundary conditions for the plane, we do not consider velocities larger than $v = L/2 = 0.5$.

The amount of time (in steps) required to reach consensus, once the velocity is sufficiently large, is shown in Figure 5.2b and exhibits a non-monotonic behavior. At low velocities, the consensus time is high and has large fluctuations, since it strongly depends on the initial conditions and the extent to which random movements favor changes towards a given majority opinion. For large values of v, we can think of the system as a complete graph with blinking edges that appear at each time step with a certain probability. The consensus time for high velocities stabilizes around 2000 steps, but with large fluctuations because the neighborhood changes completely at every time step, and every movement of the agents can potentially destabilize the local consensus achieved in the previous step. There is a minimum around $v = 0.1 \approx R$, for which opinion diffusion is very efficient, and the system reaches the global consensus rapidly in all the simulations, as shown in the example displayed in Fig. 5.2 c).

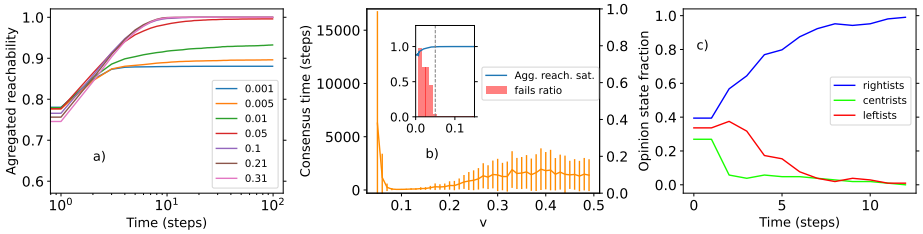

Figure 5.2: a) Aggregated reachability for the elastic case with constant velocity (see main text for explanation). Results averaged over 100 simulations. b) Number of steps needed to reach the global consensus as a function of the velocity for $\alpha = 0$ (orange), in-plot: number of simulations that does not achieve the global consensus (red bars) and saturation value of the aggregated reachability (blue line,. See main text for explanation). The grey dashed line indicates the value of v for which the fails become zero, which is very close to the value of v for which the saturation value of the aggregated reachability becomes one. Results averaged over 100 simulations. c) Particular example of temporal evolution of the number of agents in each opinion state for $\alpha = 0$ and $v = 0.1$.

5.4

Constant velocity. Non - elastic

In this section, we again consider a constant velocity of $v_i = v$ for all agents, but now we let the agents evolve following a random walk without returning to their initial position. In this case, the aggregated reachability (as defined in 5.3) never saturates to values lower than 1; instead, it always increases with time until it reaches 1, ensuring that the system eventually achieves the global consensus given enough simulation time. However, the growth rate of the aggregated reachability increases with the velocity until it saturates around $v = 0.2$, as shown in Fig. 5.3. Unexpectedly, the time needed to reach the global consensus increases with the aggregated reachability for low velocities until it reaches a peak that depends on α (see 5.3 b) and d)). In order to understand which features of two consecutive time adjacency matrices cause this behavior, we represent the probability of an agent being a first neighbor of another agent, given that they were the second neighbor in the previous step (represented by the black line), which shows a peak close to the consensus time peak (see Fig. 5.3 b) and d)). We show an example of the evolution of the fraction of agents in each opinion state for a system that evolves with a velocity around the maximum in Fig. 5.3 c). We observe switches in the majority opinion that prevent the system from achieving the global consensus quickly. Local consensus is preserved by the motion, but individual agents keep

bouncing between opinions for a large number of steps. Note that this behavior is very different from the one observed in the elastic case.

For higher velocities, the behavior is identical to that observed in the elastic case, as the position of the agents is random at each time step in both cases. Similar to the elastic case, we do not consider $v > L/2 = 0.5$ due to the symmetry imposed by the periodic boundary conditions.

The neutrality parameter α plays the most significant role in determining the opinion state of the final consensus, as shown in Fig. 5.4. These results are obtained for a system of $N = 100$ agents and a value of $R = d_c - 0.1d_c = 0.108$, which is only slightly lower than the one used in the previous section, and therefore, we do not expect significant differences. Broadly speaking, the system achieves neutral consensus for $\alpha > 1$ and a polarized global consensus otherwise. With respect to velocity, the minimum value of α required to observe neutral consensus in some simulations is very close to $\alpha = 1$ for low velocities, while for high velocities, it decreases to $\alpha = 0.8$.

This model exhibits a first-order phase transition at $\alpha = 0.8$ in the mean-field limit (55). The mean-field approximation assumes that each agent interacts with the average effect of all other agents, rather than taking into account specific interactions with every neighbor, and it is exact for the fully-connected graph. Therefore, the previous result is consistent with the notion that, for high velocities, the system behaves like a complete graph with blinking edges, where every possible pair of agents gets connected with a certain probability at each time step, regardless of their previous connections. Above $\alpha = 1$, the absorbing state is neutral consensus, regardless of velocity, as expected.

The average value of the absolute magnetization is complementary to the fraction of neutral agents, since all simulations end in a global consensus. When this consensus is polarized, both rightist and leftist consensus have an equal probability of appearing due to the opinion symmetry of the model.

5.5

Total halting

In this section, we examine how the system behaves when the velocity is adjusted at every time step following the next rule: extremists stop moving if they are surrounded by a majority of neighbors who share the same opinion state as them, and they move in a non-elastic fashion with velocity v if half or less of their neighbors share their same opinion. Neutral agents, on the other hand, are unaffected by this rule and move with a constant velocity of v at all times. The

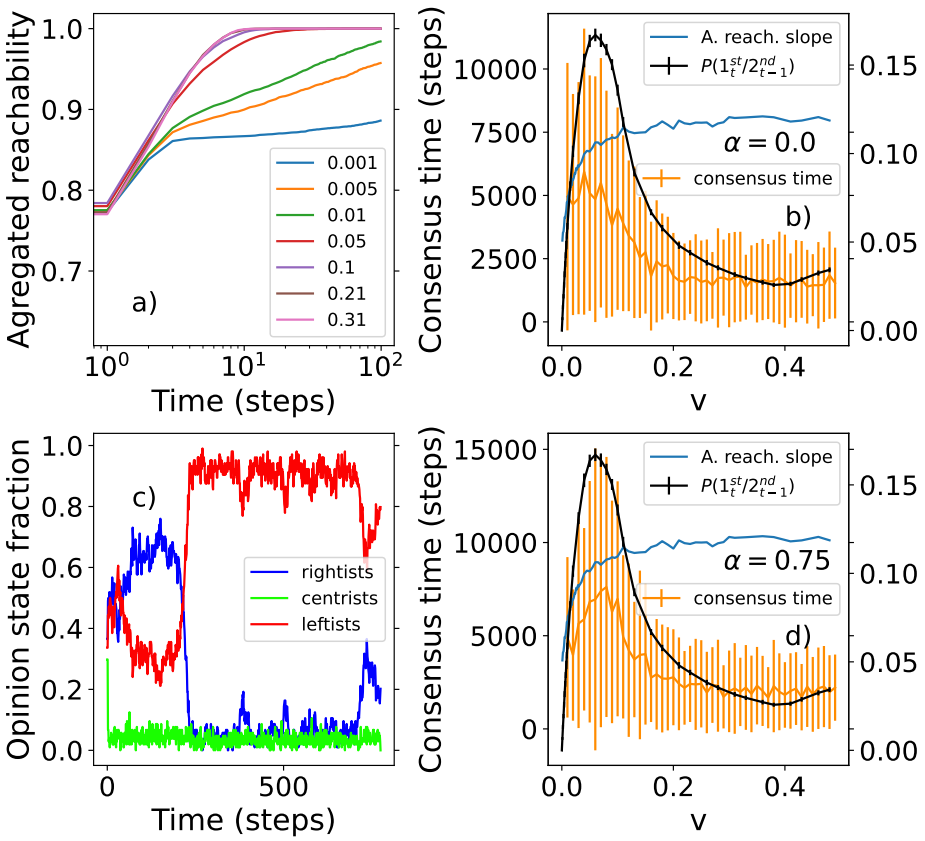

Figure 5.3: (a) Aggregated reachability for the non-elastic case with constant velocity. Number of steps needed to reach the global consensus as a function of the velocity (orange bars) for $\alpha = 0$ (b) and $\alpha = 0.75$ (d), along with the slope of the aggregated reachability as a function of the logarithm of time in the first seven steps (blue line), and the probability that an agent is the first neighbor of another agent given that in the previous step they were their second neighbor (black line). (c) Particular example of the temporal evolution of the number of agents in each opinion state for $\alpha = 0$ and $v = 0.05$. All results are averaged over 100 simulations.

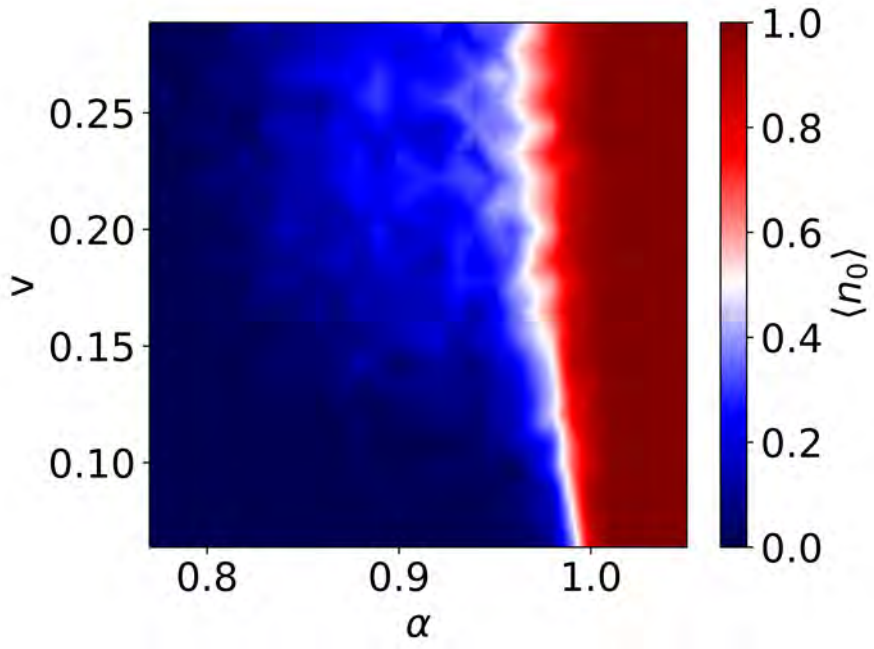

Figure 5.4: Phase diagram showing the fraction of simulations that finish with neutral consensus for the non-elastic case as a function of the velocity v and the neutrality parameter α. Results for a system of $N = 100$ agents and are averaged over 100 simulations that start from different initial positions and opinions.

simulation ends either when the system reaches a global consensus or when all the agents remain immobile. With these rules, we assume that extremists are more prone to change their links with people whose opinion is opposite to theirs. On the contrary, neutrals agents are sensitive to their neighbors' opinions regarding the opinion update, but do not selectively change their links according to their neighbors' opinion.

This type of motion favors local consensus, which by construction is always polarized, over global consensus. Additionally, it penalizes the neutral opinion, since extremists tend to form communities that capture neutral agents when they pass nearby, and convince them to change their opinion. Even for values of $\alpha > 1$ the average number of neutral agents is lower than 1, as we can see in Fig. 5.5 a). For large velocities, neutral agents, who do not stop, are able in to propagate their opinion fast enough to become a majority within the first time steps (at least in a certain number of simulations) and as a consequence $\langle n_0 \rangle$ increases. When this happens the system achieve the neutral global consensus in very few time steps (see Fig. 5.6), compared to the number of steps necessary to get partial or polarized consensus.

The average absolute magnetization strongly depends on both the velocity and the neutrality parameter α, as shown in Fig. 5.5 b). For $\alpha < 1$ and low velocities, the system reaches a local polarized consensus with a similar number of clusters in both positive and negative opinions. Therefore, $\langle |m| \rangle$ is low, and the number of neutral agents $\langle n_0 \rangle$ is approximately zero. However, when the velocity is higher, the agents travel further and the formation of local polarized clusters is faster. Any imbalance between rightists and leftists grows rapidly, leading to an increase in magnetization because the number of clusters in each polarized state is no longer equal, and the fraction of neutral agents remains close to zero.

Counterintuitively, when the neutrality parameter $\alpha > 1$, the tendency is reversed and the average value of the absolute magnetization is larger for lower velocities. This is because the abundance of neutral agents allows the system to achieve polarized global consensus in a significant number of simulations, as shown in Fig. 5.6. Due to the high value of α, neutral agents persist in time, while extremists stop and form communities. Eventually, neutral agents separate and get caught into the polarized clusters, changing their opinion to align with the community they encounter. Furthermore, the abundance of neutral agents can convert small polarized clusters to the neutral opinion, making its members move again. Later, these agents may be converted to extremism again by a larger polarized community, and eventually, the system can reach the global polarized consensus. When the velocity increases, extremist communities cannot grow enough, and in most simulations, we obtain either neutral global consensus, marked by an increase of $\langle n_0 \rangle$, or polarized local consensus with an similar number of small extremist groups, consistent with a low average magnetization.

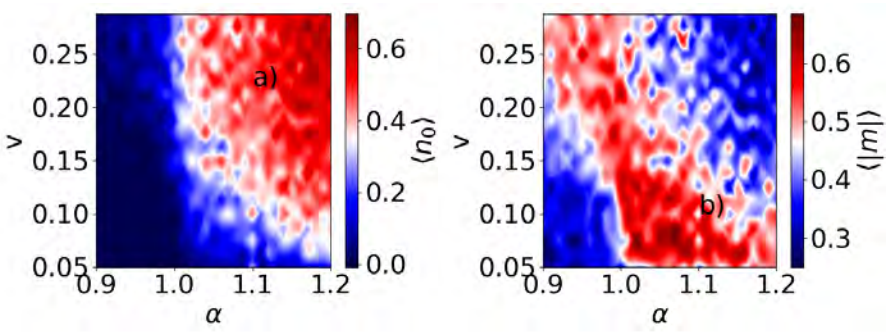

Figure 5.5: a) Final average fraction of neutral agents and b) final average absolute magnetization as a function of the velocity v and the neutrality parameter α for the total halting model. Results for a system formed by $N = 100$ agents and averaged over 100 simulations starting from different initial positions and opinions.

Figure 5.6 displays examples of the consensus time histogram for each scenario. However, it is worth noting that for $v = 0.25$ and $\alpha = 0.95$, the system only reaches local polarized consensus, despite having an average magnetization of $\langle |m| \rangle > 0$, indicating an unbalanced distribution of extremists in each state. Global neutral consensus is achieved much faster than local or global polarized consensus. Surprisingly, the value of the initial velocity v does not have a high impact on the consensus time, especially for $\alpha < 1$.

5.6

Non-accumulative acceleration

In this section, we consider a case that is similar to the previous one, except that extremists do not stop their motion completely when they have a majority of neighbors sharing their same opinion. Instead, they reduce their velocity to half the initial value ($v/2$) and, in addition, they double the initial velocity if their neighbors with an equal opinion are not a majority. This strategy enables the system to reach a global consensus, just like in the case where the velocity is constant. As a consequence, magnetization is complementary to the fraction of neutral agents.

Although the dynamics still always converges to a global consensus, the phase diagram exhibits slight differences from the case where the velocity is constant.

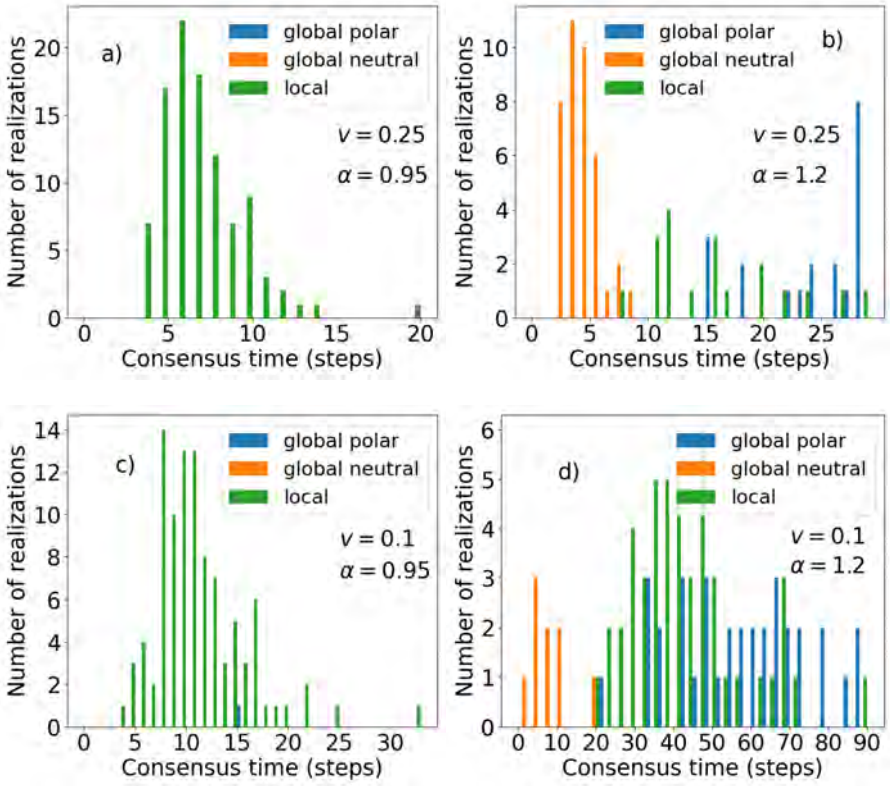

Figure 5.6: Histograms for the consensus time for the total halting model, for a) $v = 0.25$ and $\alpha = 0.95$, b) $v = 0.25$ and $\alpha = 1.2$, c) $v = 0.15$ and $\alpha = 0.95$ and d) $v = 0.15$ and $\alpha = 1.2$. Blue bars represent global polarized consensus, green bars are for global neutral consensus and yellow bars denote local polarized consensus. Results averaged over 100 repetitions, starting from different initial positions and opinions.

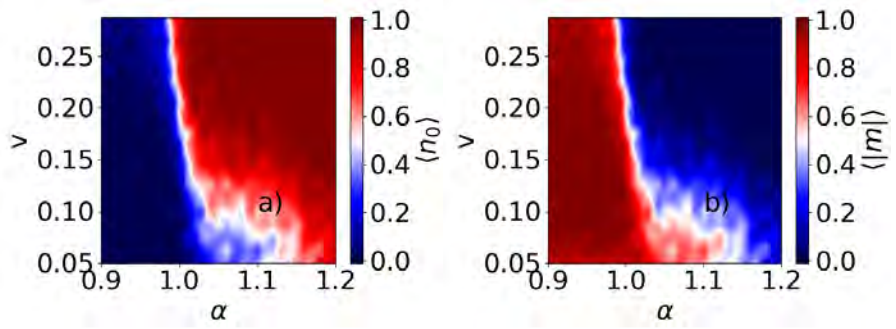

Figure 5.7: a) Average fraction of simulations that finish with consensus in the neutral opinion and b) final average value for the absolute magnetization as a function of the velocity v and the neutrality parameter α for the non-accumulative accelerated model.

In particular, for low velocities, a value of the neutrality parameter α greater than 1 is required to guarantee neutral consensus (see Figure 5.7). This is because extremists adapt their motion to their neighborhood, making them come to an agreement more efficiently. In contrast, the neutrals, which are not affected by this rule need a stronger interaction (i.e. a higher value of the neutrality parameter α) to be able to form neutral opinion groups. Therefore, for low velocities the results for the order parameters are resemblant to those obtained for the total halting case. Conversely, for high velocities, the changes in velocity are insufficient to produce this effect, and the average values of the order parameters are equal to those obtained for the constant velocity case.

Regarding the consensus time, the motion rules steer the system towards the global consensus by making the agents sensitive to the agents' opinions, while allowing all of them to move around the plane and potentially interact with any other agent. As a result, the consensus is reached in significantly fewer steps compared to agents moving with a constant velocity, as evidenced by comparing Figure 5.3 and Figure 5.8. Neutral consensus is always faster than polarized consensus, and it is enhanced by high velocities, as observed in the previous scenarios. Both increasing v or α reduce the number of steps required to achieve consensus, similar to the constant velocity case.

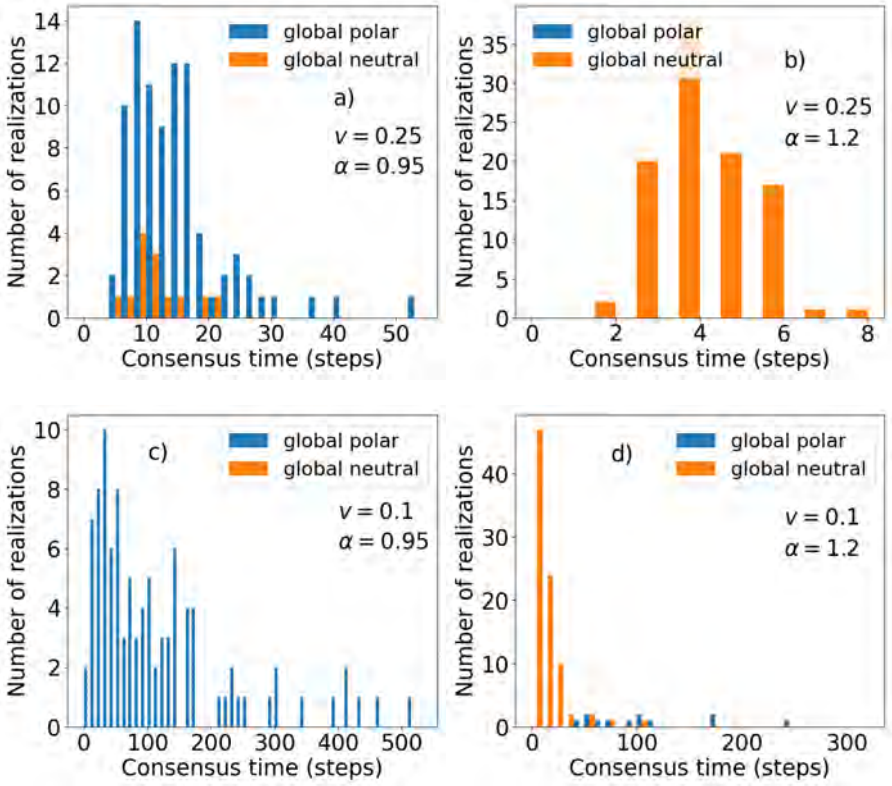

Figure 5.8: Histograms for the consensus time for the non-accumulative accelerated model, for a) $v = 0.10$ and $\alpha = 1.0$, b) $v = 0.10$ and $\alpha = 1.2$, c) $v = 0.25$ and $\alpha = 1.0$ and d) $v = 0.25$ and $\alpha = 1.14$. Blue bars represent global polarized consensus and orange bars denote global neutral consensus. Results are averaged over 100 simulations, starting from different initial positions and opinions.

5.7

Accumulative acceleration

In the case examined in this section, extremists, modify their velocity based on the proportion of neighbors who share their opinion, as in the previous sections. However, in this case, an extremist agent i reduces their velocity to $v_i(t) = v_i(t-1)/2$ when they have a majority of neighbors in their same opinion state and increases it to $v_i(t) = v_i(t-1) * 2$ otherwise (with a maximum velocity of $v_{max} = L/2 = 0.5$ to avoid higher velocities that do not make sense with periodic boundary conditions). Although the extremists' velocity can now increase, they still tend to form opinion clusters, similar to the total halting scenario. On the other hand, neutrals no longer move with the initial constant velocity v, but instead, they conserve the velocity they had acquired previously, so if a neutral agent i was polarized at some point in the past time, and they have modified its velocity to a given $v_i \neq v$, they will continue moving at their own v_i. Eventually, agents move so slowly that they are considered immobile, so we stop the simulation when the average velocity is lower than $5 * 10^{-4}$.

In most simulations, the stationary state for this scenario is local consensus for $\alpha < 1$, similar to the total halting case. While for high values of the neutrality parameter α, the system reaches a neutral consensus. The main difference now is that when an extremist changes their opinion to neutral, they conserve their velocity, which can be arbitrarily slow. Therefore, although neutral agents do not react to their neighbors' opinions, partial consensus can still contain neutral clusters, even for $\alpha = 0.95$ (see Fig. 5.10). Polar cluster formation depletes some regions of extremists, leaving empty zones that can eventually be occupied by slow neutral agents with short average displacement. As in previous scenarios, we find that higher initial velocities v favor the achievement of neutral consensus. For example, in Fig. 5.9 a), the proportion of neutrals at the end of the simulations when $\alpha = 1.2$ is $\langle n_0 \rangle \approx 1$ only for $v \gtrapprox 0.2$.

The phase diagram for the average magnetization Fig. 5.9 b) is slightly different from the one obtained for the total halting scenario. Specifically, for low α and low v, we obtain higher values for $\langle |m| \rangle$. This is because in this case, extremists do not suddenly stop their movement when surrounded by a majority of agents with the same opinion. Instead, they gradually modify their velocity, adjusting their positions, aligning their opinions, and convincing isolated neutral agents when they pass nearby. This mechanism allows them to form larger clusters, thus increasing the magnetization. For $\alpha < 1$, the system rarely reaches global neutral consensus. The average absolute magnetization increases with v, as in the total halting case, and the proportion of local consensus with neutral clusters decreases.

Regarding the typical size of opinion clusters, polarized and neutral agents behave differently, which is expected, since the movement rules are still different for both types of agents. Figure 5.9 c) shows that the largest neutral cluster found in the simulations has a number of agents $N_0 \approx 45$, while the polarized clusters can be the size of the system $N = 100$, as shown in panel d). On one hand, this is due to the fact that neutral agents' motion is not reduced when they are surrounded by other neutrals, hence any big neutral connected component can break more easily than a polarized one. On the other hand, we do not see such big polarized clusters in the case of total halting, but we do here due to the smoother movement of the extremists. It may seem counterintuitive that these big polarized clusters only appear for high values of α. However, the reason is that it takes time to form these structures and, for $\alpha < 1$, we achieve local polarized consensus too fast to give the agents time to form big opinion groups.

Our casuistic is richer than in other scenarios, particularly for $\alpha = 0.95$ and $v = 0.25$, where we observe all four possible outcomes, although a global consensus is less likely (see Figure 5.10). In contrast to the total halting case, the time required to achieve a polarized consensus is sometimes shorter than the time needed to reach a global neutral consensus. Local polarized consensus is only observed for $\alpha = 0.95$, and the time required to achieve it is similar to that of achieving global neutral consensus. The impact of v and α on the consensus time is smoother than in the non-accumulative model.

5.8

Conclusions

We use Monte Carlo simulations to investigate the impact of agents' motion on the final outcomes of our three-state opinion model with a neutrality parameter that adjusts the relevance of the neutral opinion state. Our findings indicate that both the movement and neutrality parameter play a significant role in the final outcome of the system. In particular, for a given value of α, mobility patterns can change the system's attractors in all cases studied.

We found that motion drives the system towards the global consensus, whereas the local consensus arises when the motion rules involve agent stopping. The composition of this local consensus depends on how agents adjust their velocity according to their neighbors' opinions. In the case of total halting, where polarized agents stop completely when they are surrounded by like-minded individuals, and neutrals move at a constant velocity, local consensus is always polarized. Only when neutrals inherit the extremists' velocity are they able to occupy the free space left by polarized agents and form stable clusters, even if $\alpha < 1$.

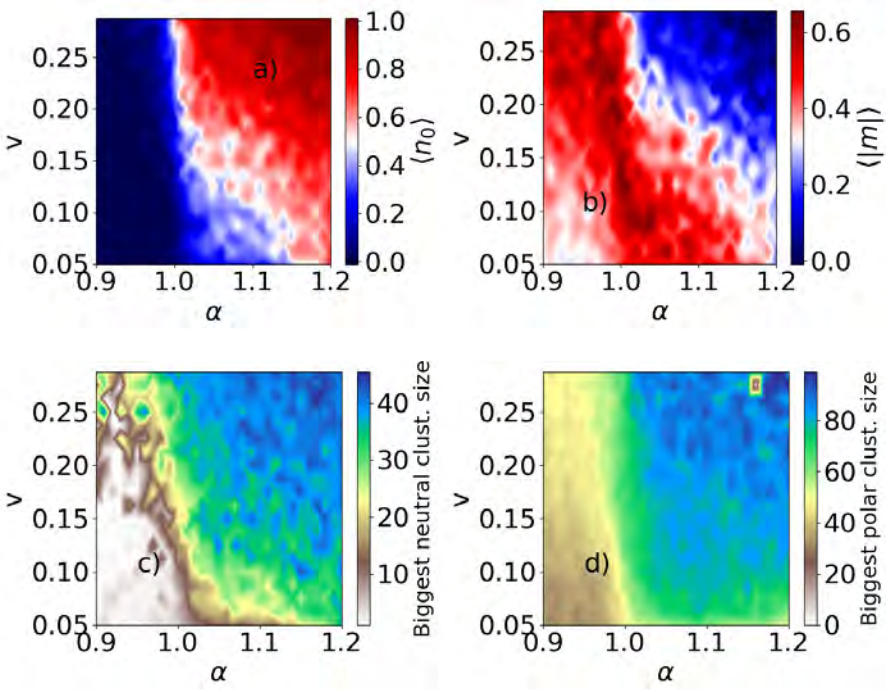

Figure 5.9: a) Average fraction of agents that finish the simulation holding the neutral opinion, and b) average final value for the magnetization as a function of the velocity v and the neutrality parameter α for the accumulative accelerated model. Size of the biggest c) neutral-connected component and d) polarized connected component. The grey dot in the upper right corner of panel d) ($\alpha = 1.16$ and $v = 0.275$) indicates that there were no polarized clusters in any of the simulations for that particular values of the parameters. Results are averaged over 100 simulations, starting from different initial positions and opinions.

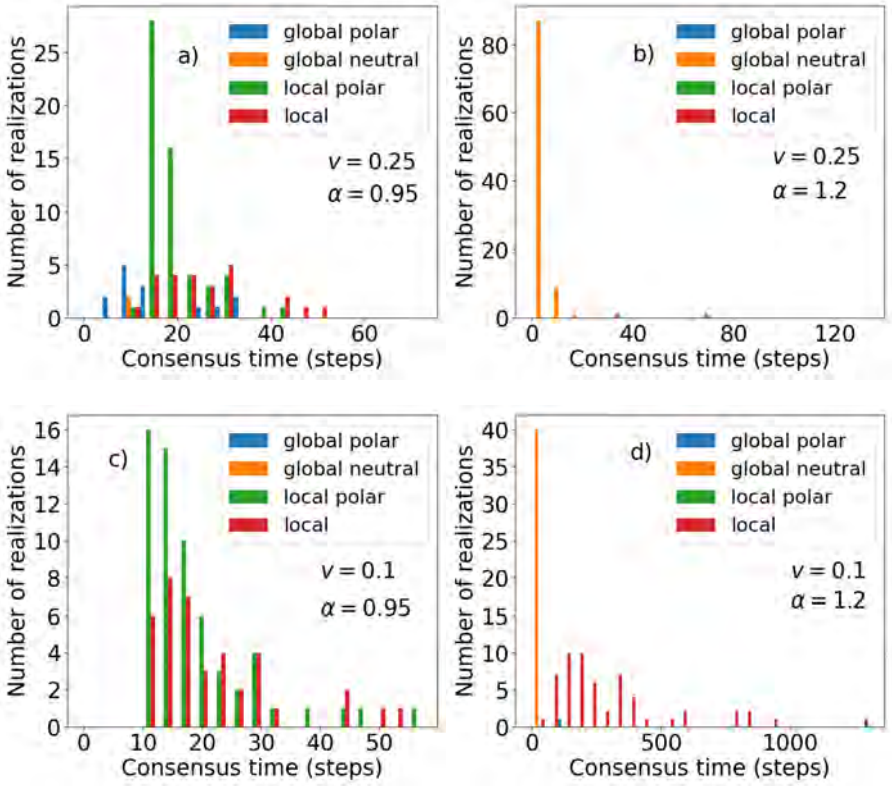

Figure 5.10: Histograms for the consensus time for a) $v = 0.10$ and $\alpha = 1.0$, b) $v = 0.10$ and $\alpha = 1.2$, c) $v = 0.25$ and $\alpha = 1.0$ and d) $v = 0.25$ and $\alpha = 1.14$ for the accumulative accelerated model. Blue bars represent global polarized consensus, orange bars are for global neutral consensus, green bars denote local consensus which only contain polarized clusters and red bars represent local consensus which contains at least 1 neutral cluster. Results for 100 simulations, starting from different initial positions and opinions.

In the limit case of a static network, a strong community structure gives rise to multiple opinion groups that may merge due to mobility effects. Performing a regular random walk at a constant velocity leads to the global consensus in all cases. However, it is interesting to note that periodically returning to a base location, even if agents do not update their opinions there, can reduce the time needed to achieve the global consensus by disrupting the formation of opinion clusters. This is true as long as the velocity is high enough to allow the system to eventually achieve an aggregated reachability of one.

Across all cases studied, high velocities favor the neutral opinion, bringing the system closer to mean-field behavior, where the neutral opinion becomes a dynamic attractor. In general, global neutral consensus is achieved faster than global or local polarized consensus, except for some marginal simulations for the accelerated accumulative model with large velocity and $\alpha < 1$, where we observe local polarized consensus at very short times. Extremists use to take advantage of longer interaction times to form large clusters and establish polarization. Once a large polarized community forms, it is hard to destabilize because opinion transitions become unlikely when agents remain clustered. In contrast, neutral agents are more prone to changing their minds, both because their movement is not influenced by the neighborhood opinion and because they have a higher probability of changing to either polarized opinion state. Interestingly, in some cases, a larger value of the neutrality parameter α can increase polarization instead of reducing it, not only for mobile agents but also for some static networks, as shown in (55).

While this work primarily concentrates on the physical plane of agent movement, there is potential to extend the concept to include ideological or emotional spaces, where the dimensions represent beliefs or emotions. In such scenarios, at lower velocities, agents would primarily interact if their ideas or emotional states are closely aligned, following the homophily principle, similar to what is done in bounded confidence models. As an example, we refer to the works by Starnini et al. (153), which explore related concepts in the context of social dynamics and opinion formation. The work "Bounded Confidence Opinion Formation Model of Periodical Interacting Agents" (Ferri, Nicolás-Olivé, Cozzo, Díaz-Guilera and Prignano), currently in preparation, also focuses on these types of spaces (Appendix B).

To summarize, we present an overview of all the mobile agent-model variants and their corresponding outcomes in Table 5.1 and Table 5.2.

Table 5.1: Table to summarize the variants of the model.

Variants of the model	**Motion Rules**	**Time step**
A. Static	$v_i = 0 = ctt \; \forall i$	Opinion update
B. Elastic	Initial positions: Same as the static case. $v_i = v = ctt \; \forall i$	Move in random direction - Opinion update - Return to the initial position
C. Non-elastic	Initial positions: Same as the static case. $v_i = v = ctt \; \forall i$	Move in random direction - Opinion update
D. Total Halting	Polarized: v = 0 if at least half their neighbors share their same opinion state; $v = v_{initial}$ otherwise Neutrals: $v = v_{initial} = ctt$	Move in random direction - Opinion update
E. Accelerated non-accumulative	Polarized: $v = v_{initial}/2$ if at least half their neighbors share their same opinion state; $v = 2 \cdot v_{initial}$ otherwise Neutrals: $v = v_{init} = ctt$	Move in random direction - Opinion update
F. Accelerated accumulative	Polarized: $v = v_{t-1}/2$ if at least half their neighbors share their same opinion state; $v = 2v_{t-1}$ otherwise ($v_{max} = L/2 = 0.5$) Neutrals: $v = v_{t-1}$	Move in random direction - Opinion update

Table 5.2: Table to summarize the outcomes of the model.

Variants	**Time for global consent**	**Stationary state**
A. Static	Only partial consensus	Network divided into opinion clusters according to: 1) the network structural partitions and 2) the value of α
B. Elastic	The system reaches global consensus only if v guarantee an aggregated reachability equal to 1 at any time step. Non-monotonic behavior with a minimum around $v = R$ and higher values with large fluctuations for slower and faster velocities.	Global consensus if $v \geq R$. • Neutral consensus if $\alpha > 1$ • Polarized consensus if $\alpha < 1$ • Partial consensus for low v: the simulation stops at the maximum time steps, and the proportion of agents in each state depends on α
C. Non-elastic	The system reaches global consensus only if $\forall\, v$. Non monotonical behavior with a maximum around $v = R$	Global consensus if $v \geq R$. • Neutral consensus if $\alpha > 1$ • Polarized consensus if $\alpha < 0.8 = \alpha_{tricritical}$(mean-field) • If $0.8 < \alpha < 1$ opinion state of the consensus depending on v (higher v favors global neutral consensus)
D. Total Halting	Partial consensus for all parameter values explored	The number of neutral or polarized agents depend on both α and v, both parameters boosting the neutral proportion of agents.
E. Accelerated non-accumulative	Global consensus, faster than in variant C	Similar to variant C. However, velocity has a greater impact favoring neutral consensus when $0.8 < \alpha < 1$
F. Accelerated accumulative	All possible outcomes: • Neutral consensus • Polarized consensus • Partial polarized consensus • Partial consensus with neutral groups	Rich casuistic. Mixture of variants D and E. See main text for details

CHAPTER 6

Belief and social networks

HUMAN beings and the belief systems that support their thought and opinion formation processes are complex in themselves. Representing opinion as a single variable offers many advantages for modeling, as it is usually simple enough to be treated analytically in some limit cases and enables the description of a wide variety of social phenomena. However, a more detailed description of each agent's opinion can be interesting and provide information on smaller scales. Robert Abelson, along with Milton J. Rosenberg, developed the concept of 'symbolic psycho-logic,' an early attempt at describing a psychological organization of attitudes and attitude consistency through an idiosyncratic type of adjacency matrix of a signed graph, which was pivotal in the development of the field of social cognition [(2)]. In this chapter, we follow this idea, exploring our vectorial three-state model embedded in a network of networks where external nodes (or supernodes) represent individuals. We focus on the role that the topology of their belief system (the inner nodes) plays in achieving both social consensus and internal coherence.

6.1

Introduction

While single-variable models are the most studied in the sociophysics literature, many recent studies consider opinions as collections of uncorrelated variables, components of a vector in a multidimensional space (15; 129; 93). Baumann et al. (2021) propose a Euclidean space spanned by a basis of topics that may overlap, indicating that intersecting arguments could apply across different topics. Indeed, it is the application of a nonorthogonal basis in their model that can

explain the emergence of an ideological phase, characterized by the polarization with alignment observed in empirical data.

Recent advancements in psychology explore graph representations of an individual's belief system (32; 166). The exploration of different themes in philosophy suggests that while the specific discussions and approaches may evolve, the fundamental human concerns like justice, ethics, and altruism remain constant over time [(125)]. While individuals are mutable entities heavily influenced by context and culture, ideas are more stable, making them more suitable as foundational elements for the study of human behavior.

Several studies have shown that when a dynamical process is embedded in a complex network, the distribution of connections between nodes significantly influences the system's behavior, leading to diverse outcomes. Although single-layer networks effectively represent many systems, recently multilayer networks have attracted attention in the study of complex systems, since they offer a more nuanced representation of real-world systems.

Networks of networks, are a type of multilayer graphs that represent different levels of complex interactions of a particular system. For instance, we can deepen our understanding of neurons' behavior by modelizing them as deep artificial neural networks, proposing a computational framework that simulates the behavior of these neurons in a detailed and nuanced manner [(38)]. In these networks, a neuron layer's activity is looped back into the same layer or preceding ones, allowing the network to combine new input with its past activities. It is also known that the brain consists of various densely linked regions that operate as units for specific tasks, and that are, in turn, interconnected forming a complex, hierarchical network, known as the connectome. [(152)].

We find another example in Zitnik et al. (2017), where authors discuss the importance and mechanics of protein-protein interactions within the larger context of cellular and tissue-level organization [(181)]. In social networks individuals interact and form various organizations contributing to higher-level networks such as schools, enterprises, associations, cities and countries [(72)].

Kim et al. (2019) studied the interplay of intracellular and extra-cellular networks revealing that the statistical properties at the macro-level were affected by the parameters set at the micro-level, but the influence did not work in the opposite direction. However, when it came to the detailed dynamics of the networks, the patterns were dominated by the macro-networks [(92; 48)].

Friedkin et al. (2016) use a matrix approach and the example of public opinion on the Iraq War to demonstrate how belief systems operate under logical constraints. They show that belief connections, combined with social influence, can

lead to a cascading effect, where a change in one belief may trigger a reevaluation of related beliefs.

Ellinas et al. (2017) proposed a model incorporating peer pressure, social rank, and internal cognitive coherence into the dynamics of belief adoption. They consider interconnected networks of beliefs and individuals to explore their interplay in organizational culture. [(45)]. Grounded in empirical data, their paper reveals that an organization might appear cohesive in its culture even when composed of individuals who are experiencing internal conflicts between their own beliefs and those adopted through social conformity. It also found that social conformity components—peer pressure and social rank—have varying degrees of influence at different levels within the organization.

Van der Maas et al. (2020) implemented a hierarchical Ising opinion model (HIOM) to explore the dynamics of polarization among individuals, testing it in Watts-Strogatz and modular networks generated by the stochastic block model. They associated the concept of temperature with the inverse of the attention individuals pay to their peers and employed a network of networks framework, where individuals are represented by networks comprising beliefs, feelings, and behaviors. [(161)]. Finally, they suggest integrating a bounded confidence approach, which they found to be effective in mitigating polarization.

The interpretations in the present work will be mainly focused on the social application of networks, in which the internal level will account for a network of beliefs interconnected in different ways, and the external network nodes will represent people [(136; 3)]

6.2

Structural considerations

As in previous Chapters, we consider a social adjacency matrix, representing the connections among individuals of a population, but here each individual is not represented by a single node, but by a network that represents the belief system of the agent. Each agent has an internal network of $\mu = \{1, \ldots, c\}$ subnodes or beliefs. Each belief has a label denoting a certain topic, which is connected to the nearest neighbors' beliefs with the same label, meaning that in a single interaction (communication act) agents discuss a specific topic. Internally, all beliefs inside an agent form a network with a certain topology. The complete structure can be obtained by performing the cartesian product of the external (social) and the internal (beliefs) adjacency matrices $A_{\text{ext}} \square A_{\text{int}}$ (see Fig. 6.1).

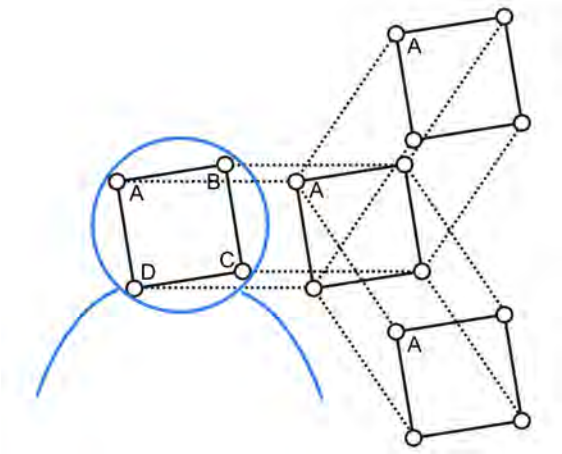

Figure 6.1: Representation of four agents with a 4-node ring-shaped internal belief topology and socially connected forming a star. Modified from [(139)].

For the social external network, we exclusively consider a fully connected graph, while in the case of the internal structures, we explore three distinct networks to represent different individual belief systems (see Fig. 6.2).:

- Clique (fully connected): as a proxy for a richly interconnected belief system
- Ring-shaped: to exemplify sparse inner connections
- Star-like topology, denoting individuals with a dominant core belief supported by all other belief components

This chapter aims to investigate how these internal topologies influence the consensus state of a population whose beliefs may align with one of the three orientations characterized by our model. So far, this work has associated temperature with social agitation, leading to a lack of opinion alignment among agents. In the case of the internal network, temperature needs to be reinterpreted. The mechanism by which an individual may tend to misalign their internal belief system is cognitive dissonance, as described by Festinger (1957) [(56)]. Cognitive dissonance is the psychological stress or discomfort experienced by individuals when they simultaneously hold two or more contradictory beliefs, ideas, or values, perform an action that contradicts their beliefs, or are confronted with new information that conflicts with existing beliefs, ideas, or values. This discomfort prompts an internal drive to reduce the dissonance, either by changing beliefs, justifying the dissonance by integrating new beliefs, or diminishing the signifi-

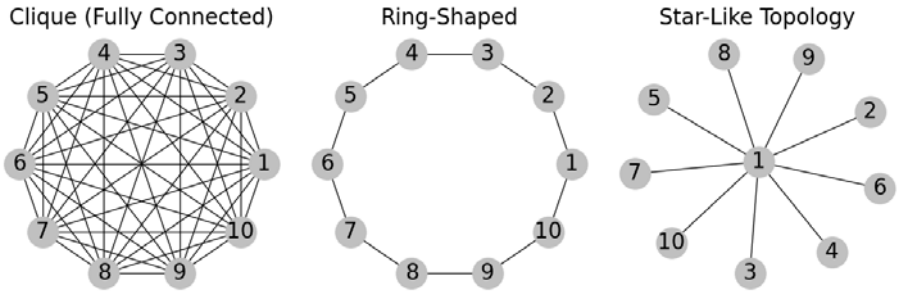

Figure 6.2: Illustration of the three network topologies used to model belief systems with a number of internal beliefs $c = 10$.

cance of the conflicting belief. We will maintain fixed the number of beliefs and the internal link weights, and focus on the change of belief state mechanism.

6.2.1 - Hamiltonian

The hamiltonian describing our system is:

$$H = -\frac{J}{z_{\text{ext}}} \sum_{\mu=1}^{c} \sum_{\langle i,j \rangle_{\text{ext}}} \mathbf{S}_{\mu}^{i} \cdot \mathbf{S}_{\mu}^{j} - \frac{J}{z_{\text{int}}} \sum_{i=1}^{N} \sum_{\langle \mu,\nu \rangle_{\text{int}}} \mathbf{S}_{\mu}^{i} \cdot \mathbf{S}_{\nu}^{i}, \tag{6.1}$$

where, z_{ext} is the external number of connections $(N-1)$ between agents; z_{int} corresponds to the average internal number of connections, which depends on each internal topology; and the vectors are belief states, for instance, $\mathbf{S}\mu^{i}$ is belief μ in agent i. The first term of the Hamiltonian extends over connected beliefs in different agents, while the second term covers the internal connections of all agents.

We calculate the contribution to the energy of each pair of connected beliefs as the scalar product of their corresponding opinion vectors, summing all contributions to compute the global energy (see Fig. 1.3). For simplicity, the positive coupling constant J is set to one, but we normalize it by the average number of connections in each term to maintain comparability between internal and external contributions. Thus, the embedded dynamics ensure an equal relevance between intra- and extra-modular links. Our goal is not to explore the relative importance of external peer pressure versus internal cognitive dissonance, as investigated by Rodriguez et al. [(136)], but to study the effects of the connection patterns in the agents' belief networks.

6.3

Finite temperature behavior

In this section we examine how the order parameters of a particular belief change with the temperature and the number of internal beliefs for each inner topology. We choose 2 values for the neutrality parameter: $\alpha = 0$, for which we expect a second-order phase transition and $\alpha = 0.85$, which is in the range of the first-order transition for the fully connected graph. We aim to know how the critical and tricritical points vary with the parameters of the system and the beliefs' topology. Since for both the clique and the ring-like topology all connections are symmetrical for all internal nodes, we will consider belief A, without loss of generality. In the case of star-like minded individuals, we will consider both A (the core belief) and B (one of the peripheral beliefs, which are topologically equivalent).

6.3.1 - Analytical approximation

Here we extend the methodology applied in Chapter 2 to a broader context. We use the Weiss mean-field approximation (MFA) to build the local hamiltonian for a particular belief A inside a given agent, and calculate the expected value for order parameters. This calculation now incorporates all possible combinations of internal contributions given by this particular belief to the global energy:

$$\langle \bar{s}^A \rangle = \frac{\mathrm{tr}\left\{ \bar{s}^A \exp\left[\beta \bar{s}^A \left(z J \bar{m} \right)_{ext} + \beta \bar{s}^A \left(\sum_\mu J \bar{s_\mu} \right)_{int} \right] \right\}}{\mathrm{tr}\left\{ \exp\left[\beta \bar{s}^A \left(z J \bar{m} \right)_{ext} + \beta \bar{s}^A \left(\sum_\mu J \bar{s_\mu} \right)_{int} \right] \right\}}, \tag{6.2}$$

where $\left(z J \bar{m} \right)_{ext} = z_{ext} J_{ext} \left(m^A, \alpha n_0^A \right)$, and he sum over μ accounts for the internal contributions from all neighbors within the network, considering three possible opinion states for belief A and its neighbors. Note that, since the external network is fully-connected, we take $z_{ext} = N - 1$, and therefore $J_{ext} = N - 1$ to ensure the preservation of energy extensivity. In the case of the clique and the ring, the sum in the second term of the exponential functions runs over the same number of neighbors, $c - 1$, for any belief, thus one can take the common factor $(c - 1)J_{int} = 1$.

Table 6.1 shows the magnetization approximations for internal networks ranging from 2 to 5 beliefs. Internal energy contributions to belief A remain consistent for ring agents, regardless of the total number of beliefs, since its number of internal neighbors is always two. However, the heterogeneous number of connections for the star agents is not accounted in Equation 6.2, which yields to the same results for clique than for star agents. Belief propagation could be used to take

into account that belief A is a hub in star agents, but this calculation is out of the scope of this thesis.

6.3.2 - Order parameters versus temperature

Here we present results for the order parameters as a function of the temperature for different numbers of internal beliefs. We compare MFA and MMC results analyzing two values for the neutrality parameter: $\alpha = 0$, which is below the tricritical point obtained in Section 2.2, and $\alpha = 0.85$, which is above.

Results for $\alpha = 0$

When $\alpha = 0$, all topologies exhibit a second-order phase transition for the number of internal beliefs studied. As observed for ER graphs (see Chapter 3), the MFA underestimates the critical temperature value, yet it qualitatively captures the influence of additional beliefs on it for the clique and ring internal topologies, as shown in Figure 6.3-a,b)).

The addition of a second belief results in a considerable increase in the critical temperature $\Delta T\,(c1 \to 2)$ compared to the single belief case analyzed in Chapter 2 (see Figure 6.3-a). The increment caused by adding a third belief $\Delta T\,(c2 \to 3)$ is smaller than $\Delta T\,(c1 \to 2)$ for the triangle agents and slightly lower for the 3-node open chain agents.

Further additions of beliefs do not affect the ring agents and all order parameter curves in Figure 6.3-b collapse, both for the MMC simulations and the MFA. However, for $c = 10$ the magnetization exhibits larger fluctuations at low temperature. This effect is due to the tendency of nodes in a circular topology to form clusters separated by boundaries. Although these boundaries are destined to annihilate when the number of beliefs is finite, the annihilation process significantly lengthens as the number of nodes in the circle increases.

On the other hand, clique and star agents continue to increase their T_c when adding more beliefs to each agent, although at different rates, as shown both in Figure 6.3-a),c), and in Figure 6.4.

The behavior of peripheral belief B in star agents is different. Magnetization curves for any number of beliefs c coincide at low temperatures, reflecting the fact that peripheral beliefs have only one internal link to the central agent, regardless of the size of the internal network. However, approaching the critical point, where all correlation lengths are significant, the curves diverge to match the critical temperature of belief A, and the system undergoes the transition as a whole.

Table 6.1: MFA Order Parameters for Different Cases

2 Beliefs

$$m^A = \frac{2\sinh(\beta m^A)(2\cosh\beta + 1)}{2\cosh(\beta m^A)(2\cosh\beta + 1) + \exp(\alpha^2\beta n_0^A)(\exp(\alpha^2\beta) + 2)}$$
$$n_0^A = \frac{\exp(\alpha^2\beta n_0^A)(\exp(\alpha^2\beta) + 2)}{2\cosh(\beta m^A)(2\cosh\beta + 1) + \exp(\alpha^2\beta n_0^A)(\exp(\alpha^2\beta) + 2)}$$

Triangle (Ring)

$$m^A = \frac{2\sinh(\beta m^A)\left[2\cosh(2\beta) + 4\cosh\beta + 3\right]}{2\cosh(\beta m^A)[2\cosh(2\beta) + 4\cosh\beta + 3] + \exp(\alpha^2\beta n_0^A)(\exp(2\alpha^2\beta) + 4\exp(\alpha^2\beta) + 4)}$$
$$n_0^A = \frac{\exp(\alpha^2\beta n_0^A)(\exp(2\alpha^2\beta) + 4\exp(\alpha^2\beta) + 4)}{2\cosh(\beta m^A)[2\cosh(2\beta) + 4\cosh\beta + 3] + \exp(\alpha^2\beta n_0^A)(\exp(2\alpha^2\beta) + 4\exp(\alpha^2\beta) + 4)}$$

Clique 4 Beliefs

$$m^A = \frac{2\sinh(\beta m^A)\left[2\cosh(3\beta) + 6\cosh(2\beta) + 12\cosh\beta + 7\right]}{Den_4}$$
$$n_0^A = \frac{\exp(\alpha^2\beta n_0^A)\left[\exp\left(3\alpha^2\beta\right) + 6\exp\left(2\alpha^2\beta\right) + 12\exp\left(\alpha^2\beta\right) + 8\right]}{Den_4}$$
$$Den_4 = 2\cosh(\beta m^A)\left[2\cosh(3\beta) + 6\cosh(2\beta) + 12\cosh\beta + 7\right] + \\ + \exp(\alpha^2\beta n_0^A)\left[\exp\left(3\alpha^2\beta\right) + 6\exp\left(2\alpha^2\beta\right) + 12\exp\left(\alpha^2\beta\right) + 8\right]$$

Clique 5 Beliefs

$$m^A = \frac{2\sinh(\beta m^A)\left[2\cosh(4\beta) + 8\cosh(3\beta) + 20\cosh(2\beta) + 64\cosh\beta + 19\right]}{Den_5}$$
$$n_0^A = \frac{2\exp(\alpha^2\beta n_0^A)\left[\exp\left(4\alpha^2\beta\right) + 4\exp\left(3\alpha^2\beta\right) + 12\exp\left(2\alpha^2\beta\right) + 16\exp\left(\alpha^2\beta\right) + 8\right]}{Den_5}$$
$$Den_5 = 2\cosh(\beta m^A)\left[2\cosh(4\beta) + 8\cosh(3\beta) + 20\cosh(2\beta) + 64\cosh\beta + 19\right] + \\ + 2\exp(\alpha^2\beta n_0^A)\left[\exp\left(4\alpha^2\beta\right) + 4\exp\left(3\alpha^2\beta\right) + 12\exp\left(2\alpha^2\beta\right) + 16\exp\left(\alpha^2\beta\right) + 8\right]$$

Results for n_0 at $\alpha = 0$ are not relevant, as they relate solely to thermal effects and are similar to those obtained in Section 2.2, but with the shifted critical temperature for each case.

Figure 6.4 displays the critical temperature for $\alpha = 0$ as a function of the number of internal beliefs. The results were obtained using MMC simulations by identifying the midpoint between the temperatures corresponding to the magnetization segment with the minimum slope.

The critical temperature for the clique increases monotonically with the number of internal beliefs within the interval $c \in [4, 10]$, though the increments diminish as c increases, presumably reaching a saturation point at or slightly beyond $c \approx 10$. In contrast, T_c for the star agents grows linearly as $T_c = 0.04c + 1.06$. Peripheral beliefs act as a support to the core belief A, making star agents behave as "zealots" for $\alpha = 0$, if the number of nodes in the internal network is large enough. The case with $c = 3$, corresponding to a 3-beliefs open chain, deviates from this linear pattern; in fact $T_c(c = 3)$ for the star topology is slightly lower than for the triangle, indicating that it is easier to destabilize consensus in the 3-beliefs open chain.

Results for $\alpha = 0.85$

When all nodes have the same degree $k_i = z$, which holds true for both ring and clique agents, all beliefs share the same magnetization such that $m_\mu = m$ and the fraction of neutral beliefs $n_{0_\mu} = n_0$, for all $\mu \in \{A, B, C, \ldots\}$. Consequently, the mean-field free-energy function $\mathcal{L}(m, n, \beta) \equiv (H_{\mathrm{MF}} - \beta^{-1} S_{\mathrm{MF}})/N$ simplifies to:

$$\begin{aligned} \mathcal{L} \quad (m, n, \beta) &= -\frac{z}{2}(m^2 + \alpha^2 n^2) + z\alpha^2 n \\ + \quad \frac{1}{\beta}&\left[\frac{n+m}{2}\ln\frac{n+m}{2} + \frac{n-m}{2}\ln\frac{n-m}{2} + (1-n)\ln(1-n)\right] \end{aligned} \tag{6.3}$$

By solving the equations presented in Table 6.1, both with and without the constraint that $m = 0$, we can determine the free energy associated with both minima. In doing so, we observe a discontinuity in the order parameters corresponding to the lowest free energy, indicative of a first-order transition, for both clique and ring agents regardless of the number of beliefs. The transition temperature rises with the number of beliefs in the case of the clique. However, when compared to the single-belief scenario, the first-order transition at $\alpha = 0.85$ is predicted to occur at a temperature that lies between which is found with MFA for two beliefs and for the triangle. This discrepancy is again attributed to the mean-field approximation's underestimation of the critical temperature.

Monte Carlo results also indicate a jump to zero magnetization, more abrupt than that observed for $\alpha = 0$, occurring at a lower temperature $T \approx 1$. On the

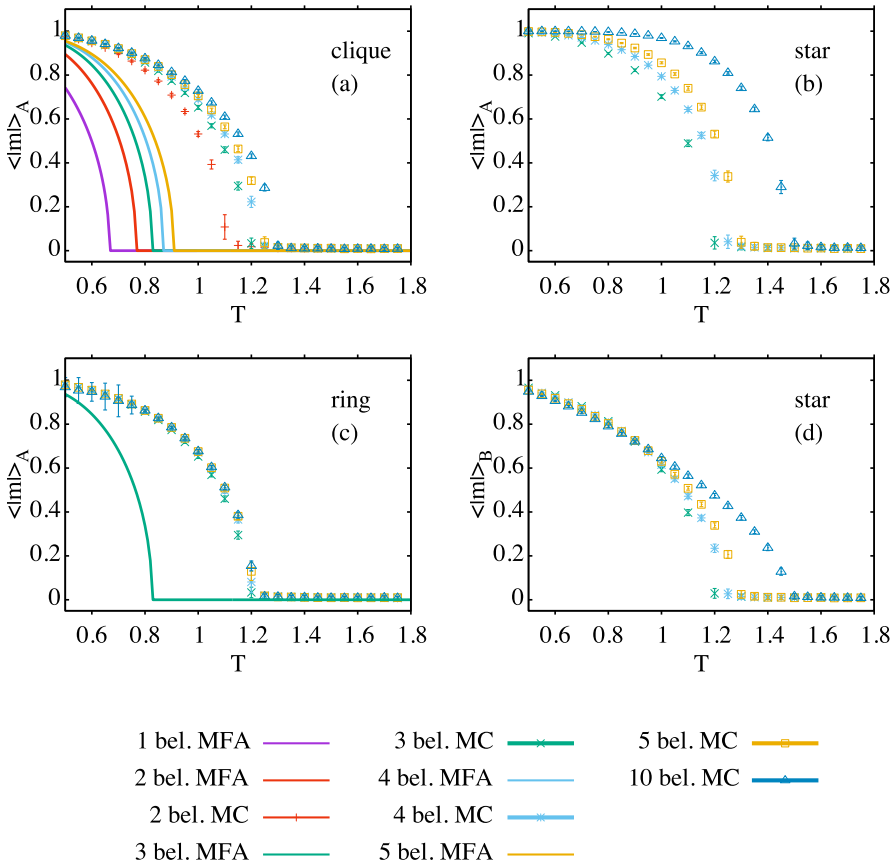

Figure 6.3: Magnetization curves for a particular belief as a function of temperature for each internal topology and different numbers of internal beliefs. Results obtained with MMC simulations for a system of $N = 10^4$ agents, neutrality parameter $\alpha = 0$, averaged over 100 repetitions with $c \cdot 10^4$ MMC steps. Comparisons with MFA results are shown for the clique and the ring.

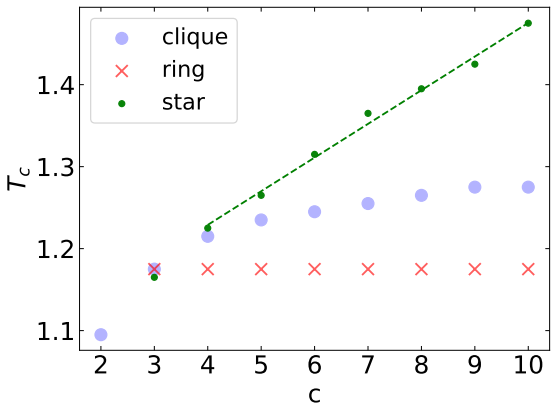

Figure 6.4: Critical temperature versus number of beliefs when $\alpha = 0$ for the clique (blue circles), the ring (red crosses), and the star-like (green dots) agent types. Results obtained averaging 100 repetitions with systems of $N = 10^4$ agents.

other hand, atsimulations tend to get trapped in a local minimum corresponding to neutral consensus, except for $c = 2$, which gets to the global minimum at an extremist consensus. At high temperatures, yet below the first-order transition threshold, the system initially trapped in neutral consensus can overcome the energy barrier separating it from the ground state, leading to a dynamical transition towards polarized consensus. Generally, this dynamic transition becomes sharper and happens at higher temperatures as the number of internal beliefs increases.

Transition temperature towards the disordered paramagnetic state in clique agents increases with the number of internal beliefs similarly to whats is observed for $\alpha = 0$, suggesting a saturation point close to 1 around $c \approx 10$. Likewise, the temperature at which the dynamical shift from neutral to extremist consensus occurs also grows with c, and probably approaches a saturation value. The temperature rise from 4 to 5 beliefs i is comparable to that from 5 to 10 beliefs, yet the precise saturation point for this transition temperature remains undetermined.

Ring agents exhibit the anticipated convergence of all results into the triangle one, except for the dynamical transition, which occurs at a temperature 0.1 k_B units higher for all ring inner topologies from $c = 4$ onwards.

For star agents, MMC results present more variations compared to the behavior at $\alpha = 0$. Notably, the decay to zero magnetization now occurs at a constant $T = 1$ for any number of beliefs, and it is particularly abrupt for $c = 10$. The dynamical transition curves, occurring at identical temperatures for both the central belief A and the peripheral belief B, solapate for the 3-node open chain and

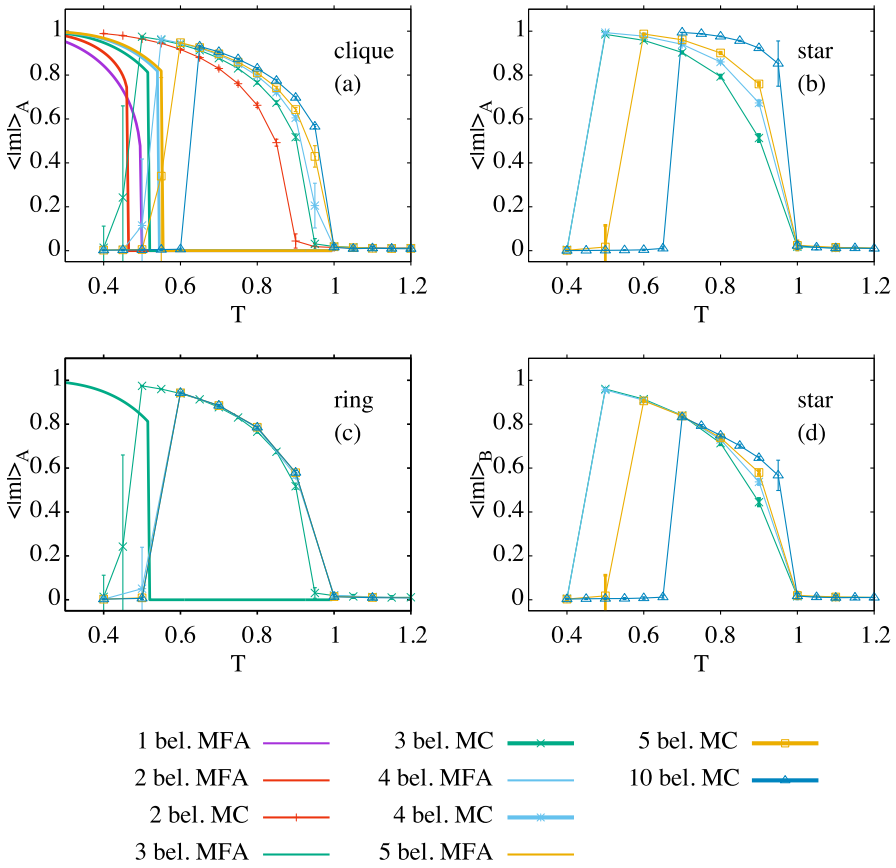

Figure 6.5: Magnetization curves for a particular belief as a function of temperature for each internal topology, and a different number of internal beliefs. Results obtained with MMC simulations for a system of $N = 10^4$ agents, with a neutrality parameter $\alpha = 0.85$, and averaged over 100 repetitions. The curves are compared with MFA results for the clique and the ring topologies.

the 4-node star. As c increases, the jump from neutral to extremist consensus happens at higher temperatures, and, as in the case of the ring agents, results suggest that this transition temperature may saturate at some c value.

6.4

Zero temperature behavior

At zero temperature, the system becomes trapped in a collection of metastable states, the nature of which depends on the system's parameters. For $\alpha = 0.85$, all beliefs reach the central state, leading to a global neutral consensus. However, at $\alpha = 0$, the system gets trapped in states with mixtures of extremist nodes, akin to the behavior seen in Erdős-Rényi graphs (see Chapter 3). Clique and star agents reach a steady state with two factions of agents who have reached an internal agreement in opposite extremist opinions, characterized by internal energy $E_{\text{int}} = -(c-1)/2$. Once internally aligned, they cannot overcome the energy barriers that would lead the dynamics to global polarized consensus. The same behavior is observed for ring agents with a low number of internal beliefs c. For these systems, which end up the simulation with all agents in internal agreement, the distribution of magnetization for belief A is the same as for any other belief and the entire system. Ring agents with larger c, on the other hand, exhibit different behavior that requires extra analysis.

In Figure 6.6 We present the distributions for the global magnetization obtained by conducting 2000 simulations for each topology with a different number of internal beliefs allowing the system to evolve for $c \cdot 10^4$ MMC steps.

The clique agents display a first peak around $|m| = 0$ followed by subsequent peaks of decreasing heights. As c increases, these later maxima shift toward lower magnetization values, suggesting that, with a sufficiently large number of beliefs, only the peak at $|m| = 0$ will persist, impliying an outcome with two opposite factions of roughly the same size in each extreme opinion.

Interestingly, for $c = 7$ the lowest peak is not located at $|m| = 0$, but at a slightly higher value; moreover, star agents also exhibit a peak in the magnetization distribution at $|m| = 0$ for $c = 4$ and $c = 10$, but not for $c = 7$. This pattern may be attributed to the fact that 7 is an odd number while 4 and 10 are even, suggesting that this detail is a minor deviation that does not significantly impact the broader interpretation of the system's macroscopic behavior.

Ring agents have a more complicated behavior. Since, the critical temperature for the one-dimensional chain is zero [(54)], ring agents do not reach internal consensus for $\alpha = 0$ unless the number of beliefs is very small. It's important to

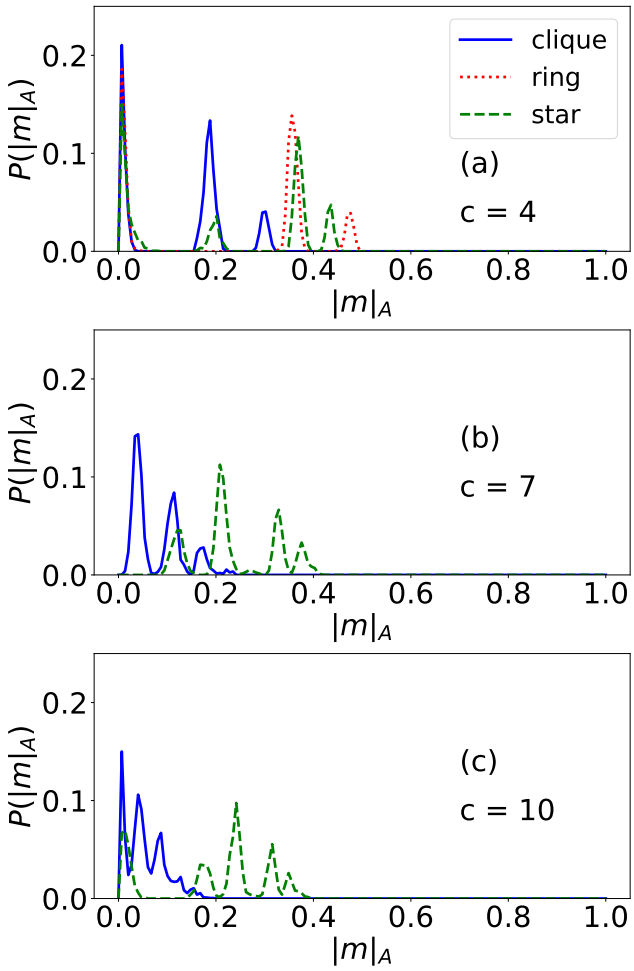

Figure 6.6: Histograms of the magnetization of belief A for systems of agents with $c = 4, 7, 10$ beliefs for (a) clique, (b) ring, and (c) star-like agent types. Results obtained from 10^4 repetitions for sytems of $N = 10^4$ agents with $\alpha = 0$, at zero temperature.

note that due to the normalization of internal and external coupling constants, this behavior is not attributable to the lesser number of connections per belief per se, but to the connection pattern of internal links.

For $c = 4$ (Figure 6.6a), their behavior closely resembles that of the clique agents, with the highest peak at $|m_A| = 0$ and two subsequent peaks at larger magnetization values. The heights of these maxima are roughly the same as those of the 4-node clique agents, but the magnetization values corresponding to the second and third peaks are larger for the ring agents.

For $c = 7$ and 10, a significant proportion of ring agents conclude the simulation in a situation of cognitive dissonance. The internal energy distributions display two peaks (see Figure 6.7a)): one at the minimum corresponding to internal coherence $E_{\text{int}} = -c/2$, and another at $E_{\text{int}} = 2 - c/2$, indicative of two internal clusters of opposing opinions separated by two domain boundaries, each contributing with an energy cost of 1. The evolution of rings towards internal agreement takes place via a domain-growth process (known as coarsening in statistical physics), in which the walls between domains of different signs perform a random walk. For $c = 7$, we observe that the lower energy peak is more prominent than the higher energy one, whereas for $c = 10$, they are of equal magnitude. It is plausible that with an increase in the number of internal beliefs, the peak at $E_{\text{int}} = -c/2$ may vanish, and new peaks at higher energies may emerge due to the formation of more than two belief domains within the rings.

In panel b) of Figure 6.7, we examine the agents corresponding to the first peak by displaying the magnetization distribution for belief A, similar to what was done in Figure 6.6, but counting only those agents that have achieved internal agreement. The magnetization peaks appear noisier compared to those from systems where all agents reach internal coherence. With an increase in c, the magnetization peaks for ring agents approach $|m| = 1$, suggesting their increasing likelihood of reaching a global extremist consensus as the number of internal beliefs grows. Same as for clique and star agents, the peak at zero magnetization does not emerge for $c = 7$, yet it does for $c = 4, 10$.

In panel c) of Figure 6.7, the distribution of the internal number of beliefs in the $\sigma_i = +1$ state is presented (the distribution for the -1 state is identical due to the model's symmetry). The pronounced peaks at 0 and c correspond to agents in internal agreement in both opposite states, indicating that most agents achieve a coherent internal state. Intermediate peaks are associated with agents having two internal clusters in opposing states, and their heights decrease monotonically as they approach $n_1 = c/2$. Given that the number of possible configurations compatible with two equally sized belief clusters is larger than for clusters of different sizes, the lower central maxima are not due to combinatorial probabilities. Instead, this effect arises because agents that achieve internal coherence influ-

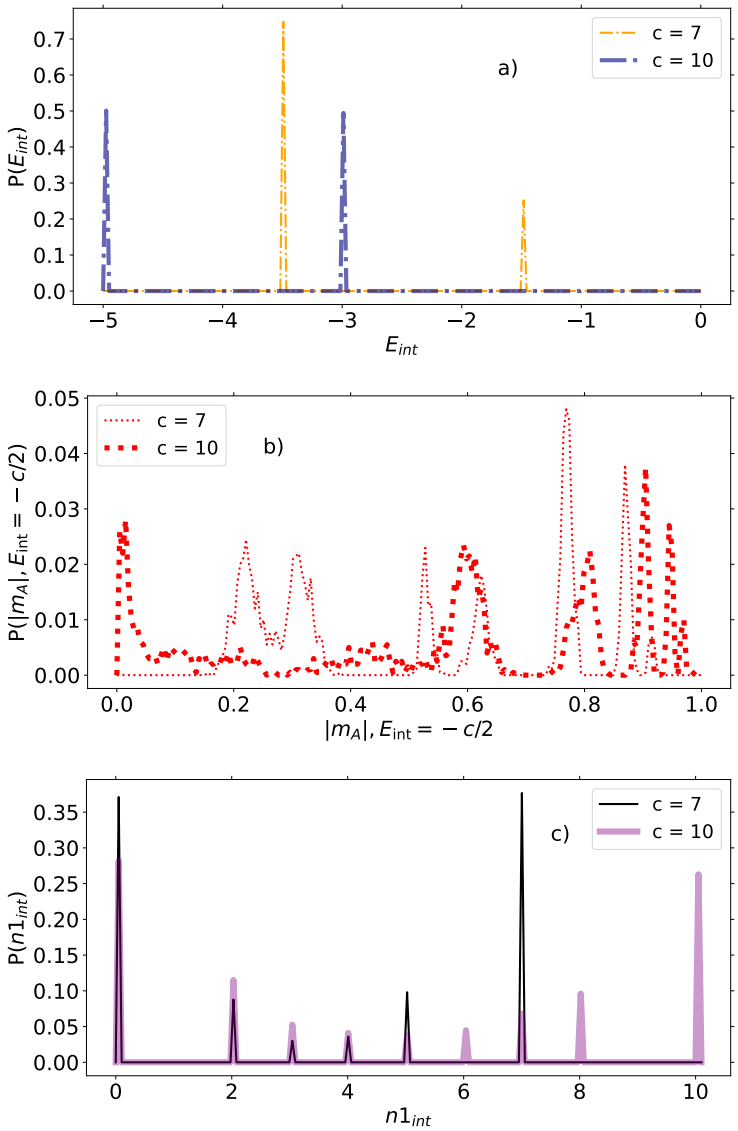

Figure 6.7: Distribution of internal parameters per agent for ring agents at temperature $T = 0$, neutrality parameter $\alpha = 0$, and number of internal beliefs $c = 7, 10$. In panel (a) distribution probability fo the internal energy, in panel (b) distribution of magnetization for the agents that reach internal agreement and in panel (c) distribution of number of internal beliefs in state $+1$. Results obtained for systems of $N = 10^4$ agents and 2000 simulations with different initial conditions.

ence other agents to adopt higher internal magnetizations. The distribution of extremist beliefs inside each agent becomes flatter as c increases because the time required for internal consensus in the ring grows with the number of nodes, thus we expect that it tends to a uniform distribution for larger c. There are no peaks at $n_1 = 1$ or $n_1 = -1$ because such values would correspond to a single internal belief in a state opposite to the rest of the beliefs within that agent, which would energetically favor a change in the state of belief B.

It is worth remarking that all distributions in Figure 6.7 remain unchanged even when the system evolves for a number of MMC steps ten times larger; the states reached by ring agents with a large number of internal beliefs are stable. The reason is that once a particular belief—such as belief B—achieves a majority of positive state across all agents, those agents with neighboring beliefs A and C also in the +1 state will not accept any change for belief B, even if the rest of their internal beliefs are in the negative state. Consequently, the configuration becomes frozen, as happens with the agents that achieve internal coherence.

Star agents exhibit a series of peaks similar to those of the clique agents; however, unlike cliques, their maxima do not consistently converge toward $|m| = 0$ when c increases, nor is the tallest peak the one with the lowest magnetization value. The peaks for star agents are found within the range $|m| \in [0, 0.5]$ and maintain a similar profile across all studied numbers of beliefs, being the only remarkable difference is the absence of a peak at zero magnetization for $c = 7$. Star agents are more likely than cliques to reach a steady state in a polarized, bipartite scenario with a dominant majority of one of the two extremist factions, rather than in a situation with two equally sized opposing groups.

6.5

Mixed topologies

We have seen that agents exhibit diverse behaviors depending on the topology connecting their internal beliefs. A natural question arises: do agents with a specific inner topology maintain consistent behavior when interacting with different types of agents? To address this, we have conducted Monte Carlo simulations, mixing two types of agents in equal proportions. Instead of the order parameter for a particular belief, we focus on the internal order parameters of the agents. We present results at temperatures near the transitions, where agents exhibit more behavioral diversity, and we choose the largest number of internal beliefs considered in previous sections, $c = 10$, which presents the greater differences among internal topologies.

6.5.1 - Second-order transition

For $\alpha = 0$ (Figure 6.8-top row) we present results for $T = 1.2$, which is close to the second-order transition. Distributions are generally broad, presenting all internal magnetization values, with medians at 4 or 5, with star agents exhibiting distributions more sharply peaked around the median. At $\alpha = 0$, the distribution of neutral internal beliefs is only due to thermal fluctuations and remains approximately the same across all topologies, regardless of whether agents are isolated or mixed with another type. The median of $N_{0_{\text{int}}}$ is 3 (2 for stars mixed with rings), which is roughly $c/3$, the value expected as $T \to \infty$.

We observe that when mixed with ring agents (blue-shaded plot), clique agents display slightly lower internal magnetizations compared to when they are alone (black line), indicating that ring agents lead to equalize the number of internal beliefs in states $+1$ and -1 inside the cliques. Taking into account that $N_{0_{\text{int}}}$ is around $c/3$, this distribution of internal beliefs for clique agents closer to having one third of their beliefs in each possible state of the model, indicative of maximal cognitive dissonance. By contrast, star agents (pink-shaded plot) lead to higher internal magnetization, promoting greater internal coherence and polarization towards one of the extreme opinions in cliques.

Rings, with their tendency to form internal clusters of opposite magnetizations of similar size, exhibit a distribution skewed towards low internal magnetization when isolated. Presumably, the neutral beliefs are situated at the boundaries between the extremist clusters, facilitating their separation, since the energy cost of a chain segment $\{+1 \cdots +1, 0, -1 \cdots -1\}$ is equivalent to that of $\{+1 \cdots +1, -1 \cdots -1\}$. Both clique and star agents shift the rings towards higher M_{int} (although star agents have a stronger effect), pushing the rings closer to a state of maximal cognitive dissonance.

Star agents are the only ones that do not experience the influence of being mixed with another agent type. Their "zealot" behavior at $\alpha = 0$ remains evident in mixed simulations as the shape of their internal order parameter distribution stays consistent whether they are alone or mixed with cliques or rings. They maintain $M_{\text{int}} = 5$, and the distribution is slightly skewed towards higher magnetizations, indicating a stronger internal preference for one of the extremist states.

6.5.2 - First-order and Dynamical transitions

For $\alpha = 0.85$ (Figure 6.8-bottom row), we chose a temperature $T = 0.63$ corresponding to the change in the basins of attraction. This represents a dynamical, not an equilibrium, effect. Here, we observe distributions that are more skewed towards one of the two limits: 0 or 10. The values for $N_{0_{\text{int}}}$ are no longer merely thermal fluctuations, but complement M_{int}, meaning that when $M_{\text{int}} = 0$, it is

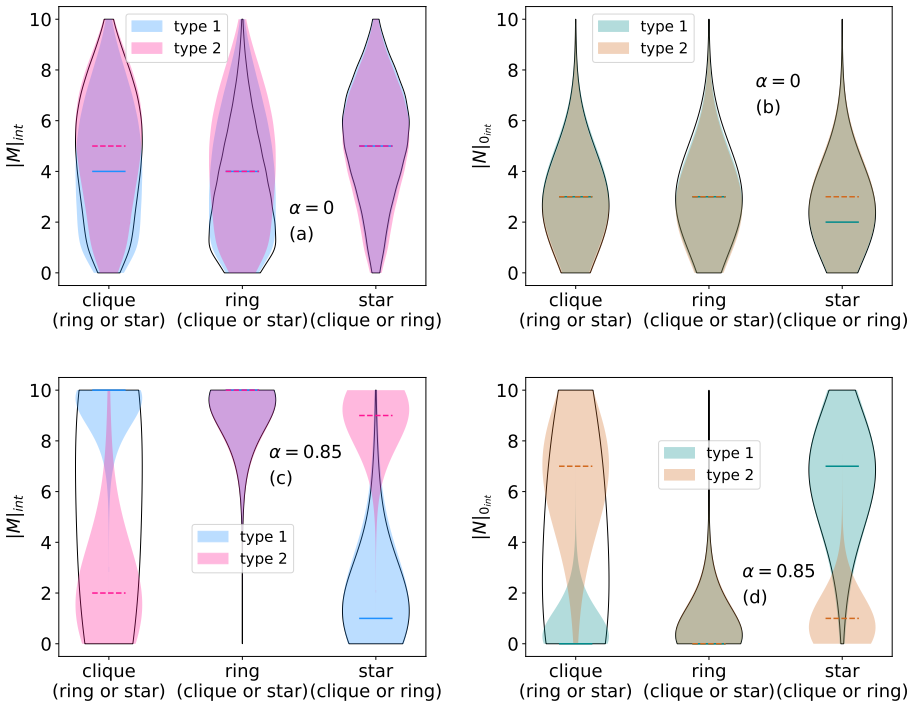

Figure 6.8: Distribution of the absolute values of internal magnetization (first column) and the number of internal neutral beliefs (second column) for agents of each topology when mixed with another type in a 50% proportion. Values for internal magnetization are represented in blue (and green for neutral beliefs) when agents were mixed with the first type listed in parentheses beneath them, and in pink (and orange for neutral beliefs) when mixed with the second type. Lines indicate the medians. Results were obtained from 10^4 repetitions with systems of $N = 10^4$ agents at a temperature of $T = 1.2$ and neutrality parameter $\alpha = 0$ (top row), and at $T = 0.63$ and $\alpha = 0.85$ (bottom row).

not due to an equal number of opposite beliefs, but because there is neutral internal agreement. In this scenario, rings, rather than stars, are the dominant structure.

When cliques are alone, they display an almost flat distribution for both order parameters, indicating that any number of beliefs from 0 to 10 are equally likely to be in any of the three possible states. However, when mixed with rings, they become entirely extremist, with M_{int} close to $c = 10$ and $N_{0_{\text{int}}}$ around zero. In fact, they adopt the same distribution as the rings alone. The opposite effect is observed when cliques are mixed with stars; here, cliques assume the same order parameter distributions as the stars alone, characterized by a median $N_{0_{\text{int}}}$ of 7 and a low value for M_{int}.

As mentioned before, rings, characterized by high internal magnetization with a median equal to $c = 10$ and a median of zero for internal neutral beliefs, are not affected by mixing with cliques or stars. Their system maintains a ferromagnetic global phase, corresponding to the ground state of the system, despite the high value of the neutrality parameter and any perturbations caused by mixing with other agents. This stability makes them a catalyst for causing other types to converge towards the ground extremist global minima.

Star agents, when alone, have low internal magnetization values, with a median of 1, and are mostly neutral. Mixing them with clique agents does not alter their internal order parameter distributions; however, as previously mentioned, rings pull them towards extremism, completely changing their behavior.

6.6

Conclusions

The networks discussed in this chapter can be seen as a special case of graphs with well-defined community structures. The interpretability of the modular structure at two operational levels is valuable from a qualitative perspective and can potentially be extended to other multilevel systems. Despite these graphs being non-trivial, the selection of simple symmetrical structures for the internal and external networks allows for an analytical analysis of the system.

When the neutrality parameter α is low, in the region of the second-order transition, adding more belief nodes to each agent generally increases the critical temperature. This increase in T_c may reach saturation at an upper bound number of beliefs, depending on the topology of the internal belief network. Furthermore, additional beliefs complicate the energy landscape, steering the system dynamics toward metastable states at low temperatures.

With high α, on the other hand, central agents are not merely undecided individuals but play a significant role in the opinion-spreading process. When the neutrality parameter exceeds the tricritical point for one internal belief, all topologies undergo a first-order transition at a temperature that depends solely on α, except for 2-belief and triangle agents whose critical temperature is slightly lower. Furthermore, all systems exhibit neutral consensus as a dynamic attractor at low temperatures, but they transition to global energy minimum corresponding to the extremist consensus at a given temperature, prior to the first-order transition. This dynamical transition temperature is influenced by both the internal topology and the number of beliefs.

Mixing agents with different internal topologies in the same simulation significantly impacts their behavior. Agents far from a transition point are more likely to retain their behavior when mixed with agents closer to their critical temperature. These stable agents may influence the behavior of the other type, pulling it closer to their own. Overall, when mixing at $\alpha = 0.85$, close to the temperature corresponding to the change in dynamical basins of attraction, the impact is more significant than when close to the second-order phase transition at $\alpha = 0$. In general, we expect that the phenomena related to mixing agent types strongly depend on the selected temperature and neutrality parameter, further exploration is necessary to fully understand how these parameters influence each system's behavior.

In clique agents, internal all beliefs support each other. With increasing c, the order parameters approach a saturated regime where agents act as a supernode. Their beliefs are tightly coherent, functioning as a single unit, leading to a extremist bipartisan situation at zero temperature and low α.

When in their equilibrium state, rings with any number of internal beliefs are effectively equivalent to triangles. However, at low temperatures, $\alpha = 0$ and large c values, they exhibit a more complex behavior characterized by local minima and internal cognitive dissonance. This difficulty in reaching internal consensus quickly enhances the influence of peer pressure and pushes the system towards a global polarized consensus. Therefore, when $\alpha = 0$, ring agents are most likely to reach high levels of global extremist consensus at $T = 0$, but at the expense of maintaining a subset of agents in a state of internal cognitive dissonance.

Star agents, with a large enough number of peripheral beliefs supporting their core beliefs, act as "zealots" and maintain a global extremist consensus phase that is difficult to destabilize. Even when mixed with other agent types near the transition temperature, they remain uninfluenced by their presence, retaining the same internal order parameters as if isolated. However, this is only true for low α. As neutral beliefs gain strength, star agents undergo a first-order phase transition just at the same temperature as cliques or rings. Moreover, during the dynamic

shift from neutral to extremist consensus, it is the star agents that are influenced by the rings, which dominate the dynamics when mixed with other types in this parameter region.

Besides the possible social interpretation of this study, its results are also significant due to their novelty in the realm of Ising-based models on multilayer networks. This area of study has been considered in a few previous works [(76; 85; 29; 95; 179)], yet the existing body of literature is still limited. It could be interesting to extend this work to include other structures for the external network, such as scale-free or modular graphs, and examine their impact on the phase diagram and the dynamical attractors of the system.

To summarize, the network of networks multilayer approach is still in its initial phase of development and holds great potential for application across various fields, ranging from biological to technical. Incorporating asymmetric, weighted, or even complex adjacency matrices and embedding other dynamics could lead to interesting findings with wide applicability.

Conclusions

CHAPTER 7

Conclusions and outlook

This final chapter provides an overview of the research presented in this thesis and the key findings from all chapters, highlighting some open questions that would require further investigation. Structurally, the chapter is segmented into three parts. The initial two sections maintain the organization of the thesis's main content, with discussions on Chapters 2 to 4 grouped together, followed by an analysis of Chapters 5 and 6. It concludes with a general summary that closes the thesis.

7.1

Remarks on Single Layer topologies

Connections are at the core of complex systems, and humans are perhaps some of the most elusive agents to model. Yet, it can be advantageous for society to understand why and how relationships shape our ideas both individually and collectively. When designing models, we aim to capture some relevant aspects of human behavior to understand a problem, so it seems natural that we first focus on extracting conclusions about the model's features. However, considering its interplay with temporal or structural features is a logical extension that exploits the model in a more realistic context.

An extensive topological study of an opinion model like the one considered in this work is useful from various perspectives. It ranges from isolating the essential structural properties that contribute to opinion spreading and consensus formation to extending the model for a multiscale description of social phenomena.

The model has the potential to describe a large number of social situations. Its rich energy landscape, especially when the topology is non-trivial, implies mul-

tiple dynamic attractors that depend on both the connection patterns and the system's parameters. This allows for the identification of key aspects that enhance the probability of observing a specific social phenomenon, such as the formation of a central consensus—even when extremist agents have stronger convictions, represented by larger contributions to the system's energy—or the fragmentation of the population into opinion clusters that can vary in size even within the same topology, depending on the temperature or neutrality parameter values. For instance, at low temperatures—where agents pay significant attention to their neighbors' opinions over other factors—individuals in different communities belong to separate opinion groups. However, they can reach a global agreement with an increase in temperature.

The mean-field analysis of the system's transitions demonstrates that the model can reproduce various scenarios with social interpretability under specific parameter conditions. The results provide insights into how a neutral faction behaves and how temperature influences the system in different ways, depending on the level of neutral engagement in opinion transmission. Low neutral conviction leads to continuous transitions from extremist consensus to disorder, driven by temperature. Surprisingly, central consensus can become a dynamics attractor, even when neutral convictions are lower than those held by extremists, highlighting the significant role a neutral party can play. These intermediate levels of neutral conviction are associated with jumps from neutral consensus to extremist consensus and then to disorder again, with the coexistence of ordered and disordered phases.

A three-state opinion spreading dynamics on a network can be metaphorically visualized as three fluids moving through a system of pipes and cavities. In this analogy, communities are akin to cavities where fluids (opinions) tend to accumulate due to larger cross-sectional areas, while inter-community links are represented by narrower pipes. Both temperature and neutrality parameters modify the 'viscosity' of these fluids, affecting how easily each opinion state flows; temperature impacts all states uniformly, whereas neutrality specifically facilitates the flow of neutral opinions over extremist ones. Although this analogy simplifies complex interactions and neglects the conservation of matter—unless sinks and sources are introduced at each node—it provides a heuristic model to conceptualize and potentially explore new questions regarding dynamic processes on networks, including the investigation of structural and entropic barriers [(160)]. It is important to note that this analogy serves purely as a conceptual tool and should not be interpreted as a strict physical representation of the dynamics of opinions or fluids.

When applied to modular and real networks, our model primarily serves as a tool to understand how opinion groups emerge as a consequence of structure, temperature, and dynamics. It also acts secondarily as a multiresolution community

detection method, which could be extended to include signed and/or weighted networks, potentially offering further insights.

Regarding real-world applications, Twitter networks represent just an initial approach to analyzing social structures. A more comprehensive analysis using additional real datasets could yield further insights. Moreover, comparing this model with other opinion models on the same real networks could provide a complementary cross-view analysis of model-topology interactions, further elucidating how model construction and topological effects interplay. When it comes to calibrating the model with real data, it is advantageous that the neutrality parameter models relative conviction values, rather than absolutes ones.

7.2

Remarks on temporal and multilayer networks

Coevolving opinion states and network links offer a fresh reinterpretation of the model. With the addition of self-propulsion, the model enters into a non-equilibrium regime, which presents more complex analytical challenges. Nevertheless, the interplay between neighborhood selection and opinion formation has a significant influence on opinion dynamics and remains a topic of interest in the sociophysics literature [(96; 109)].

Movement patterns can disrupt established opinion groups, going beyond the static community structure of a network and introducing a temporal dimension to the analysis. Consequently, consensus time becomes more significant, demonstrating that resonating patterns between opinion changes and link reconfiguration rates can significantly accelerate the path to consensus.

When the model combines selective rewiring processes with persistence in like-minded neighborhoods, it can achieve a local consensus outcome, characterized by groups of agents who share the same opinion but differ from one group to another. In these scenarios, polarization exhibits non-monotonic behaviors, influenced both by the agents' velocity in the physical plane and the conviction of neutral agents. Generally, polarized clusters, when formed, are larger than neutral ones; however, it is the neutral consensus, the outcome that is achieved more quickly.

The network of networks approach represents the most state-of-the-art project of this thesis; therefore, it involves significant simplifications in both external and internal network structures. However, we expect it to serve as a tool for understanding nested complex networks that may mimic multiscale system structures. Coarse-graining is an important step in modeling, yet fine-tuning specific sys-

tem characteristics can help to deepen into different nuances of complex systems. Effectively managing this balance is essential in this context.

Network representations and interpretations of belief systems are a current research line in psychology, and as a result, the availability of data for studying such networks is steadily increasing. It could be interesting to adapt traditional psychological questionnaires and fine-tune them for a more accurate testing of the model.

The multilayer approach offers a versatile framework for analyzing social-belief systems from both bottom-up and top-down perspectives. In a bottom-up approach, researchers can examine the topology of belief networks within population samples to infer the potential impact of their topology on the social dynamics and collective behavior of the aforementioned population. On the other hand, the top-down approach could be used to understand psychological states such as cognitive dissonance through a social analysis of an individual's network of social contacts.

7.3

General concluding remarks

This thesis represents a foundational exploration into the topological aspects of a discrete opinion model, rather than an exhaustive study. Future research may broaden the scope of the model to include weighted networks, signed networks, or networks with complex weights (i.e $[a_{ij}] \in \mathbb{C}$), hinting the next steps in this line of research.

Like covering a vast sphere with small patches, sociophysics literature strives to overlap adequately to afford a comprehensive understanding of the surface, thus building a more general framework and integrating insights from each study.

In decision-making processes, the ability to see the bigger picture can be paramount. A formal, methodical understanding of the interplay across multiple social mechanisms is crucial for achieving meaningful results. These studies stand out for their ability to condense information and results into a format that is manageable and broadens the global perspective. Deliberative processes across political contexts, cooperative enterprises, or neighborhood communities can benefit from the insights derived from these analyses.

Appendices

APPENDIX A

Algorithms

HERE we present a compilation of all algorithms used to generate simulation data used in this thesis.

Algorithm 1 Calculate correlations

Require: multiple initial set of opinions $\{\mathbf{S}_i\}_{initial}$ and the adjacency matrix of the embedding network A_{ij}. Number of repetitions N_{reps}

Ensure: a correlation matrix C_{ij} that contains the number of times a pair of nodes has the same final opinion in the steady state when running a Metropolis algorithm N_{reps} times

set $\hat{C}_{ij} = 0 \; \forall i, i$
set $rep = 0$
repeat
  set initial opinion $\{\mathbf{S_i}\}_{\mathbf{initial}}$ uniformly at random
  call a Metropolis algorithm
  define correlation value for each pair of nodes
  for all $\mathbf{S_i}, \mathbf{S_j} \in \{\mathbf{S_i}\}_{\mathbf{final}}$ with i, j $\in 1, ..., N$ **do**
    if $\mathbf{S_i} = \mathbf{S_j}$ **then**
      $\boldsymbol{\hat{C}_{ij} \leftarrow \hat{C}_{ij} + 1}$
    else
      $\boldsymbol{\hat{C}_{ij} \leftarrow \hat{C}_{ij} - 1}$
    end if
  end for
  $rep \leftarrow rep + 1$
until $rep = N_{reps}$
return $\hat{C}_{ij}/N_{reps}$ as C_{ij} correlation matrix

Algorithm 2 Sorting links

Require: C_{ij} correlation matrix

Ensure: a correlation matrix C_{ij} that contains in the secondary diagonal the pairs of nodes that always share the same opinion in the steady state, regardless of the initial set of opinions. Rows and columns are sorted in such way that the structure of the network can be inferred from its visual representation

set $pivot = C_{ij}$ dimension
sort from lowest to highest correlation value $C_{pivot,node}$ all nodes from 1 to pivot
repeat
  set the new pivot
  for all $i \in C_{pivot,i}$ **do**
    if $C_{pivot,i} = 1$ **then**
      $pivot \leftarrow i - 1$
    end if
  end for
until $pivot = 1$
return C_{ij} sorted correlation matrix

A.0.1 - Mobility pseudocode

Algorithm 3 Perform an agent-based simulation using the three-state opinion model and a random walk

Require: Initial set of opinions $\{\mathbf{S}_i\}_{initial}$ and initial set of positions $\{\mathbf{x}_i\}_{initial}$ The number of Monte Carlo steps N_{steps}. A lower bound tol for the average velocity v

Ensure: Getting to one of the attractors of the dynamics, given a sufficiently large N_{steps}

set $step = 0$
repeat
  set initial opinion $\{\mathbf{S}_i\}_{initial}$ uniformly at random
  set initial positions $\{\mathbf{x}_i\}_{initial}$ uniformly at random
  update agents positions following a random walk with velocity v_i for each agent i, given by each variant of the model
  call a $Metropolis - Hastings$ algorithm
  if $\mathbf{S}_i = +1$ **or** $\mathbf{S}_i = 0$ **or** $\mathbf{S}_i = -1$ **then**
    $global\, consensus =$ **True**
    Break
  else
    if $\langle v_i \rangle < tol$ **then**
      $local\, consensus =$ **True**
      Break
    end if
  end if
until $step = N_{steps}$
return $\{\mathbf{S}_i\}_{final}$ set of final opinion states and number of steps when the simulation stops

APPENDIX B

Bounded Confidence Model

THE bounded confidence model represents a widely adopted framework for modeling opinion dynamics wherein actors have a continuous-valued opinion (O) and interact and approach their positions in the opinion space only if their opinions are within a specified confidence threshold. Here, we propose a framework where the confidence bound is determined by a decreasing function of their emotional arousal, an additional independent variable distinct from the opinion value. Additionally, our framework accounts for agents' ability to broadcast messages, with interactions influencing the timing of each other's message emissions. Our findings underscore the significant role of synchronization in shaping consensus formation. Furthermore, we demonstrate that variable confidence intervals alter the impact of step length when navigating the opinion space, leading to deviations from observations in the traditional Deffuant model [(41; 40; 170; 143; 14)].

B.1

Introduction

Our model is designed to simulate deliberative spaces, involving agents capable of potential interactions without any specific underlying network topology influencing their interaction patterns, which are solely conditioned by the confidence interval. In practice this can involve a joint interpretation of the stroboscopic time and the step longitude, accounting for the average agent displacement after a round of interactions. Scenarios represented by the model can range from a debating chamber, representing a deliberation that takes place over a period of hours with relatively minor displacements between interactions, to discussions extended over a longer period (e.g., virtual discussions spanning months), allowing

ample time for interactions among all participants. The latter situation could be effectively modeled by employing larger alpha values.

We study two different population sizes $N = 200$ and $N = 1000$ living in the same O-EA square with $L = 1$. Larger initial agent density implies increased initial opinion diversity and reduced opinion distance among neighbor agents in the initial state. Since agents are closer they can mediate interactions more easily, however, this scenario might not be very realistic. There are several reasons why the initial distribution of opinions may not be uniform across the opinion space; instead, it might be concentrated around specific areas influenced by past experiences, culture, and other shared traits among individuals. Hence, lower densities may represent not just a smaller number of individuals, but rather a coarse-graining of a larger population initially spread across N positions in the O-EA plane.

We investigate several limit cases (see Table B.1, which enable us to establish connections between our model and previous studies in the field. By employing geometrical reasoning, we derive analytical approximations for the number of final clusters in the synchronized case.

B.2

The Model

We consider a population of N integrate-and-fire oscillators, which are initially uniformly and randomly distributed on an O-EA plane represented in Fig. B.1. Similar to the classical bounded confidence model, opinion is treated as a continuous variable ranging between the two extremes of the x-axis, which, for simplicity and without loss of generality, are set to 0 and 1. We assign to each agent a confidence bound that determines the maximum distance along the opinion axis within which they react to messages from an emitter. Emotional arousal, a continuous variable, also ranging from 0 to 1 and represented on the y-axis, governs the width of each agent's confidence bound through the following relation:

$$d_i = 2d \cdot (1 - EA_i), \tag{B.1}$$

where d is the basal confidence bound of the model that represents the confidence bound of an agent with $EA = 0$. The bounded confidence interval is considered open, hence an agent with $EA = 1$ behaves as a zealot and never reacts to a message, even if the emitter's opinion is exactly the same. Each oscillator is assigned an initial internal phase ϕ_i, uniformly distributed at random between 0 and 1, except for the pairwise and the synchronized limit cases (see Table B.1). The phases increase uniformly with a period T until reaching a maximum value

Table B.1: Table to summarize the variants of the model.

Variants of the model	**Internal phases**	**Time step**
A. Pairwise	Agents have no internal phases	Two agents, one emitter and one receiver, are randomly selected. The receiver moves towards the emitter if they are within the receiver's interaction area.
B. Sequential	Initial random phases $\phi_i \in [0, 1]$.	$\epsilon = 0$ Sequential firing in a consistent decreasing phase order.
C. Broadcasted with local synchronization	Initial random phases $\phi_i \in [0, 1]$.	$\epsilon \neq 0$ Firing in an order dictated by decreasing phases. Phases increase upon message reception causing message cascades and leading to progressive cluster synchronization.
D. Fully synchronized	Initial phases $\phi_i = 1\ \forall i$.	All agents firing at once since the beginning.

of 1, at which point a firing (communication) event occurs, and the phase is reset to zero. During a firing event, an oscillator influences other agents within its confidence area (see Fig. B.1-a) multiplying their phases by a factor $(1 + \epsilon)$. This mechanism induces local synchronization, which can lead to multiple agents emitting messages simultaneously, known as a cascade of messages. Once a pair of oscillators achieve the same phase, they remain synchronized until the end of the simulation. Following phase updating and firing events, all oscillators move towards the barycenter formed by the n emitters located within their confidence bound, following the equation below:

$$\begin{aligned} O_j(t+1) &= O_j(t) + min(\alpha/d_{C_j}, 1)\frac{\sum_{i=1}^{n}(O_i - O_j)}{n+1}, \\ EA_j(t+1) &= EA_j(t) + min(\alpha/d_{C_j}, 1)\frac{\sum_{i=1}^{n}(EA_i - EA_j)}{n+1}, \end{aligned} \tag{B.2}$$

where d_{C_j} is the distance between the j^{th} oscillator and the barycenter formed by the n emitters inside their confidence area. The system evolves until

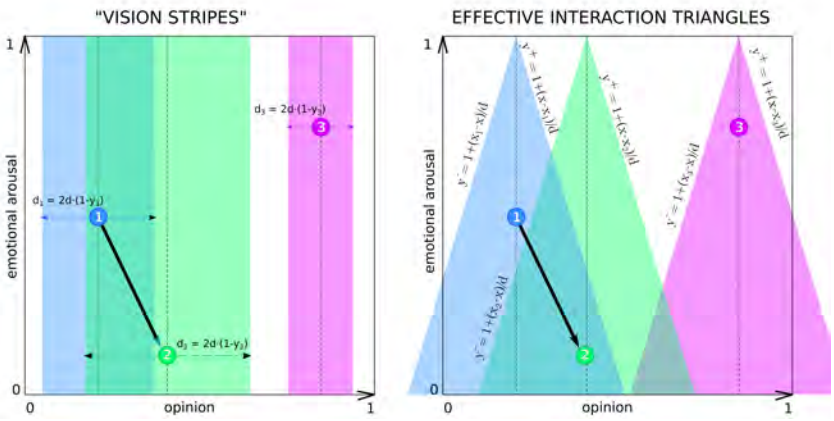

Figure B.1: (Left) Confidence area: the region within an emitter must be located for a receiver at a given opinion position O_j to listen to their message. (Right) Affectation area: the region within which receivers will be affected by emitters at a given opinion position O_i.

all the interacting oscillators collapse into single points in the O-EA plane. At the end of the simulation, all agents belonging to the same opinion group fire synchronously for $\epsilon > 0$. We define this firing cycle as our time unit, referred to as a stroboscopic cycle. In the case of pairwise interaction, where there is no reference agent, we define the unit time as the number of firing events divided by the system size, enabling comparison with other scenarios. See Appendix B.5.1 for more details about the dynamics implementation.

In line with previous studies on the bounded confidence model, our primary focus is to investigate the formation of opinion groups, specifically assessing the number of opinion groups obtained at the end of the simulation, with a particular interest in consensus and bipartisanship. We define an opinion group as a subgroup of agents that are connected by interactions, where an agent i is considered to interact with or be linked to agent j if agent i moves when agent j emits a message. Due to the variation in confidence interval widths resulting from different levels of emotional arousal, the resulting interaction network is directed, as shown in Fig. B.1. Therefore, we define an opinion group as a weakly connected component of this directed interaction network.

In certain cases, small groups that separate from the main cluster may appear for certain parameter values. These small groups, referred to as "wings" in (41), are excluded from the statistical analysis when counting the final number of

opinion clusters, unless otherwise specified. To be included in the counting, an opinion group must be larger than 5% of the size of the largest cluster.

It is worth noting that in our model, opinion groups can break but they cannot merge. All interactions are attractive, but by definition, two separated opinion clusters cannot interact and, as a result, they cannot attract each other to merge. Any agent that could potentially mediate the interaction between the opinion groups would necessarily be connected to both groups, resulting in a single weakly connected component instead of two. An exception occurs in Section B.3.3 where we take into account strongly connected components, which may potentially merge.

Whenever the final outcome is not consensus, we pay close attention to the polarization of the system, with a particular focus on the case of bipartisanship. The measure of polarization used in this study follows the definition provided by Esteban et al. in (49):

$$P(\pi, O) = K \sum_{i=1}^{n} \sum_{j=1}^{n} \pi_i^{1+\beta} \pi_j |O_i - O_j|, \tag{B.3}$$

where the summation is carried out over the n final opinion groups. Here, K represents a normalization constant that is calculated based on the most polarized situation possible, which corresponds to two clusters of size $N/2$ each, located at the extremes of the opinion segment. The exponent β is numerically determined in (49) and has a value of 1.6, therefore $K = N(N/2)^{2.6}$

B.3

Results and Discussion

B.3.1 - Trajectories

We aim to investigate the impact of the different control parameters on the number of opinion clusters that emerge in the stationary state. Due to the model's complex behavior and the non-trivial interplay between these parameters, our objective is to demonstrate how the step length α, and the synchronization factor ϵ, influence the system's behavior in a particular simulation that leads to consensus. To ensure consensus is reached, we set a sufficiently large value for the confidence interval, $d = 0.8$ and we assign random initial positions to $N = 200$ agents, verifying that consensus is achieved in all explored cases. Under these conditions, we track the trajectory of a reference agent for four different combinations of α and ϵ, with both small and large values for each parameter (see Fig. B.2). Each dot represents a displacement associated with a firing event, including any resulting

cascades. Our observations reveal distinct trajectory lines and equilibrium points at which the system reaches consensus.

The red line, corresponding to low values of both α and ϵ, exhibits an almost vertical displacement in the initial movements. The red agent increases their emotional arousal, and after a while, they simultaneously start shifting their opinion toward the left extreme of the opinion space. When the reference agent reaches the highest point in their trajectory, they suddenly changes the movement direction for both axes, approaching directly to the consensus point at $O = 0.43$ and $EA = 0.69$. The movement of the red agent can be explained by the fact that dense regions attract agents from less populated areas (77). In fact, the red agent does not move directly upwards, but rather in a random fashion during a few initial displacements, since the density of agents is still homogeneous. It is only after these initial firing events, when the average emotional arousal (EA) has increased due to the asymmetry in connections that favors the reception of messages from agents in the upper part of the opinion space, that the movement becomes steadily upward. The low synchronization factor contributes to the vertical movement since the emission is almost sequential at the beginning, therefore the red agent cannot potentially receive several simultaneous messages from the bulk of central agents that would pull them towards the center, as is the case when ϵ is larger (blue agent). The drift towards the left is attributed to a small group of agents located in the upper left corner of the opinion space, acting as "zealots". These "zealots" have such a narrow interaction band that they do not receive messages from the rest of the agents. However, once the reference agent's band becomes narrow enough to stop receiving messages from the "zealots", they start moving toward the rest of the group and eventually collapse at the consensus point. The group of "zealots" in the upper left corner ends up separated from the large consensus group, but they represent a very small percentage of the population and are classified as a wing.

The blue line, corresponding to small α and large ϵ, exhibits a behavior similar to the red line in the first few movements when the synchronization factor has not yet significantly affected the system. However, in these initial movements, synchronization allows the system to pull the "zealots" who formed the wing in the previous scenario and connect them to the larger group. Consequently, the consensus is achieved without wings, resulting in a reduction in the equilibration time, lower final emotional arousal, and a final opinion closer to the center at $O = 0.5$.

Trajectories for a large value of the step parameter α are represented by the green and purple lines, corresponding to a small and a large synchronization factor ϵ, respectively. Both exhibit similar behavior and achieve consensus near the

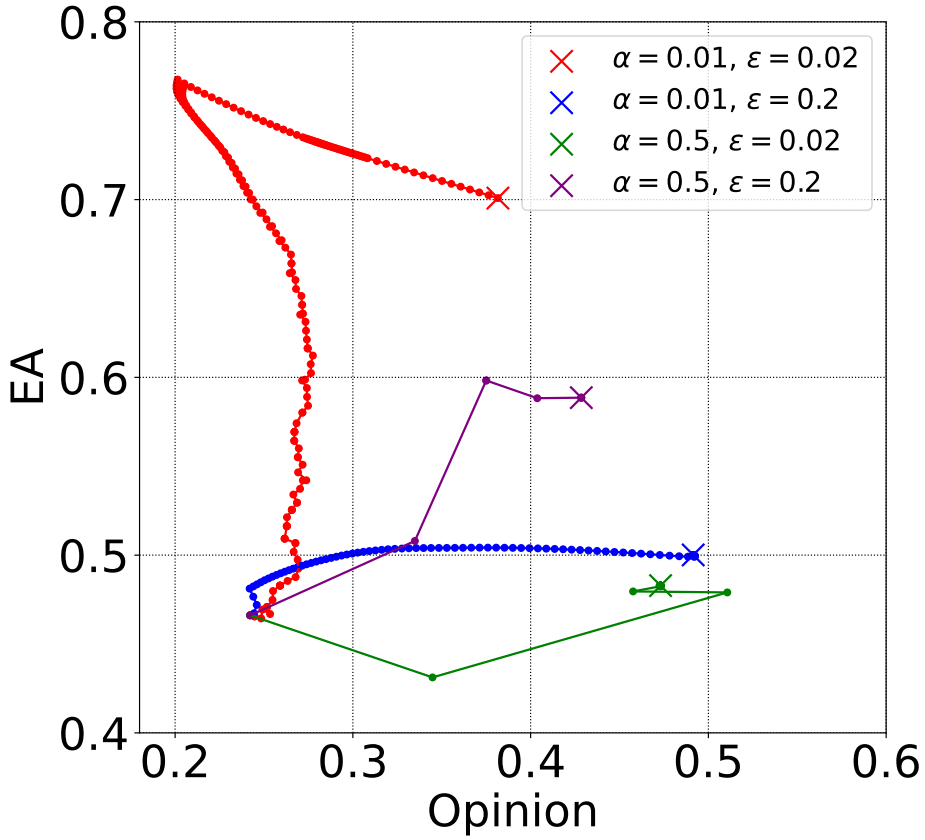

Figure B.2: Examples of one-agent trajectories for different step lengths α and synchronization factors ϵ in the plane formed by the opinion axis (vertical) and the emotional arousal axis (horizontal) for systems consisting of $N = 100$ agents with basal confidence bound $d = 0.5$.

center of the opinion space in just a few iterations. Moreover, no wings were observed in these simulations. The green trajectory shows more frequent changes in direction due to the sequential emission characteristic of low ϵ values. In contrast, the purple line represents a scenario where the reference agent is simultaneously influenced by multiple synchronized emitters. When multiple emitters collectively attract receivers to their barycenter instead of pulling from different points in each firing event, the resulting overall displacement appears smoother, having fewer changes of direction.

It is important to highlight that all outcomes shown in Fig. B.2 are significantly influenced by the initial conditions, as the position of the first emitter can dramatically affect the early dynamics, particularly for large values of α. This strong dependence on the early dynamics has also been discussed elsewhere (89).

In Fig. B.3, we present specific examples that illustrate the effect of synchronization on the entire system. We choose a bounded confidence interval of $d = 0.5$ for a system of $N = 100$ agents and set random initial positions and phases. To facilitate visualization of the agents' trajectories, we use a smaller value for the step longitude, $\alpha = 0.001$, compared to the rest of the sections. However, it is important to note that the precise value of α is not crucial in this section, as our aim is to provide qualitative insights into the system's behavior.

The first row in Fig. B.3 shows the evolution of opinions as a function of time steps, while the second row depicts the corresponding emotional arousal. The colors represent the membership to an opinion cluster (weakly connected component), and they change over time as the clusters break. It is worth noting that the chosen bounded confidence interval is much larger than the value corresponding to the percolation transition, $d_{\text{perc}} \approx 0.02$. Consequently, there is a single opinion cluster (red) in all cases at $time = 0$.

The first column corresponds to the pairwise case, which is similar to the model proposed by Deffuant et al. (41), with the addition of the emotional dimension. In the stationary state, the system is fragmented into five clusters, evenly distributed along the opinion axis due to the symmetric interaction along this axis. Since the interaction is also attractive the extremes of the segment O = 0 and O = 1 are devoid of agents. Conversely, along the EA axis, we observe all clusters accumulated in the upper part with $EA > 0.75$. Specifically, the green-colored cluster that concludes the simulation has EA = 1, and its opinion is close to 0.5. The average initial width of the interaction bands is approximately 0.25, which corresponds to the consensus transition in the original model by Deffuant et al. (41). However, since agents with higher levels of EA receive fewer messages, the overall system's EA increases over time, and this

average width is reduced, resulting in a more fragmented outcome.

The second column corresponds to the purely sequential case, with broadcasted interactions and a coupling factor $\epsilon = 0$. This case is similar to the previous one, but the number of final clusters is reduced to four instead of five because, thanks to the multi-body interactions, agents can group more easily. Furthermore, convergence is much faster, requiring only 800 stroboscopic cycles compared to 20.000 cycles in the pairwise case. Another notable difference is that with multi-body interactions, the system is unable to merge already separated clusters, whereas in the pairwise case, opinion groups can both fragment and reunite. Both in the sequential and the pairwise case fragmentation occurs during the early steps of the simulation.

The third column exhibits significant differences compared to the previous two. In the final scenario, bipartisanship is observed, with two large clusters separated by a distance close to $d = 0.5$ between them, and positioned at $d/2 = 0.25$ from the extremes of the segment, as in the original model by Deffuant et al. (41),. However, since the EA of both clusters is approximately 0.5, their interaction bands at that position are half the width of those in the original model. The transient regime also differs in this case, as the displacements are smoother, but the convergence time is similar to the sequential case, indicating that synchronization does not significantly affect this quantity.

The fourth column corresponds to a high value of ϵ, resulting in rapid synchronization of agents' emissions. The outcome can be considered as a consensus, with the second cluster, consisting of only 3 agents, classified as a wing. This wing exhibits high EA and an "extreme" opinion value, close to zero. For more details on the number and position of wings depending on the model parameters, refer to the Supplementary Material B.5.2. The main opinion cluster is located at the center of the opinion space, coinciding with the equilibrium point for the consensus outcome. The last column presents a limiting case in which all agents fire simultaneously from the beginning of the simulation, and ends with a consensus with no wings. Both the convergence time and the smoothness of the trajectories are similar to the two previous examples with $\epsilon > 0$.

From these examples, as we witness a gradual decrease in the number of final clusters with heightened synchronization, we can infer that both multi-body interactions via broadcasted messages and synchronized emission play important roles in preventing opinion fragmentation. Furthermore, synchronization also helps in avoiding an increase in emotional arousal.

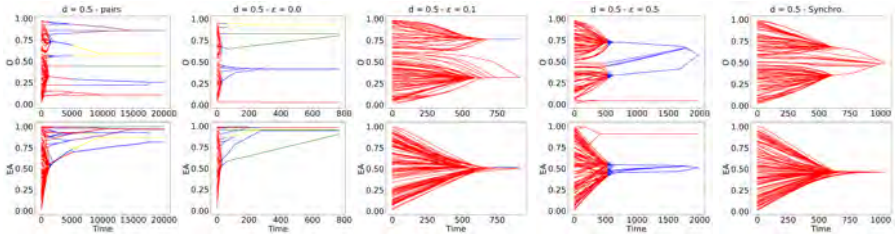

Figure B.3: Examples of agents trajectories for different parameters in the opinion axis (up) and the emotional arousal axis (down) for systems formed by $N = 100$ agents, $d = 0.5$ and $\alpha = 0.001$. Colors are tags denoting the belonging to an opinion cluster. We use the sequence of colors [red, blue, green, yellow, purple] to represent agents belonging to different opinion groups. All simulations start with a single connected component colored in red. When a second cluster emerges, it is designated as blue, and so forth. Agents receive color assignments at each time step, regardless of their previous color. The grey vertical dashed lines serve as visual guides to aid in identifying the time steps at which the groups fragment.

Note that in the pairwise case, stroboscopic time defined as number of attempted interactions/firing events over N.

In all cases, we can distinguish between two movement regimes: the first, characterized by numerous displacements at each time step, and the second, in which most agents have already collapsed into a few opinion clusters that evolve slowly until reaching the stationary state.

B.3.2 - Number of clusters

Here, we investigate the number of opinion groups (after filtering out the wings) for various model parameter values. We perform 300 independent simulations with different initial positions and phases for each parameter set and present the results in figure B.4, which illustrates the distribution of different outcomes. We focus on four distinct stationary states: consensus, bipartisanship, and fragmentation into three or four opinion groups. As expected, the average number of final opinion groups increases with the parameter d across all parameter combinations. However, the specific transition to consensus or the value of d at which a particular outcome has the highest probability of occurring depends on the step size, synchronization factor, and system size.

Variation on d for different fixed values of the remaining parameters

We observe that increasing α leads to broader and noisier distributions, making it impossible to ensure consensus in any case for $\alpha = 0.5$. These effects can be attributed to a higher sensitivity to initial conditions, which is related to the fact that agents experience larger movements when they interact. Consequently, the system tends to break into smaller clusters more easily during the initial steps of the simulation.

The system size also plays a significant role in the outcome distributions. For $\alpha = 0.01$, increasing the system size N decreases the value of the basal confidence bound d required for the consensus transition, and all the peaks corresponding to fragmented outcomes shift to the left. Surprisingly, for $\alpha = 0.5$ and low ϵ, we observe the opposite effect, and for $\alpha = 0.5$ and $\epsilon = 0.2$, there appears to be no noticeable effect of the system size. It is worth noting that having a sharper transition to consensus for smaller N, as depicted in Fig. B.4 - (d), is not a commonly observed result. The underlying reason is that a higher agent density amplifies fragmentation caused by sequential firing during the initial steps of the simulation, as a larger number of receivers are affected by these initial interactions. From a social perspective, this implies that denser initial groups are more likely to become fragmented if individuals strongly influence one another and several agents' opinions are significantly altered after a single interaction, without considering alternative viewpoints. However, the study of other values of N to determine the scaling behavior is out of the scope of this paper.

On the other hand, increasing ϵ has a smoothing effect on the system, closing the gap between the $N = 200$ and $N = 1000$ curves and reducing the noise. In terms of the consensus transition, we once again observe differences depending on α. For $\alpha = 0.01$, increasing ϵ subtly enhances the position of the consensus transition, and shifts to the left the probability peaks corresponding to fragmented outcomes. However, for $\alpha = 0.5$, the effect of ϵ depends on N, with a more pronounced effect observed in smaller systems. Notably, the transition to consensus occurs at larger d for $\epsilon = 0.05$, deviating from the monotonic trend observed in other cases.

The interplay of the model parameters becomes non-trivial, particularly when the system undergoes larger changes in each interaction (higher step length α) and the movement does not involve multiple emitters firing simultaneously (lower coupling factor ϵ). In such cases, the dynamics of the system exhibit a complex behavior and is more sensitive to variations in the initial conditions, leading to a larger variety of outcomes.

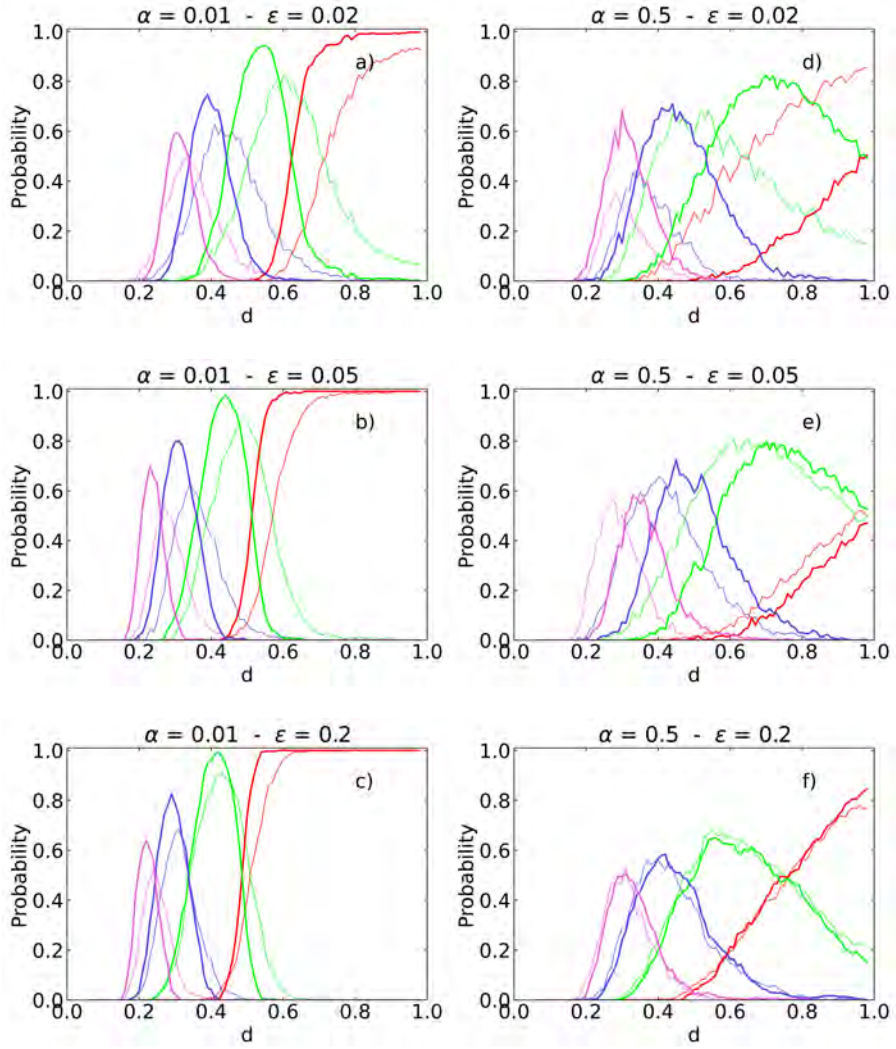

Figure B.4: Proportion of final scenarios as a function of the parameters. Colors denote the different outcomes: red for consensus, green for bipartisanship, blue for fragmentation into three opinion groups, and pink for fragmentation into four opinion groups. Results obtained for a system of $N = 200$ agents (thin line) and $N = 1000$ agents (thick line), running 300 simulations with different initial conditions for each parameter set.

The synchronized case

Here we present the simulation results for the synchronized limit case where all agents emit messages at once at every time step since the beginning. Since this variant lacks random initial phases and depends only on the initial positions, we can provide a semi-analytical estimation for the proportion of clusters based on the following assumptions (see Fig. B.5):

- For each outcome, there exists an equilibrium position in the opinion axis for the opinion clusters, given by the original model, which corresponds to $\bar{O}_i = i/(n+1)$, where n is the number of final clusters.
- Each equilibrium position $\bar{O}_i$ has an associated area $2d \cdot L/2 = d$ that corresponds to the affecting triangle of an agent placed at this equilibrium point ($L = 1$ corresponds to the height of the opinion space).
- The normalized total attraction area associated with all the equilibrium points of a given outcome is $A(n,d) = d/D_n$, where $D_n = 2/n$ is twice the distance between the opinion axis boundary and the first equilibrium point, representing the maximum base of a triangle that contains only one equilibrium position.
- The probability of a given outcome is equal to the probability that initially at least half of the agents lie within the attraction area associated with this outcome, minus the probability that initially at least half of the agents lie within the attraction area associated with an outcome with fewer clusters. Since initial positions are sampled from a uniform distribution, we have:

$$P(n) = \sum_{k=N/2}^{N} A(n,d)^k \left(1 - A(n,d)\right)^{N-k} - \sum_{\eta=1}^{n-1} \left(\sum_{k=N/2}^{N} \left(A(\eta,d)\right)^k \left(1 - A(\eta,d)\right)^{N-k} \right) ; n \geq 1 \tag{B.4}$$

Based on these assumptions, the probability of achieving consensus is 1 if at least $N/2$ agents lie initially inside the affectation triangle whose peak is at O, EA $= L/2, 1$, and has a base length $L = 1$ (see Figure B.5-a)). This estimation tends to overestimate the value of d for the transition to consensus and the position of the peaks for the other outcomes, as observed in our simulations for all parameter values explored. However, it provides a closer approximation for lower step longitude values (α) as shown in Figure B.6. It is important to note that this approximation is not influenced by the presence of wings (which are more abundant for higher α) since not filtering the wings from the results obtained with the simulations only introduces noise and distorts the results. But with the wing filtered the probability distributions exhibit no noise, even for $\alpha = 0.5$ (Figure B.6-right column), indicating that the sensitivity to

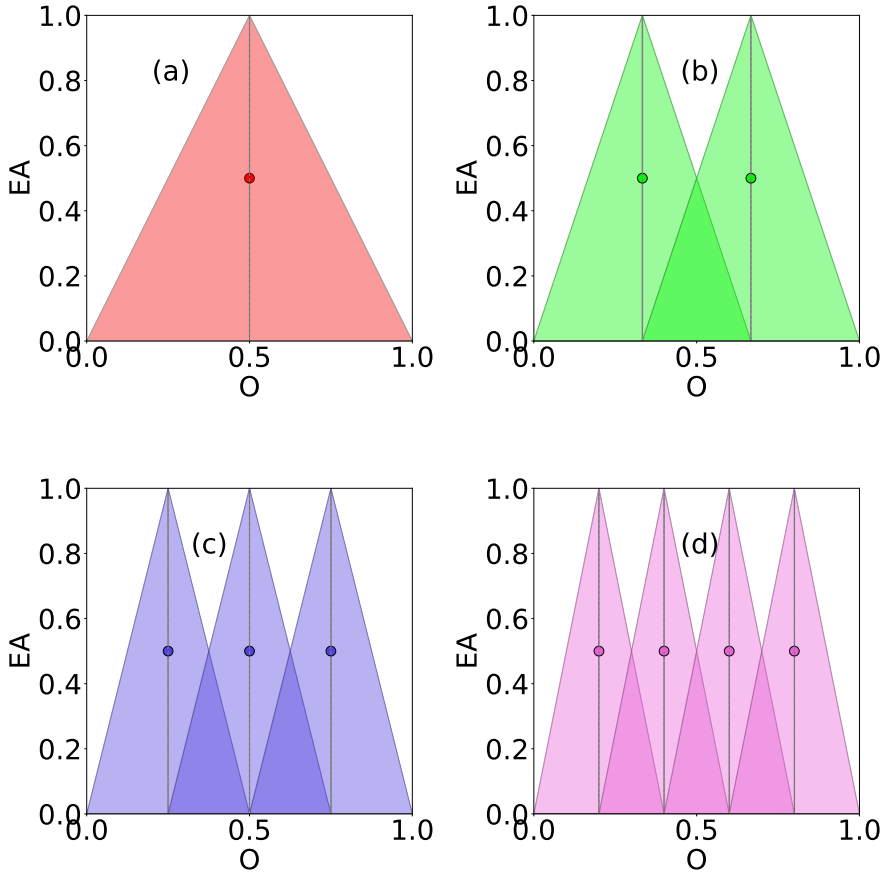

Figure B.5: Basins of attractions and theoretical equilibrium points of (a) consensus, (b) bipartisanship, (c) fragmentation in 3 clusters, and (d) fragmentation in 4 clusters in the synchronized case.

initial conditions is primarily related to the phases that determine the emitter in the first time steps. With perfect synchronization from the beginning, a larger step does not promote system fragmentation but drives it toward consensus at smaller values of the confidence interval d.

If we modify the lower bound of the sum in Equation B.4, requiring a greater number of agents to lie initially within the considered attraction area, we can improve the estimation. Although we see that the analytical expression for this bound is an increasing function of α and N, the exact formula is beyond the scope of this paper, however, some approximated corrections to the original estimation can be found in Section B.5.3. What occurs is that, while agents may not be initially within this area, the attractive dynamics lead them to reach it at earlier times for larger α. Since they do so in a cohesive manner, influenced by all other agents simultaneously, this does not result in fragmentation. The analytical approximation captures the shape of the transition, which becomes sharper for larger N but remains centered around the same d values. Furthermore, it accurately represents the tendency for the peaks of other outcomes to decrease and narrow.

The pairwise case

To establish a connection between our results and the classical case involving pairwise interactions, we conducted additional investigations on our two-dimensional opinion space with pairwise interactions. Since the pairs can be chosen in any order, the final outcome can be dramatically affected by the particular pair selection. For $\alpha = 0.01$ we observe consensus for certain values of d when $N = 200$ (thin lines in Figure B.6-e), but it cannot be guaranteed for any $d \in [0.05, 1]$, resembling the behavior exhibited for $\alpha = 0.5$ and $\epsilon = 0.05$ but with broader peaks. However, a non-monotonic behavior in the proportion of consensus and bipartisanship, unique to this limit case and parameter combination, emerges for $N = 1000$ (thick lines). In both cases, two peaks are observed, with the peak for three opinion clusters being the highest. This characteristic, with an approximate probability of 90% for having 3 opinion clusters in the stationary state when $d \approx 0.7$, is also exclusive to this specific parameter combination.

For $\alpha = 0.5$, the final configuration becomes significantly more fragmented. The number of opinion groups, which increases with higher N, decreases supra-exponentially as d varies within the range $d = [0.05, 1]$ (see Fig. Figure B.6-f). The maximum average number of clusters, corresponding to $d = 0.05$, is approximately $\langle n \rangle = 40$ for $N = 200$ and $\langle n \rangle = 80$ for $N = 1000$. This proportion is maintained for all d values, reaching a minimum around $\langle n \rangle = 10$ for $N = 200$

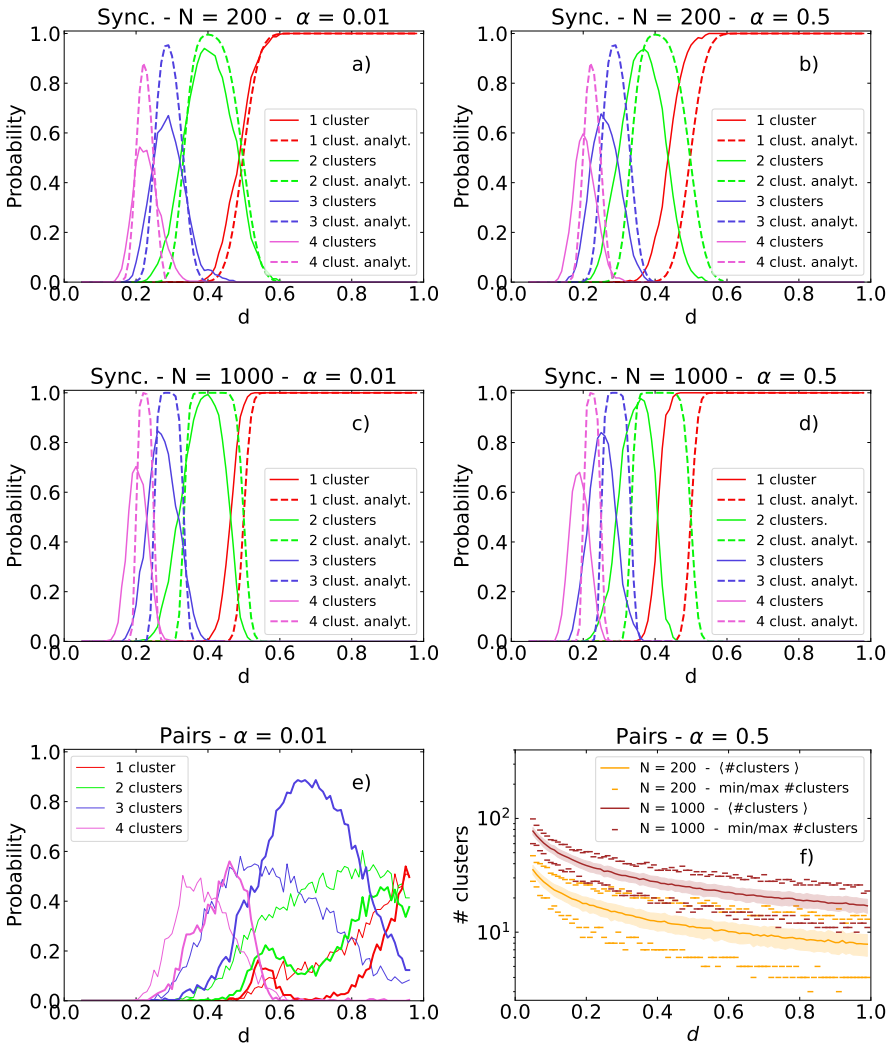

Figure B.6: Proportion of final scenarios as a function of the basal confidence bound d for a) synchronized interactions, step longitude $\alpha = 0.01$ and system size $N = 200$, (b) synchronized interactions, $\alpha = 0.5$ and $N = 200$, c) synchronized interactions, $\alpha = 0.01$ and $N = 1000$, d) step $\alpha = 0.5$ and $N = 1000$ and e) pairwise interactions, $\alpha = 0.01$ and $N = 200, 1000$. f) Average maximum and minimum number of final clusters as a function of d for pairwise interactions, $\alpha = 0.01$ and $N = 200, 1000$. Results were obtained for 300 simulations with different initial conditions.

and $\langle n \rangle = 20$ for $N = 1000$ at $d = 1.0$.

A higher overall density implies having more agents in the extremes on the opinion axis, which could lead to the formation of 3 clusters more easily than when N is smaller.

The behavior of the pairwise variant, which exhibits significantly more noise, is attributed to the wide range of confidence intervals associated with randomly selected interacting pairs. We explain the formation of double peaks for consensus and bipartisanship when $N = 1000$ in Section B.3.3.

The most important changes in this limit case are due to the value of α. The system size also plays a qualitatively significant role in the basins of attraction for $\alpha = 0.01$.

Variation on ϵ for different fixed values of the rest of parameters

Here we conduct a detailed investigation on the impact of the coupling factor ϵ within the range $[0, 1]$ (including the sequential limit case $\epsilon = 0$) for two values of the maximum confidence interval, $d = 0.1$ and $d = 0.5$ (see Fig. B.7). We compare the results of the sequential limit case at $\epsilon = 0$ with those obtained for the pairwise limit case, as well as the results for $\epsilon = 1$ with the synchronized limit case. The pairwise and synchronized cases are represented by diamond dots at $\epsilon = 0$ and $\epsilon = 1$, respectively. It is important to note that each value of the parameter d corresponds to a distinct region of potential outcomes. In the case of $d = 0.5$, we separate the results obtained for each system size.

For $d = 0.1$, we do not expect to observe any of the four focused outcomes. Therefore, we pay attention to the average number of opinion groups, its standard deviation, and the maximum and minimum number of clusters for each value of ϵ. We clearly distinguish two regimes for both values of α: a coupling-dependent region for ϵ below approximately 0.1, and above this value, a region that is nearly independent of the coupling and exhibits an average number of opinion groups around $n = 10 \pm 2$ for both system sizes and step longitudes. The coupling-dependent regime is more extensive for $\alpha = 0.5$ and depends on the system size. Specifically, for $N = 1000$ and $\alpha = 0.01$, the average number of opinion groups peaks at $\epsilon \approx 0.02$ and shows a relative minimum around the same value for $\alpha = 0.5$. On the other hand, for $N = 200$, there is a monotonic decay for both values of α. When $\alpha = 0.01$, $\langle n \rangle$, $n_{\min}$, and $n_{\max}$ are larger for $N = 200$ than for $N = 1000$ for all ϵ. However, when $\alpha = 0.5$, these quantities are more similar for each system size, and their magnitudes depend on the value of ϵ. In general, in this fragmented region of parameter space, higher agent densities and larger coupling factors tend to result in less frag-

mentation, except for the specific values of $\alpha = 0.5$ and $\epsilon \in [0, 0.4]$, approximately.

When approaching the region where consensus is observed, at $d = 0.5$, we again observe non-monotonic behaviors for low values of the coupling factor. For $\alpha = 0.01$ (see Fig. B.7 (c) and (e)), the probability of consensus transitions from a value close to zero for $\epsilon \to 0$ to a finite probability, which is higher for larger system sizes. The probability of bipartisanship is complementary to the probability of consensus, as fragmentation into three or four clusters, despite having some representation at $\epsilon \to 0$, rapidly decays to zero with increasing coupling factor. The shape of the curves remains unchanged when increasing N, but the transition to consensus becomes sharper and the bipartisanship peak becomes narrower and higher. As a result, fragmentation into three or four opinion groups becomes more residual compared to the smaller system size. At $\epsilon = 0$, the sequential limit case yields results that closely resemble those obtained for the pairwise limit case, particularly when $N = 200$. On the other hand, when the coupling factor is 1, the results resemble those obtained for the synchronized case for both system sizes.

On the contrary, for $\alpha = L/2 = 0.5$, the pairwise and synchronized limit cases do not match the results for $\epsilon = 0$ and $\epsilon = 1$ (see Fig. B.7 d, f). The probability curves exhibit more noise due to the larger step length and show a non-monotonic behavior for low values of ϵ. The probability of consensus is zero at $\epsilon = 0$ for both system sizes and increases linearly with ϵ until it reaches a value around 0.4. Consensus also exhibits a narrow peak of height 0.3 approximately at $\epsilon = 0.1 \pm 0.1$ for $N = 200$. Bipartisanship shows a peak and a minimum at $\epsilon < 0.1$ for both system sizes. Concurrent with the minimum for bipartisanship, there are peaks for the outcomes with 3 and 4 opinion groups, which are higher and occur at lower values of the coupling factor for larger N. However, the effect of N is only noticeable for low ϵ, while in the range $\epsilon > 0.2$, there are no significant differences between the two system sizes. In fact, the behavior is similar to the case with $\alpha = 0.01$, but with increased fragmentation across the entire range of studied ϵ values and a much slower transition to consensus. It is interesting to note that for this value of the maximum confidence bound $d = 0.5$, an increase in ϵ can promote fragmentation for any system size when the step length is large enough.

B.3.3 - Emotional Arousal and Fragmentation

We have generated ϵ-d and ϵ-α phase diagrams to analyze the final average number of clusters and the average level of emotional arousal $\langle EA \rangle$. We observe a significant correlation between $\langle EA \rangle$ and the ratio between the final and initial average number of strongly connected components $\langle n \rangle_{fin} / \langle n \rangle_{ini}$ when wings were not filtered. However, applying the wing filtering process disrupts this correla-

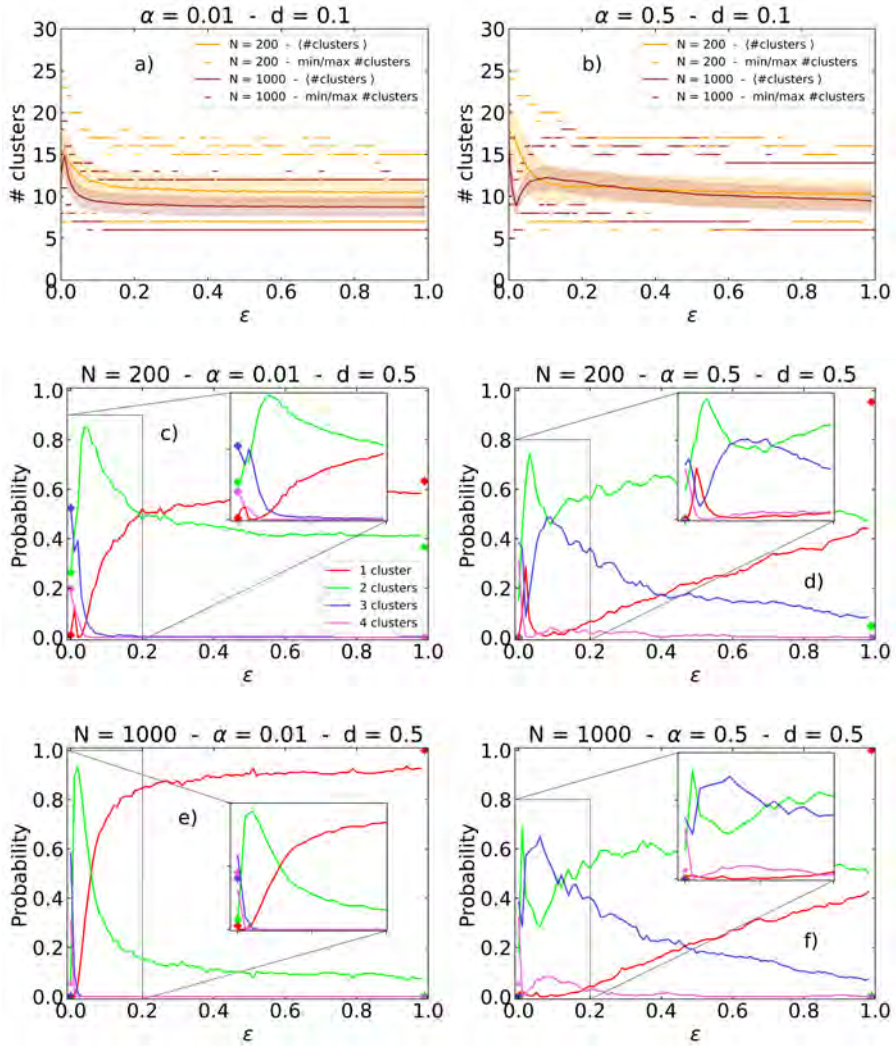

Figure B.7: Average, maximum, and minimum number of clusters as a function of the coupling factor ϵ for different parameters values. Results obtained by performing 300 simulations with different initial conditions for each parameter set, except for the inset plots in panels c) and d), where 1000 simulations were performed with finer resolution in parameter values.

tion. The average level of emotional arousal remained relatively consistent across all parameter ranges since the wings, being small by definition, do not contribute significantly to the overall average. Instead, the ratio $\langle n \rangle_{fin}/\langle n \rangle_{ini}$ could decrease or remain the same, depending on the number of wings filtered out (it cannot increase because wings are only defined for the final state). Furthermore, the presence of wings exhibited a strong dependence on the model parameters, as discussed in Section B.5.2. Note that in this context we are considering strongly instead of weakly connected components, therefore the ratio $\langle n \rangle_{fin}/\langle n \rangle_{ini}$ can be smaller than one (i. e. groups can merge).

Phase diagram d-ϵ

We present the results for two values of the step longitude $\alpha = 0.01, 0.5$ in the range of $d \in [0.005, 1.0]$ and $\epsilon \in [0, 0.5]$, and compare them to those obtained for the synchronized and the pairwise cases (B.8). We first analyze the phase diagrams for the average final values of the emotional arousal and the ratio between initial and final strongly connected components as a function of d and ϵ (shown in Fig. B.8-a and c, respectively), obtained for small α, where we can clearly distinguish four regions:

1. The vertical band on the left corresponds to $d < 0.02$, marking the percolation transition (see Sec. B.2). In this region, the dynamics have a minimal effect due to the small confidence interval, resulting in a highly fragmented situation with small opinion groups scattered across the O-EA plane. Both magnitudes, $\langle EA \rangle$, and $\langle n \rangle_{fin}$, remain unchanged from the beginning to the end of the simulation.

2. The brown region (panel a) and red region (panel b) corresponding to $d > 0.02$ and low ϵ. However, there are discrepancies in the shape of the figures for high d. While $\langle EA \rangle$ increases monotonically with d, the behavior of the ratio of strongly connected components varies.

3. The upper-right area represents the consensus region, where $\langle EA \rangle$ and $\langle n \rangle_{fin} \leq 1$. Here $\langle EA \rangle$ is approximately equal to the initial value of 0.5. The reason why $\langle n \rangle_{fin}$ can be smaller than one is that strongly connected components can merge, contrarily to the weakly connected components examined in Sec. B.3.1

4. The transition region, colored in green in both panels. This zone exhibits a relative maximum along the ϵ axis at around $d \approx 0.05$, just above the percolation threshold. In this region, both $\langle EA \rangle$ and $\langle clusters \rangle_{final}$ decrease with increasing ϵ towards a saturation value that depends on d. This decay is faster for larger values of d.

Overall, these results demonstrate the dependence of the system behavior on the values of d and ϵ, revealing distinct regions characterized by different dynamics and outcomes. The profiles of both $\langle EA \rangle$ and $\langle n \rangle_{fin}/\langle n \rangle_{ini}$ are generally similar, except when we are close to the sequential case, in the limit $\epsilon \to 0$ (region II). In this limit, $\langle EA \rangle$ monotonically increases with d (as observed in the pairwise case), and $\langle n \rangle_{fin}/\langle n \rangle_{ini}$ exhibits a relative maximum around $d = 0.3$ and then decays towards $\langle n \rangle_{fin}/\langle n \rangle_{ini} \approx 2$. When we are close to the sequential case, an increase in d primarily benefits agents located in the upper part of the O-EA plane. These agents act as "zealots", influencing the rest of the agents and causing fragmentation into multiple opinion groups with high emotional arousal. Eventually, with sufficiently high d fragmentation can be reduced, but the average emotional arousal will keep increasing with the confidence interval, resulting in narrower confidence bounds. Consequently, a new agent introduced into the system after reaching the stationary state would face more difficulties in being listened to by the existing agents. When the coupling factor increases the situation reverses and both $\langle EA \rangle$ and $\langle n \rangle_{fin}$ decrease monotonically with d.

Since the coupling factor ϵ leads to synchronization, it is not surprising that the results tend towards the synchronized limit case for high values of ϵ. As previously shown, the outcome in the synchronized case is always consensus for $d > 0.5$, therefore the fluctuations observed in this range are only caused by the different number of strongly connected components in the initial state. We observe as well an increase in fluctuations around $d = 0.5$ that corresponds to the transition to consensus. It is worth noting that highly synchronized systems tend to have average levels of emotional arousal close to 0.5, even for fragmented outcomes, whereas systems without synchronization exhibit considerably higher emotional arousal levels despite having less fragmentation.

Interestingly, the results for $\epsilon = 0$ tend to resemble those obtained for the pairwise case, at least in terms of $\langle EA \rangle$. However, in terms of the ratio of opinion groups, the correlation only exists for low values of d. While $\langle n \rangle_{fin}/\langle n \rangle_{ini}$ starts decreasing at higher d for $\epsilon = 0$, it continues to increase until $d = 1.0$ in the pairwise case. Filtering the wings does not reverse this tendency but rather smoothens it (see Section B.5.2), indicating that wings play a more significant role in the pairwise case compared to the sequential case.

When $\alpha = 0.5$ (Figure B.8 (b) and (d)) the results are resemblant but with some differences. Fragmentation and average emotional arousal are, in general, higher except below the percolation at $d = 0.02$ (region I), since agents do not interact, regardless of the step longitude. Only for large values of d and ϵ, where we have consensus, $\langle n \rangle_{fin}/\langle n \rangle_{ini}$ drops to 1. The relative maximum in region III disappears in the $\langle EA \rangle$ heatmap and, above the percolation $\langle EA \rangle$ decreases depending only on ϵ. The ratio of opinion groups, on the other hand, does

experiment a decrease with both d and ϵ when $d > 0.02$ (regions III and IV). The most noticeable difference is the overall increase in $\langle EA \rangle$, which becomes independent of d above the percolation and is larger than 0.5, even at $d = 1$ and $\epsilon = 0.5$, where consensus is guaranteed

So, the way agents with a high EA drag up the other agents via their interactions has a direct correlation with the number of final opinion groups, taking into account the minorities (usually with a high $\langle EA \rangle$, as we can see in Section B.5.2) Excluding the pairwise case, the highest level of EA is not reached in either the most fragmented situation or the least one, but in the parameter zone that corresponds to sequential firing and large basal confidence bound, and is always larger for larger α. When the set of parameters yields multiple outcomes, the most fragmented scenario corresponds to the one exhibiting a higher average emotional arousal $\langle EA \rangle$, as we see in Figure B.9. This observation is drawn from examining the EA distributions for a system of $N = 1000$ with a step length of $\alpha = 0.01$, across two values of the basal confidence bound d. These values result in a combination of bipartisanship and fragmentation into 3 clusters ($d = 0.35$), and a mix of consensus and bipartisanship ($d = 0.5$).

Phase diagram α-ϵ

We examine the range of $\alpha \in [0.005, 0.5]$, since smaller or larger step longitudes are not interesting from a social point of view, and $\alpha > 0.5$ would not be comparable with the classical bounded confidence model.

The system behaviors when varying α and ϵ are more straightforward, but the correlation between the final $\langle EA \rangle$ and $\langle n \rangle_{fin}/\langle n \rangle_{ini}$ hold for all the parameter range explored. The coupling factor always diminishes $\langle EA \rangle$ making it tend to average initial value 0.5, while alpha always increases it. However, when α is low, decay of $\langle EA \rangle$ occurs for $\epsilon < 0.05$ and is fast, and this transition becomes smoother as α increases. For $d = 0.5$ we confirm that $\langle EA \rangle$ is higher at low ϵ for any α A larger confidence bound implies a higher number of interactions, in particular with agents that have a higher EA and, since their k_{out}/k_{in} degree is larger, they are privileged from a communicative point of view. Therefore a large d leads to a low number of clusters since agents interact among them, regardless thbasal confidence boundey are far away on the opinion axis. During the trajectory to a consensus, however, they considerably shrink their confidence interval and they lose their mediator role.

The fact that these effects are contraposed is the cause of the double peak for consensus and bipartisanship in the pairwise case for $N = 1000$ and $\alpha = 0.01$ (see Fig. B.6 (e). For instance, in the approximate interval $d \in (0.6, 0.8)$ agents have a basal confidence bound d large enough to ascend rapidly in the O-EA. However, this parameter it is not large enough to maintain a wide confidence interval,

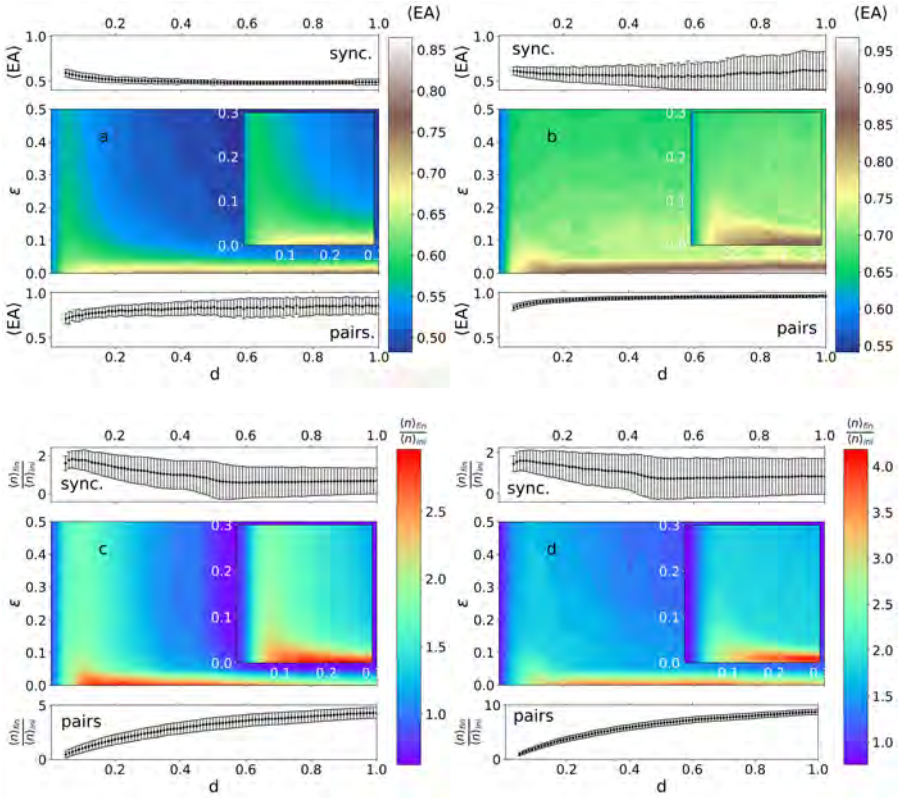

Figure B.8: Final values of average emotional arousal $\langle EA \rangle$ (upper row) and ratio between average number of final and initial opinion groups $\langle n \rangle_{fin} / \langle n \rangle_{ini}$ (lower row), for a range of basal confidence bound d and coupling factor ϵ when the step longitude $\alpha = 0.01$ (a, c) and $alpha = 0.5$ (b, d). Results correspond to a system formed by $N = 200$ agents and are averaged over 100 simulations with different initial conditions. The inset plot shows a smaller range with more resolution. The upper and lower subpanels in each subfigure correspond to the synchronized and pairwise cases for the corresponding set of parameters.

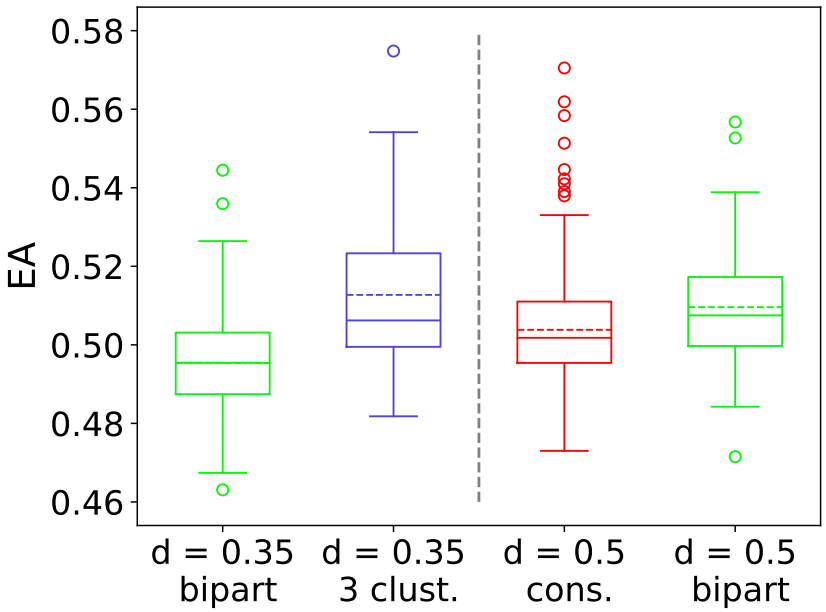

Figure B.9: Final EA distributions of a system of $N = 1000$ agents, longitude step $\alpha = 0.01$, synchronization factor $\epsilon = 0.2$ and different values of the basal confidence bound d for those repetitions that end up in consensus, bipartisanship and 3 clusters. Results obtained for 300 simulations with different initial conditions for each value set of parameters.

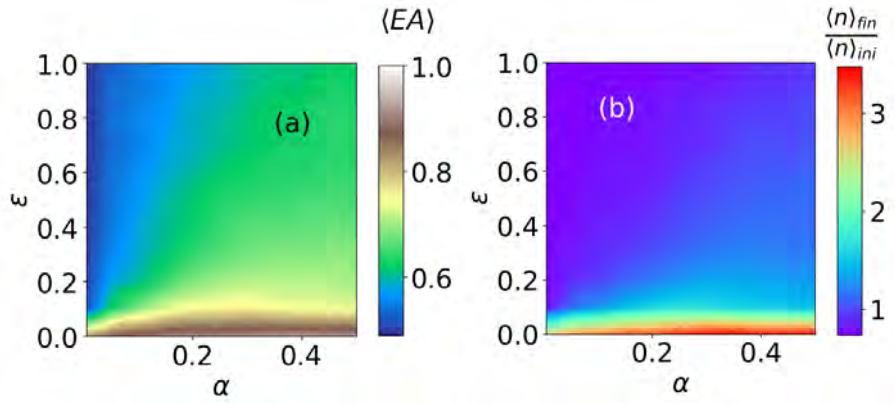

Figure B.10: Final values of a) average emotional arousal $\langle EA \rangle$ and b) ratio $\langle n \rangle_{fin}/\langle n \rangle_{ini}$ for a range of the step longitude α and coupling factor ϵ. Results correspond to a system formed by $N = 200$ agents and are averaged over 100 simulations with different initial conditions. The basal confidence bound is set to $d = 0.5$.

hindering the achievement of consensus. Counterintuitively, a lower value of d can result in consensus, as the upward movement is not as fast. Synchronization prevents this from occurring by diminishing the impact of "zealots" (i.e., agents with high EA). This is because individuals simultaneously consider not only the viewpoints of highly emotional agents but also the arguments presented by less emotional individuals.

B.3.4 - Polarization

Polarization reaches its theoretical peak value $P = 1$ for the bipartisan outcome when two clusters of size $N/2$ are positioned at $O = 0$ and $O = 1$ (see Eq. B.3). In our simulations, we observe a maximum average value of $\langle P \rangle = 0.5$, achieved in the synchronized scenario for the range of d where the outcome is consistently bipartisan, regardless of the initial conditions or the step length α. In contrast, other cases exhibit a mixture of outcomes, resulting in a reduced overall average polarization.

Low α

For smaller step lengths α, the average polarization exhibits a distinct peak around $d = 0.4$ across all synchronization factors $\epsilon > 0.1$. This aligns with the region where the system tends to converge towards a bipartisan outcome

more frequently. Notably, this peak shifts towards higher d values for lower ϵ, correlating with a higher tendency for fragmentation as the system approaches the sequential limit. As highlighted in Section B.3.2, the synchronized case shows a sharp transition towards consensus, here, we observe a rapid decline in polarization at the value of the basal confidence bound d where this transition occurs. On the other hand, the pairwise case exhibits more fluctuations and a smoother decrease in polarization when increasing d.

When analyzing the lower range of ϵ in detail (refer to Fig. B.11 - inset), we find a non-monotonic behavior. For instance, following the vertical line at $d = 0.2$, we see that the average polarization is $\langle P \rangle \approx 200$ for $\epsilon = 0$, decreases to a minimum of $\langle P \rangle \approx 75$ around $\epsilon = 0.02$, and rises again to approximately $\langle P \rangle \approx 200$ at $\epsilon = 0.1$. Beyond $\epsilon = 0.1$, the average final polarization primarily depends on d only.

For $\epsilon > 0.05$, the system achieves consensus if $d > 0.6$, resulting in zero average polarization. When ϵ is below this threshold, the average polarization value $\langle P \rangle$ decreases with both d and ϵ.

Note that low polarization values at both low d correspond to a highly fragmented outcome, while at high d, they indicate a consensus.

High α

For large step length, polarization presents a different behavior, especially noticeable for low ϵ and high d, where it exhibits greater values compared to scenarios with smaller α. For instance, taking the vertical line $d = 0.6$ (Fig. B.11 (b)), we observe a peak at $\epsilon \approx 0.05$. Additionally, the previously observed non-monotonic behavior for small ϵ and $0.1 < d < 0.3$ is inverted. In the vertical line at $d = 0.3$, we have a peak in the average polarization instead of a valley at a slightly larger $\epsilon \approx 0.05$. The peak across all $\epsilon > 0.1$ along $d = 0.4$ persists.

The results in the limit of high ϵ no longer converge to the synchronized case. With a larger step length, the initial steps, where the system has not synchronized yet, become crucial, inducing fragmentation, and thereby increasing polarization. This effect is prevented only when the system is fully synchronized from the beginning, leading to consensus.

This transition, more abrupt for the synchronized case, as usual, is absent in the pairwise scenario."

Polarization peak

As observed, the system's global polarization peak strongly correlates with the bipartisan peak. This correlation becomes clearer when we compare Figures B.4 and B.12. With low α, an increase in agent density sharpens this transition,

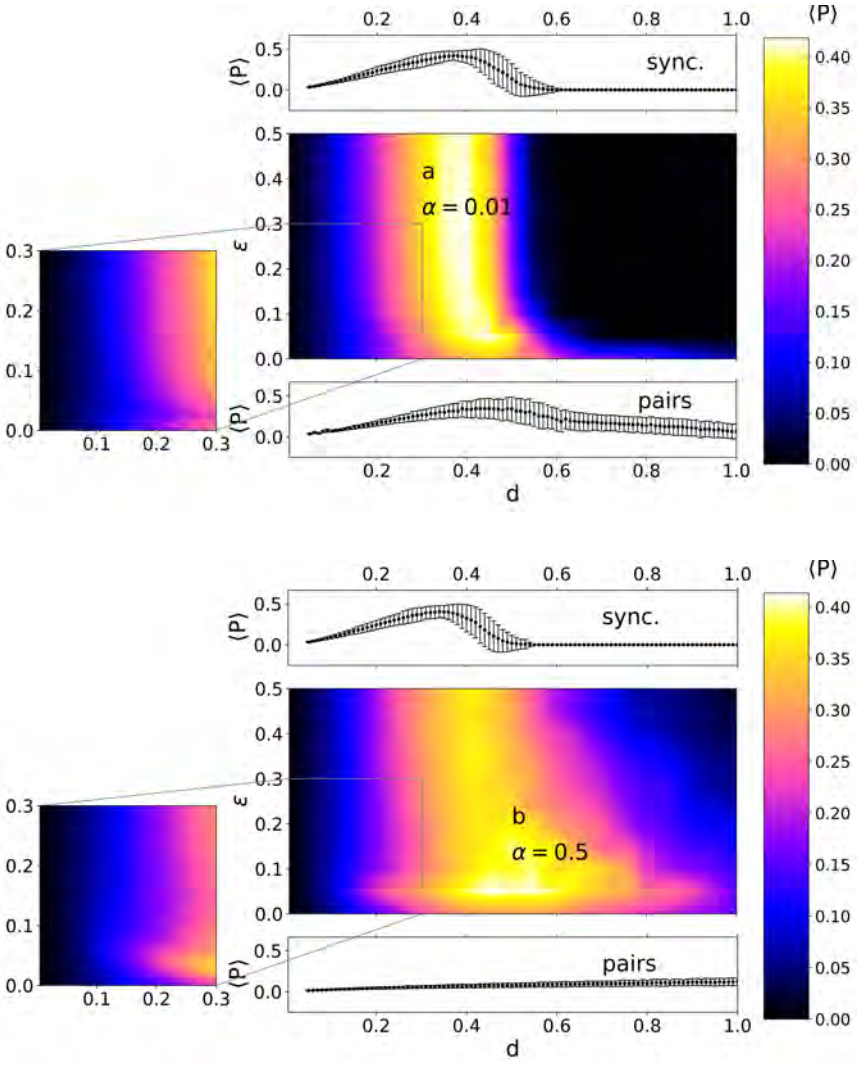

Figure B.11: Total average polarization of the system as a function of the basal confidence bound d and the synchronization factor ϵ for (a) step length $\alpha = 0.01$, (b) $\alpha = 0.5$. Results obtained for a system of $N = 200$ agents and 100 simulations with different initial conditions. The inset plot shows a smaller range with more resolution. The upper and lower subpanels in each subfigure correspond to the synchronized and pairwise cases for the corresponding set of parameters.

as is typical in second-order transitions. When α increases, heightened fluctuations and disruptions in clusters lead to a scenario where N no longer influences the average total polarization at low ϵ. Moreover, a larger step smoothens the transition at high ϵ.

Polarization per outcome α

When examining average polarization levels based on outcomes (Fig. B.13), the average polarization $\langle P \rangle$ increases proportionally with the basal confidence bound d in scenarios where the system fragments into 3 or 4 clusters, in the same way the system increases the average level $\langle EA \rangle$. On the other hand, for the bipartisan outcome $\langle EA \rangle$ maintains the increasing tendency, while $\langle P \rangle$ decreases.

Within the range of d values where systems exhibit the coexistence of 2 and 3-cluster outcomes, realizations where the system significantly raises the $\langle EA \rangle$result in more significant loss of connections among agents, causing the system to break into 3 clusters and resulting in decreased average polarization. In contrast, systems maintaining lower EA levels prevent fragmentation, leading to a bipartisan outcome and higher polarization levels. The final outcome is solely determined by initial conditions (position in the plane and first emitter).

At higher ϵ these tendencies become sharper (see Fig. B.13 (c) and (d)). Longer steps are not shown in Fig. B.13) because the increased number of fluctuations outgrow the aforementioned behaviors.

B.3.5 - Bipartisanship

In this subsection, we examine the bipartisan outcome, a common scenario in various social contexts such as presidential elections (e.g., U.S., France) and leadership contests within political parties. In Fig. B.13, we analyze the polarization levels of realizations ending in 2 clusters depending on the model parameters. Polarization hinges on the relative sizes and distances between clusters. Since the two clusters tend to be similar in size (with fluctuations depending on parameter ranges), we are focusing on the distance between them.

We present results for a step length $\alpha = 0.01$ because larger α blurs effects due to increased fluctuations. For larger steps, the initial messages become crucial, especially when emitters possess high initial EA, since they may draw some agents upward in the O-EA plane but not others. When d is high this fosters bipartisanship over consensus, and clusters generally exhibit different EAs, contingent on the first emitters on each side of the opinion space, who attract agents to each cluster, and their respective EA levels. However, for small α, the vertical distance on the emotional arousal axis fluctuates around zero, with fluctuations decaying approximately as $1/\sqrt{N}$ (Fig. B.14 (a) and (b)).

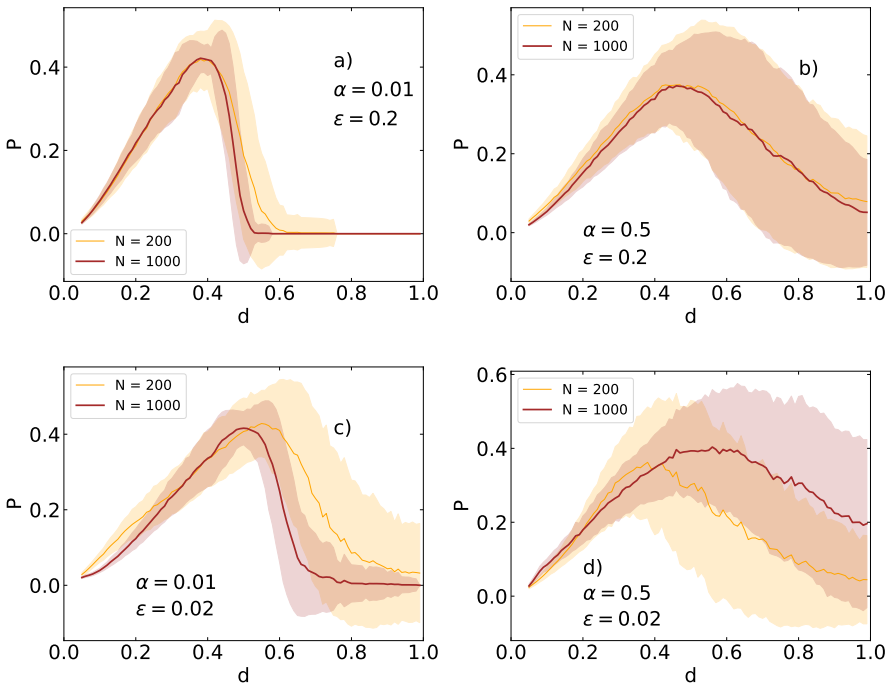

Figure B.12: Total polarization of the system as a function of the basal confidence bound d for (a) step $\alpha = 0.01$ and coupling factor $\epsilon = 0.2$, (b) $\alpha = 0.5$ and coupling factor $\epsilon = 0.2$, (c) step $\alpha = 0.01$ and coupling factor $\epsilon = 0.02$, and (d) $\alpha = 0.5$ and coupling factor $\epsilon = 0.02$. Results obtained for a system of $N = 200$ agents (thin light line) and $N = 1000$ agents (thick dark line) and 300 simulations with different initial conditions.

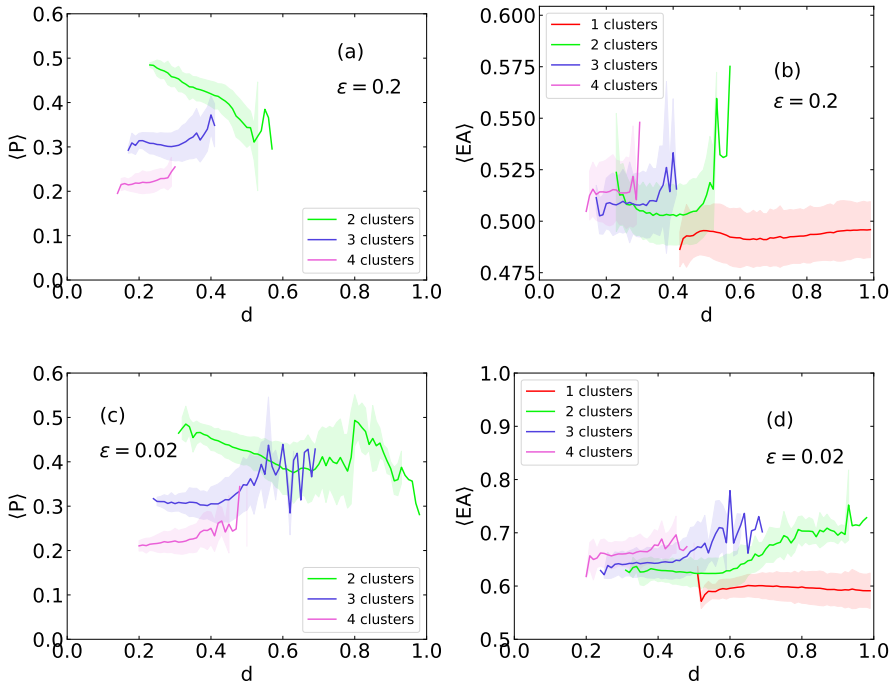

Figure B.13: Average polarization (left) and average final EA (right) of each outcome system as a function of the basal confidence bound d Results are shown up to 4 clusters and are obtained for a system of $N = 1000$ agents, synchronization factor $\epsilon = 0.2$ (up) and $\epsilon = 0.02$ (down), step longitude $\alpha = 0.01$, and 300 simulations with different initial conditions.

On the other hand, the distance on the opinion axis for small α depends on the synchronization level. In the fully synchronized case (Fig. B.14 (a)), the distance decreases with the basal confidence bound d as larger confidence bounds bring clusters closer. In contrast, with pairwise interactions (Fig. B.14 (b)), it increases with d, because of the increased EA levels reached in this case.

To explore slope changes, we fitted linear regressions to the data for both the synchronized and the pairwise case, and across various ϵ values (Fig. B.14 (c)). Similar to the results we expose in previous sections, sequential case results with $\epsilon = 0$ tend to converge to pairwise results, (more accurately for $N = 200$), while results for larger ϵ converge to synchronized case results. The emotional arousal axis distance maintains a flat slope in all cases, with fewer fluctuations for larger N.

In contrast, the opinion axis distance undergoes a transition from positive to negative slopes around an ϵ transition value of approximately 0.05. The slope stabilizes for $\epsilon > 0.2$, matching synchronized case values. Slopes have larger absolute values and fewer fluctuations for larger N. At the transition value, local synchronization is achieved fast enough to have entire clusters firing at once early in the dynamics, when the system still forms a single connected component, which contributes to a cohesive approach in both the opinion and the EA axis, leading to lower levels of EA and closer clusters in the bipartisan outcome, so even in bipartisanship.

B.4

Conclusions

Our study reveals different stationary states for the proposed system, depending on the parameters set and the initial conditions. In general, we observe that the dynamics leads to an increment in the average of emotional arousal level of the system and a fragmentation of the initial number of clusters into several final opinion groups. However, for some specific set of parameters, a less fragmented situation is more probable. The synchronization factor ϵ significantly influences these aspects, reinforcing their effects when it is small and mitigating their intensity when is large.

Total synchronization emerges as a unifying factor that not only facilitates consensus and prevents fragmentation at lower basal confidence bound values, but also eliminates fluctuations, the outcome becoming more predictable, and sharpens transitions between different outcomes. Fully synchronized systems even reach consensus at lower confidence bounds for larger step longitudes. However, this scenario poses challenges in replicating real-world debates effectively.

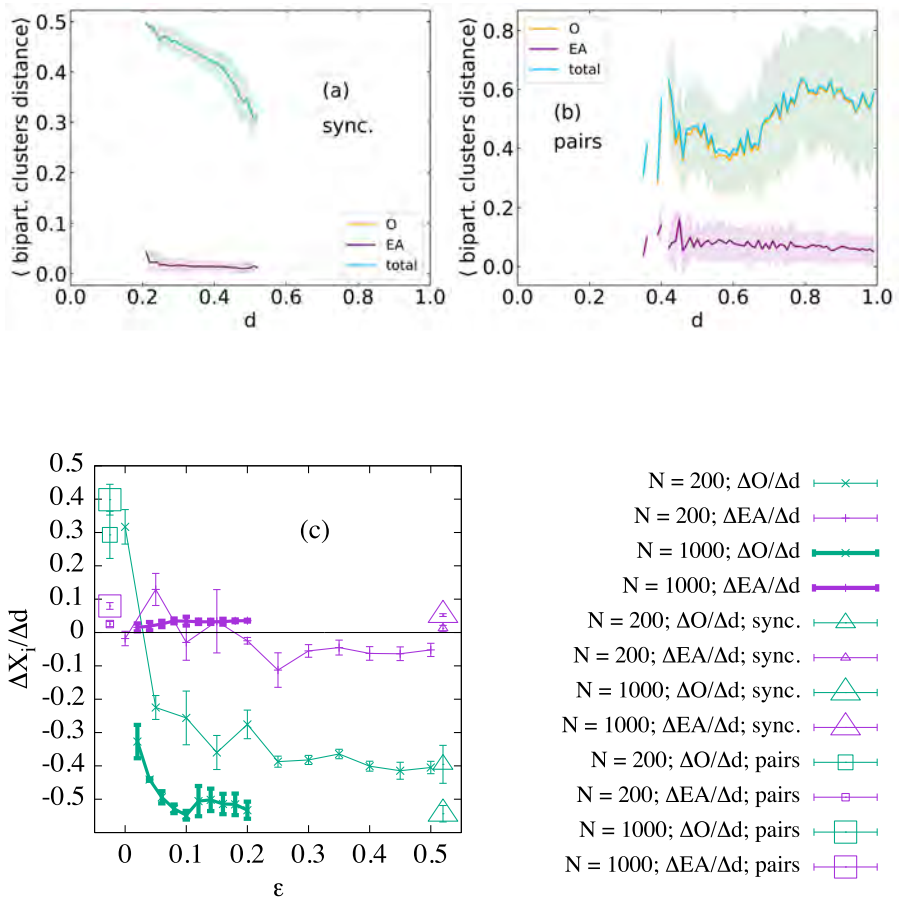

Figure B.14: Distance between the two clusters observed in realizations with a bipartisan outcome, shown on both the opinion axis O (in light blue) and the emotional arousal axis EA (in purple), plotted against the basal confidence bound d for both (a) the synchronized case and (b) the pairwise case. (c) Slopes derived from linear regressions fitted to the O distance (in light blue) and the EA distance (in purple) between these clusters against d, accompanied by their respective errors, as a function of ϵ. The results are based on systems with $N = 1000$ agents for (a) and (b), and $N = 200, 1000$ agents in (c), conducting 300 repetitions with different initial conditions for each set of parameters. Values of d with less the 10 percent of repetitions ending in bipartisanship were discarded for the linear regression.

Synchronization, above all factors, appears as the most favorable to consensus attainment. Furthermore, the position of the consensus cluster has a lower EA than the initial average $\langle EA \rangle$. Additionally, in the synchronized case there is a narrow range of the basal confidence bound d, around 0.4, within which the outcome is always bipartisanship regardless of initial conditions, the exact position of this d range shifts slightly with N and α towards lower d. Furthermore, synchronization not only fosters consensus but also diminishes opinion distance between clusters as d increases in bipartisan outcomes. In contrast, in pairwise and sequential cases, this distance expands with d.

Phase diagrams for d and ϵ show more complex profile demonstration a more intrincate interplay between these two parameters than between α and ϵ. A larger α disrupts transitions toward consensus, except for synchronized systems where in contrast larger α achieve consensus at lower d.

Agent density plays a relevant role in shaping the distribution of the system's basins of attraction as well. Having people holding opinions in between other people builds more links in the system and as a consequence higher agent densities tend to diminish the final number of opinion groups, particularly within parameter regions that lead to fragmentation into multiple clusters (low ϵ, low d, and high α)

The system is very dependent on the initial positions of the agents in the O-EA plane and on the relative position of the first emitter.

The emotional arousal dimension enhances the relevance of small opinion groups, called wings. For instance, the presence of highly emotional minorities, although filtered, notably impacts final levels of emotional arousal, because they are capable of triggering a general increase in $\langle EA \rangle$ before segregating from the bigger groups. Small opinion groups, which used to appear only in the extremes of the opinion segment for the unidimensional model can now emerge in moderate opinions, especially for large step lengths. They also appear with lower levels of emotional arousal for small α.

High α and low d scenarios consistently result in highly fragmented situations, but in general fragmentation is intricately influenced by interaction patterns related to synchronization and step length per interaction. In practical scenarios, these magnitudes would reflect intrinsic attributes, different for each agent. However, as an initial approximation, considering the mean values of participating agents in the modeled scenario suffices. Navigating the interplay between various system parameters becomes complex, particularly in promoting consensus within deliberative spaces. Achieving consensus can be a sensitive endeavor due to multiple influencing factors.

Our model, designed to simulate deliberative spaces, involves agents capable of potential interactions without any specific underlying network topology affecting their interaction patterns, which are conditioned only by the confidence interval. the model could be applied to describe opinion formation in debating chambers, representing hours-long deliberations with presumably short displacements after a round of interactions. Another potential scenario involves extended online discussions on media platforms, occurring over months, thus allowing again to consider a complete underlying graph. Larger alpha values probably model more effectively the latter situation.

Another viewpoint on interpreting the parameters of the model pertains to the level of fragmentation or the number of active parties during country elections. A greater number of parties often correlates with longer step lengths contributing to opinion fragmentation, except in fully synchronized cases. Similarly, reducing synchronization or a decline in the basal confidence bound may increase the final number of opinion groups. The actual scenario likely results from a blend of multiple contributing factors.

B.5

Supplementary material

B.5.1 - The algorithm

Algorithm 4 Performs an agent-based simulation using the broadcasting bounded confidence model with emotional arousal and synchronization dynamics.

Require: Number of agents N. A length step α, a basal confidence bound d (confidence bound at $EA = 0$) and a synchronization factor ϵ. A tolerance μ to consider stationarity.

Ensure: Getting to one of the stationary attractors of the dynamics, given a sufficiently large N_{steps}

set $step = 0$
set $step_{sync} = 0$
set initial positions $\{\mathbf{O}_i\}_{initial}$ and $\{\mathbf{EA}_i\}_{initial}$ uniformly at random in the range $[0, 1]$
set initial phases $\{\phi_i\}_{initial}$ uniformly at random in the range $[0, 1]$ (or $\{\phi_i\}_{initial} = 1$ in the sync. case
repeat
  $\Delta\phi = 1 - \phi_{max}$
  Update all agents phases $\{\phi_i\} = \{\phi_i\} + \Delta\phi$
  repeat
    for all ϕ_i ϕ_j with i, j $\in 1, ..., N$ **do**
      if $\phi_i = 1$ **then**
        $dist_{ij} = \sqrt{(O_i - O_j)^2 + EA_i - EA_j)^2}$
        if $dist_{ij} < d$ **then**
          $c = min\{1, \alpha/dist\}$
          $\mathbf{O_j} = \mathbf{O_j} + c\mathbf{O_j}$
          $\mathbf{EA_j} = \mathbf{EA_j} + c\mathbf{EA_j}$
          $\phi_j = \epsilon\phi_j$
        end if
      end if
    end for
  until $\{\phi_i \neq 1$
  $step = step + 1$
  if $\phi_i = \phi_j$ $\forall$ i, j $\in$ same connected component **then**
    $step_{sync} = step_{sync} + 1$
  end if
until $\{|\mathbf{\Delta O_i}|\}$, $\{|\mathbf{\Delta EA_i}|\} < \mu$
return $\{\mathbf{O}_i\}_{final}$ and $\{\mathbf{EA}_i\}_{final}$, $step$ and $step_{sync}$ set of final positions states, number of steps when the simulation stops and number of step after local syncronization

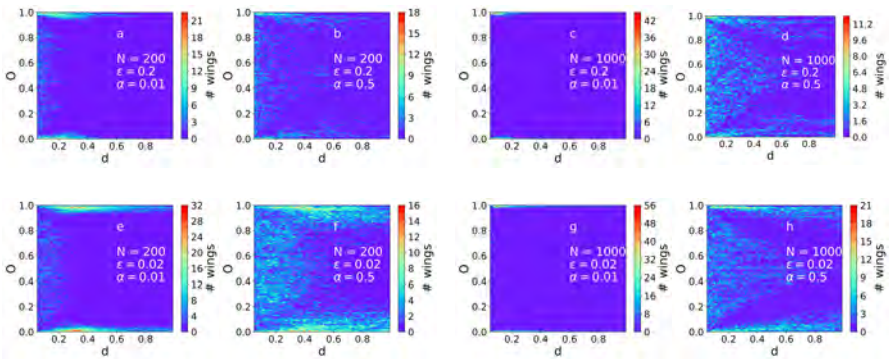

Figure B.15: Number of wings as a function of their opinion and the basal confidence bound d for a coupling factor $\epsilon = 0.2$ (upper row) and $\epsilon = 0.02$ (lower row), system sizes $N = 200$ (a, b, e, f) and $N = 1000$ (c, d, g, h) and step longitude $\alpha = 0.01$ (a, c, e, g) and $\alpha = 0.5$ (b, d, f, h). Results for 300 simulations with different initial conditions.

B.5.2 - Wings

In the one-dimensional model (41), wings were disregarded due to their negligible role. However, in the model proposed in this study, wings assume greater significance, exhibiting a notable dependence on all parameters. Contrary to their mere appearance at the extremes of the opinion axis, these wings manifest not only at these endpoints but also emerge across various opinion positions, particularly prominent for low d values, as shown in Fig. B.15. A larger step longitude accentuates the dispersion of wings along the opinion axis. For a system of $N = 200$ agents, a small step longitude α, and a high synchronization factor ϵ (Fig. B.15 (a)), these wings tend to appear near the equilibrium points of clusters within the range $0.15 < d < 0.3$ (refer to Subsection B.3.2). This suggests that these points are system attractors for the fully synchronized case, extending their significance beyond their role as preferred positions for the primary clusters.

In our model, wings have typically a large EA, and that's why they become isolated from the rest of the system. However, in some cases, wings can also have lower EA (see Fig. B.16), especially in the parameter region with a clear predominance of a bipartisan outcome.

B.5.3 - The approximation for the synchronized case

We can improve the estimation for the different outcomes in the synchronized case if we modify the lower bound of the second sum in Eq. B.4, requiring a

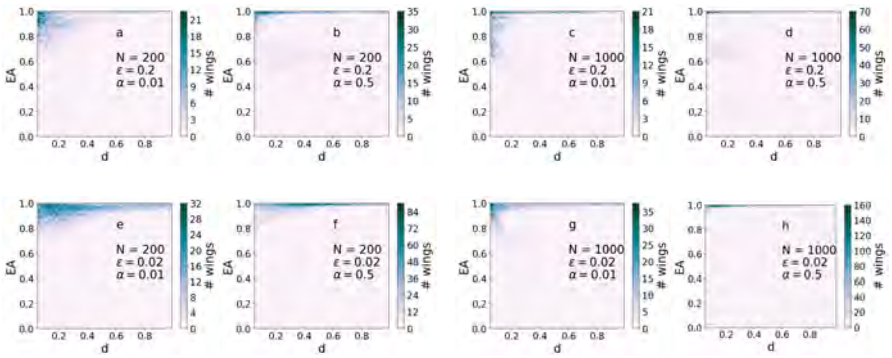

Figure B.16: Number of wings as a function of their emotional arousal and the basal confidence bound d for a coupling factor $\epsilon = 0.2$ (upper row) and $\epsilon = 0.02$ (lower row), system sizes $N = 200$ (a, b, e, f) and $N = 1000$ (c, d, g, h) and step longitude $\alpha = 0.01$ (a, c, e, g) and 0.5 (b, d, f, h). Results for 300 simulations with different initial conditions.

Table B.2: Table illustrating the minimum number of agents required to initially lie within each outcome's affectation area in order to estimate its probability, for different system sizes N and step lengths α.

N	α	**Sum lower bound Eq. B.4**
200	0.01	$N/2$
200	0.5	$N/2 - N/18$
1000	0.01	$N/2 - N/25$
1000	0.5	$N/2 - N/12$

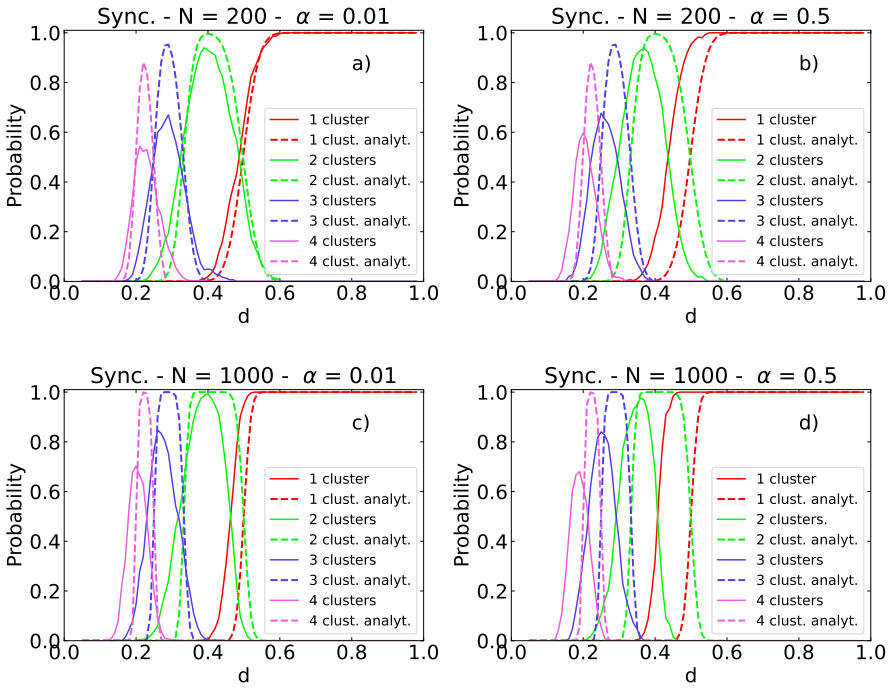

Figure B.17: Proportion of final scenarios as a function of the basal confidence bound d for a) synchronized interactions, step longitude $\alpha = 0.01$ and system size $N = 200$, (b) synchronized interactions, $\alpha = 0.5$ and $N = 200$, c) synchronized interactions, $\alpha = 0.01$ and $N = 1000$, d) step $\alpha = 0.5$ and $N = 1000$. Results were obtained for 300 simulations with different initial conditions. Continuous lines correspond to simulations while dashed lines are for the semi-analytical approximation.

lower minimum number of agents to lie initially within the considered attraction area. Although we see that the analytical expression for this bound is an increasing function of α and N. In this Appendix, we present the shifted predictions obtained by relaxing the summation lower bound as indicated in Table B.2. A finite size scaling in a broad step length range could give us the exact expression.

B.5.4 - The experiments

A series of ongoing experiments titled Dialoguem! (meaning *Let's talk!* in Catalan) aims to validate and potentially calibrate the model in its synchronized variant. In Dialoguem!, participants are presented with a question via a Telegram chatbot, and are encouraged to express their opinions anonymously within the model's defined opinion segment. Following this, they articulate a sentence to elucidate their stance. Subsequently, participants engage in reading and rating all other participants' sentences, then they assess their inclination to reach an agreement with the sender of each statement (i.e., if they fall within the model's interaction threshold). As the process unfolds, if participants modify their initial opinions, they adjust their position within the opinion segments. This iterative process continues until all participants confirm they do not wish to change their positions within the opinion segments any further. The evaluation of other participants' statements holds significant importance as self-assessment of opinions tends to be subjective and inconsistent. However, aggregating ratings from all participants regarding a given opinion yields more accurate predictions of shifts within the opinion segments between rounds. Nonetheless, it's noteworthy that the experiment's results are still inconclusive from a statistical perspective.

Bibliography

[1] Abelson, R. (1964). Mathematical models of the distribution of attitudes under controversy. In Fredericksen, N. and Gullicksen, H., editors, *Contributions to mathematical psychology*. Holt, Rinehart & Winston, New York. [Cited on page 6]

[2] Abelson, R. P. and Rosenberg, M. J. (1958). Symbolic psycho-logic: A model of attitudinal cognition. *Behav. Sci.*, 3(1):1–13. [Cited on page 95]

[3] Aiyappa, R., Flammini, A., and Ahn, Y.-Y. (2023). Weighted belief networks unify simple and complex contagion dynamics. Submitted on 6 Jan 2023. [Cited on page 97]

[4] Albert, R. and Barabási, A.-L. (2002). Statistical mechanics of complex networks. *RMP*, 74(1):47–97. [Cited on page 13]

[5] AlSonosy, O., Rady, S., Badr, N., and Hashem, M. (2018). *Business Behavior Predictions Using Location Based Social Networks in Smart Cities*, pages 105–122. Springer Singapore, Singapore. [Cited on page 7]

[6] Arenas, A., Díaz-Guilera, A., and Pérez-Vicente, C. J. (2006). Synchronization reveals topological scales in complex networks. *Phys. Rev. Lett.*, 96:114102. [Cited on pages 55 and 61]

[7] Arenas, A., Fernández, A., and Gómez, S. (2008). Analysis of the structure of complex networks at different resolution levels. *New J. Phys.*, 10(5):053039. [Cited on pages 11 and 56]

[8] Axelrod, R. (1997). The dissemination of culture: A model with local convergence and global polarization. *J. Conflict Resolut.*, 41(2):203–226. [Cited on page 5]

[9] Baek, Y., Ha, M., and Jeong, H. (2012). Absorbing states of zero-temperature Glauber dynamics in random networks. *Phys. Rev. E*, 85(3):031123. [Cited on page 53]

[10] Balenzuela, P., Pinasco, J. P., and Semeshenko, V. (2015). The undecided have the key: Interaction-driven opinion dynamics in a three state model. *PLOS ONE*, 10(10):1–21. [Cited on page 45]

[11] Barabási, A.-L. and Albert, R. (1999). Emergence of scaling in random networks. *Science*, 286(5439):509–512. [Cited on page 13]

[12] Baravi, T., Feinerman, O., and Raz, O. (2022). Echo chambers in the ising model and implications on the mean magnetization. *Journal of Statistical Mechanics: Theory and Experiment*, 2022(4):043402. [Cited on pages 4, 18, and 23]

[13] Baronchelli, A. and Díaz-Guilera, A. (2012). Consensus in networks of mobile communicating agents. *Phys. Rev. E*, 85:016113. [Cited on page 73]

[14] Baumann, F., Lorenz-Spreen, P., Sokolov, I. M., and Starnini, M. (2020). Modeling echo chambers and polarization dynamics in social networks. *Phys. Rev. Lett.*, 124(4):048301. [Cited on pages 4, 18, and 129]

[15] Baumann, F., Lorenz-Spreen, P., Sokolov, I. M., and Starnini, M. (2021). Emergence of polarized ideological opinions in multidimensional topic spaces. *Phys. Rev. X*, 11(1):011012. [Cited on page 95]

[16] Benjamini, I., Chan, S.-O., O'Donnell, R., Tamuz, O., and Tan, L.-Y. (2016). Convergence, unanimity and disagreement in majority dynamics on unimodular graphs and random graphs. *Stoch. Process. their Appl.*, 126(9):2719–2733. [Cited on page 48]

[17] Bergstrom, C. T. and Bak-Coleman, J. B. (2019). Information gerrymandering in social networks skews collective decision-making. *Nature*, 573(7772):40–41. [Cited on page 19]

[18] Bianconi, G. (2002). Mean field solution of the Ising model on a barabási–albert network. *Phys. Lett. A*, 303(2-3):166–168. [Cited on page 48]

[19] Binder, K., Stauffer, D., and Müller-Krumbhaar, H. (1975). Theory for the dynamics of clusters near the critical point. i. relaxation of the glauber kinetic ising model. *Phys. Rev. B*, 12:5261. [Cited on page 23]

[20] Blume, M., Emery, V. J., and Griffiths, R. B. (1971). Ising model for the transition and phase separation in He3-He4 mixtures. *Phys. Rev. A*, 4(3):1071–1077. [Cited on pages 25 and 27]

[21] Bollobás, B. (2001). *Random Graphs*. Cambridge Studies in Advanced Mathematics. Cambridge University Press. [Cited on page 12]

[22] Bonato, A., Lozier, M., Mitsche, D., Pérez-Giménez, X., and Prałat, P. (2015). The domination number of on-line social networks and random geo-

metric graphs. In *Theory and Appl. Models Comput.*, volume 9076 of *Lect. Notes Comput. Sci.*, pages 196–207. Springer, Cham. [Cited on page 15]

[23] Bordogna, C. M. and Albano, E. V. (2007). Dynamic behavior of a social model for opinion formation. *Phys. Rev. E*, 76:061125. [Cited on page 24]

[24] Bovet, A. and Makse, H. A. (2019). Influence of fake news in twitter during the 2016 US presidential election. *Nat. Commun.*, 10(1):7. [Cited on page 18]

[25] Bray, A. J. (1994). Theory of phase-ordering kinetics. *Adv. Phys.*, 43(3):357–459. [Cited on page 23]

[26] Castellano, C., Fortunato, S., and Loreto, V. (2009). Statistical physics of social dynamics. *Rev. Mod. Phys.*, 81(2):591–646. [Cited on pages 19 and 23]

[27] Castelló, X., Eguíluz, V. M., and Miguel, M. S. (2006). Ordering dynamics with two non-excluding options: bilingualism in language competition. *New J. Phys.*, 8(12):308–308. [Cited on page 24]

[28] Chen, H. and Hou, Z. (2011). Optimal modularity for nucleation in a network-organized ising model. *Phys. Rev. E*, 83(4). [Cited on page 56]

[29] Chmiel, A., Sienkiewicz, J., and Sznajd-Weron, K. (2017). Tricriticality in the q-neighbor ising model on a partially duplex clique. *Phys. Rev. E*, 96:062137. [Cited on pages 23 and 116]

[30] Comte, A. (1855). *The Positive Philosophy*. American Mathematical Society, New York. [Cited on page 4]

[31] Couzin, I. D., Krause, J., James, R., Ruxton, G. D., and Franks, N. R. (2002). Collective memory and spatial sorting in animal groups. *J. Theor. Biol.*, 218(1):1–11. [Cited on page 73]

[32] Dalege, J. and van der Does, T. (2022). Using a cognitive network model of moral and social beliefs to explain belief change. *Sci Adv*, 8(33). [Cited on page 96]

[33] Dall, J. and Christensen, M. (2002a). Random geometric graphs. *Phys. Rev. E*, 66:016121. [Cited on page 15]

[34] Dall, J. and Christensen, M. (2002b). Random geometric graphs. *Phys. Rev. E*, 66:016121. [Cited on page 76]

[35] Danon, L., Díaz-Guilera, A., Duch, J., and Arenas, A. (2005). Comparing community structure identification. *J. Stat. Mech.: Theory Exp.*, 2005(09):P09008–P09008. [Cited on pages 55 and 61]

[36] Das, T. K., Abeyasinghe, P. M., Crone, J. S., Sosnowski, A., Laureys, S., Owen, A. M., and Soddu, A. (2014). Highlighting the structure-function rela-

tionship of the brain with the Ising model and graph theory. *BioMed Res. Int.*, 2014:1–14. [Cited on page 7]

[37] Dasgupta, S., Pan, R. K., and Sinha, S. (2009). Phase of ising spins on modular networks analogous to social polarization. *Phys. Rev. E*, 80:025101. [Cited on page 23]

[38] Davison, A. P. and Appukuttan, S. (2022). Computational neuroscience: A faster way to model neuronal circuitry. *eLife*, 11:e84463. [Cited on page 96]

[39] De Martino, D., Bradde, S., Dall'Asta, L., and Marsili, M. (2012). Topology-induced inverse phase transitions. *EPL*, 98(4):40004. [Cited on page 48]

[40] Deffuant, G., Amblard, F., Weisbuch, G., and Faure, T. (2002). How can extremism prevail? a study based on the relative agreement interaction model. *J. Artif. Soc. Soc. Simul.*, 5(4). [Cited on pages 6 and 129]

[41] Deffuant, G., Neau, D., Amblard, F., and Weisbuch, G. (2000). Mixing beliefs among interacting agents. *Adv. in Compl. Syst.*, 3(4):87–98. [Cited on pages 6, 129, 132, 136, 137, and 164]

[42] DeSteno, D., Petty, R., Rucker, D., Wegener, D., and Braverman, J. (2004). Discrete emotions and persuasion: The role of emotion-induced expectancies. *J. Pers. Soc. Psychol.*, 86:43–56. [Cited on page 6]

[43] Dorogovtsev, S., Goltsev, A. V., and Mendes, J. F. F. (2008). Critical phenomena in complex networks. *Rev. Mod. Phys.*, 80(4):1275–1335. [Cited on page 48]

[44] Dunn, J. and Schweitzer, M. E. (2005). Feeling and believing: The influence of emotion on trust. *J. Pers. Soc. Psychol.*, 88(5):736–748. [Cited on page 6]

[45] Ellinas, C., Allan, N., and Johansson, A. (2017). Dynamics of organizational culture: Individual beliefs vs. social conformity. *PLoS ONE*, 12(6):e0180193. [Cited on page 97]

[46] Engel, A., Monasson, R., and Hartmann, A. K. (2004). On large deviation properties of erdös-rényi random graphs. *Journal of Statistical Physics*, 117(3–4):387–426. [Cited on page 24]

[47] Erdös, P. and Rényi, A. (1959). On random graphs I. *Publ. Math. Debr.*, 6:290–297. [Cited on page 12]

[48] Escobar, L. A., Kim, H., and Gershenson, C. (2019). Effects of antimodularity and multiscale influence in random boolean networks. *Complexity*, 2019:1–14. [Cited on page 96]

[49] Esteban, J. M. and Ray, D. (1994). On the measurement of polarization. *Econometrica*, 62:819–851. [Cited on page 133]

[50] Farías, C. and Davis, S. (2021). Multiple metastable states in an off-lattice potts model. *Physica A: Statistical Mechanics and its Applications*, 581:126215. [Cited on page 73]

[51] Fernandes, F. P. and Lima, F. W. S. (2008). Persistence in the zero-temperature dynamics of the q-states potts model on undirected-directed barabÁsi–albert networks and erdÖs–rÉnyi random graphs. *International Journal of Modern Physics C*, 19(12):1777–1785. [Cited on page 24]

[52] Fernandez, M. A., Korutcheva, E., and de la Rubia, F. J. (2016). A 3-states magnetic model of binary decisions in sociophysics. *Physica A*, 462:603–618. [Cited on pages 24 and 26]

[53] Ferri, I., Gaya-Àvila, A., and Díaz-Guilera, A. (2023). Three-state opinion model with mobile agents. *Chaos*, 33:093121. [Cited on page 30]

[54] Ferri, I., Palassini, M, Pérez-Vicente, C., and Díaz-Guilera, A. (2022a). Three-state opinion model on complex topologies. [Cited on pages 30, 33, 54, 58, 74, 75, and 107]

[55] Ferri, I., Pérez-Vicente, C., Palassini, M., and Díaz-Guilera, A. (2022b). Three-state opinion model on complex topologies. *Entropy*, 24(11). [Cited on pages 30, 55, 74, 75, 80, and 92]

[56] Festinger, L. (1957). *A Theory of Cognitive Dissonance*. Stanford University Press, Stanford, CA. [Cited on page 98]

[57] Fortunato, S. (2002). Site percolation and phase transitions in two dimensions. *Phys. Rev. B*, 66:054107. [Cited on page 23]

[58] Fortunato, S. (2010a). Community detection in graphs. *Phys. Rep.*, 486(3-5):75–174. [Cited on pages 15 and 24]

[59] Fortunato, S. (2010b). Community detection in graphs. *Phys. Rep.*, 486(3-5):75–174. [Cited on page 55]

[60] Fortunato, S. and Hric, D. (2016). Community detection in networks: A user guide. *Phys. Rep.*, 659:1–44. [Cited on page 10]

[61] Gaisbauer, F., Olbrich, E., and Banisch, S. (2020). Dynamics of opinion expression. *Phys. Rev. E*, 102(4):042303. [Cited on page 18]

[62] Galam, S. (1997). Rational group decision making: A random field ising model at t = 0. *Physica A*, 238(1-4):66–80. [Cited on pages 5 and 20]

[63] Galam, S. (2012). *Sociophysics*. Springer US. [Cited on page 18]

[64] Galam, S. (2013). Modeling the forming of public opinion: An approach from sociophysics. *Glob. Econ. Rev.*, 18(1):2–11. [Cited on page 18]

[65] Galam, S. and Jacobs, F. (2007). The role of inflexible minorities in the breaking of democratic opinion dynamics. *Physica A*, 381:366–376. [Cited on page 20]

[66] Galam, S. and Martins, A. (2015). Two-dimensional Ising transition through a technique from two-state opinion-dynamics models. *Phys. Rev. E*, 91(1):. – . [Cited on pages 20 and 23]

[67] Gauvin, L., Nadal, J.-P., and Vannimenus, J. (2010). Schelling segregation in an open city: A kinetically constrained blume-emery-griffiths spin-1 system. *Phys. Rev. E*, 81:066120. [Cited on page 25]

[68] Gauvin, L., Tizzoni, M., Piaggesi, S., Young, A., Adler, N., Verhulst, S., Ferres, L., and Cattuto, C. (2020). Gender gaps in urban mobility. *Hum. Soc. Sci. Commun.*, 7(1). [Cited on page 73]

[69] Gilks, W. R., Richardson, S., and Spiegelhalter, D. J. (1996). *Markov Chain Monte Carlo in Practice*. Chapman and Hall/CRC, 1st edition. [Cited on page 74]

[70] Girvan, M. and Newman, M. E. J. (2002). Community structure in social and biological networks. *Proc. Natl. Acad. Sci. U.S.A.*, 99(12):7821–7826. [Cited on page 75]

[71] Goldenfeld, N. (1992). *Lectures on Phase Transitions and the Renormalization Groufp*, volume 85 of *Frontiers in Physics*. Addison-Wesley, Reading, MA. [Cited on pages 21 and 33]

[72] Granovetter, M. S. (1973). The strength of weak ties. *American Journal of Sociology*, 78(6):1360–1380. [Cited on page 96]

[73] Granovsky, B. L. and Madras, N. (1995). The noisy voter model. *Stoch. Process. their Appl.*, 55(1):23–43. [Cited on page 20]

[74] Gross, T. and Sayama, H. (2009). *Adaptive Networks: Theory, Models and Applications*. Springer Publishing Company, Incorporated, 1st edition. [Cited on page 74]

[75] Guimerà, R., Sales-Pardo, M., and Amaral, L. A. N. (2004). Modularity from fluctuations in random graphs and complex networks. *Phys. Rev. E*, 70:025101. [Cited on page 7]

[76] Gómez-Gardeñes, J., de Domenico, M., Gutiérrez, G., Arenas, A., and Gómez, S. (2015). Layer–layer competition in multiplex complex networks. *Philos. Trans. R. Soc. A*, 373(2056):20150117. [Cited on page 116]

[77] Hegselmann, R. and Krause, U. (2002). Opinion dynamics and bounded confidence, models, analysis and simulation. *J. Artif. Soc. Soc. Simul.*, 5(3):2. [Cited on pages 6 and 134]

[78] Herrero, C. P. (2002). Ising model in small-world networks. *Phys. Rev. E*, 65(6):066110. [Cited on page 23]

[79] HOHNISCH, M., PITTNAUER, S., SOLOMON, S., and STAUFFER, D. (2005). Socioeconomic interaction and swings in business confidence indicators. *Physica A: Statistical Mechanics and its Applications*, 345(3–4):646–656. [Cited on page 26]

[80] Holley, R. A. and Liggett, T. M. (1975). Ergodic Theorems for Weakly Interacting Infinite Systems and the Voter Model. *Ann. Probab.*, 3(4):643 – 663. [Cited on pages 5 and 19]

[81] Holme, P. and Kim, B. J. (2002). Growing scale-free networks with tunable clustering. *Phys. Rev. E*, 65(2):026107. [Cited on page 12]

[82] Hurtado-Marín, V. A., Agudelo-Giraldo, J. D., Robledo, S., and Restrepo-Parra, E. (2021). Analysis of dynamic networks based on the ising model for the case of study of co-authorship of scientific articles. *Sci. Rep.*, 11(1):5721. [Cited on page 23]

[83] Ising, E. (1925). Beitrag zur theorie des ferromagnetismus. *Zeitschrift für Physik*, 31(1):253–258. [Cited on pages 5 and 20]

[84] Jacobs, M. and Walch, O. (2018). A partial differential equations approach to defeating partisan gerrymandering. [Cited on page 19]

[85] Jang, S., Lee, J. S., Hwang, S., and Kahng, B. (2015). Ashkin-teller model and diverse opinion phase transitions on multiplex networks. *Phys. Rev. E*, 92:022110. [Cited on page 116]

[86] Janke, W., Christiansen, H., and Majumder, S. (2019). Coarsening in the long-range ising model: Metropolis versus glauber criterion. *Journal of Physics: Conference Series*, 1163:012002. [Cited on page 23]

[87] Jensen, H. J. (2022). *Complexity Science: The Study of Emergence*. Cambridge University Press. [Cited on page 3]

[88] Jia, X. (2004). Wireless networks and random geometric graphs. In *Proceedings of the 7th International Symposium on Parallel Architectures, Algorithms and Networks (ISPAN 2004)*, pages 575–579. [Cited on page 15]

[89] Kan, U., Feng, M., and Porter, M. A. (2023). An adaptive bounded-confidence model of opinion dynamics on networks. *Journal of Complex Networks*, 11(1):415–444. [Cited on page 136]

[90] Kaufman, M., Kaufman, S., and Diep, H. T. (2022). Statistical mechanics of political polarization. *Entropy*, 24(9):1262. [Cited on page 18]

[91] Kaufman, M., Kaufman, S., and Diep, H. T. (2024). Social depolarization: Blume–capel model. *Physics*, 6(1):138–147. [Cited on page 18]

[92] Kim, H., Pineda, O. K., and Gershenson, C. (2019). A multilayer structure facilitates the production of antifragile systems in boolean network models. *Complexity*, 2019:1–11. [Cited on page 96]

[93] Korbel, J., Lindner, S. D., Pham, T. M., Hanel, R., and Thurner, S. (2023). Homophily-based social group formation in a spin glass self-assembly framework. *Phys. Rev. Lett.*, 130:057401. [Cited on page 95]

[94] Kossinets, G. and Watts, D. J. (2009). Origins of homophily in an evolving social network. *Am. J. Sociol.*, 115(2):591–646. [Cited on page 20]

[95] Krawiecki, A. (2018). Spin glass transition in a simple variant of the ising model on multiplex networks. *Physica A*, 506:773–790. [Cited on page 116]

[96] Kureh, Y. H. and Porter, M. A. (2020). Fitting in and breaking up: A nonlinear version of coevolving voter models. *Phys. Rev. E*, 101(6):062303. [Cited on pages 20 and 121]

[97] Kutner, R., Ausloos, M., Grech, D., Matteo, T. D., Schinckus, C., and Stanley, H. E. (2019). Econophysics and sociophysics. *Physica A*, 516:240–253. [Cited on page 18]

[98] Lazarsfeld, P. F. and Merton, R. K. (1954). Friendship as a social process: a substantive and methodological analysis. *Freedom and Control in Modern Society*, pages 18–66. [Cited on page 20]

[99] Leone, M., Vázquez, A., Vespignani, A., and Zecchina, R. (2002a). Ferromagnetic ordering in graphs with arbitrary degree distribution. *Euro. Phys. J. B*, 28(2):191–197. [Cited on pages 29 and 48]

[100] Leone, M., Vázquez, A., Vespignani, A., and Zecchina, R. (2002b). Ferromagnetic ordering in graphs with arbitrary degree distribution. *Euro. Phys. J. B*, 28(2):191–197. [Cited on page 49]

[101] Li, H.-J., Wang, Y.-C., Wu, L.-Y., Liu, Z.-P., Chen, L., and Zhang, X.-S. (2012). Community structure detection based on Potts model and network's spectral characterization. *EPL*, 97(4):48005. [Cited on pages 24 and 56]

[102] Li, L., Fan, Y., Zeng, A., and Di, Z. (2019). Binary opinion dynamics on signed networks based on Ising model. *Physica A*, 525:433–442. [Cited on pages 20 and 23]

[103] Li, L., Zeng, A., Fan, Y., and Di, Z. (2022). Modeling multi-opinion propagation in complex systems with heterogeneous relationships via potts model on signed networks. *Chaos: An Interdisciplinary Journal of Nonlinear Science*, 32(8). [Cited on page 24]

[104] Li, X., Jin, Y. Y., and Chen, G. (2003). Complexity and synchronization of the world trade web. *Physica A*, 328(1-2):287–296. [Cited on page 7]

[105] Lu, D., Tian, Y., Liu, V. Y., and Zhang, Y. (2015). The performance of the smart cities in china—a comparative study by means of self-organizing maps and social networks analysis. *Sustainability*, 7(6):7604–7621. [Cited on page 7]

[106] Lü, L., Chen, D.-B., and Zhou, T. (2011). The small world yields the most effective information spreading. *New J. Phys.*, 13(12):123005. [Cited on page 18]

[107] Marinazzo, D., Pellicoro, M., Wu, G., Angelini, L., Cortés, J. M., and Stramaglia, S. (2014). Information transfer and criticality in the ising model on the human connectome. *PLoS ONE*, 9:e93616. [Cited on page 7]

[Metropolis et al.] Metropolis, N., Rosenbluth, A. W., Rosenbluth, M. N., Teller, A. H., and Teller, E. Equation of state calculations by fast computing machines. *J. Chem. Phys.*, 21(6). [Cited on page 74]

[109] Min, B. (2023). Coevolutionary dynamics of group interactions: coevolving nonlinear voter models. *Frontiers in Complex Systems*, 1. [Cited on page 121]

[110] Mitchell, M. (2009). *Complexity: A Guided Tour*. Oxford University Press. [Cited on page 3]

[111] Mobilia, M. (2003). Does a single zealot affect an infinite group of voters? *Phys. Rev. Lett.*, 91(2):028701. [Cited on pages 20 and 24]

[112] Mobilia, M., Petersen, A., and Redner, S. (2007). On the role of zealotry in the voter model. *J. Stat. Mech. Theory Exp.*, 2007(08):P08029. [Cited on page 24]

[113] Moreno, Y., Nekovee, M., and Pacheco, A. F. (2004). Dynamics of rumor spreading in complex networks. *Physical Review E*, 69(6). [Cited on page 18]

[114] Naderer, B., Rieger, D., and Schwertberger, U. (2023). An online world of bias. the mediating role of cognitive biases on extremist attitudes. *Communications*, 49(1):51–73. [Cited on page 74]

[115] Naskar, M., Acharyya, M., Vatansever, E., and Fytas, N. G. (2021). Metastable behavior of the spin-s Ising and Blume-Capel ferromagnets: A Monte Carlo study. *Phys. Rev. E*, 104(1):014107. [Cited on page 26]

[116] Newman, M. E. J. (2004). Fast algorithm for detecting community structure in networks. *Phys. Rev. E*, 69(6):066133. [Cited on page 15]

[117] Newman, M. E. J. (2006). Modularity and community structure in networks. *Proc. Natl. Acad. Sci. U.S.A.*, 103(23):8577–8582. [Cited on page 10]

[118] Newman, M. E. J. (2010). *Networks: An Introduction*. Oxford Univ. Press, Oxford, UK. [Cited on pages 8 and 12]

[119] Newman, M. E. J. and Girvan, M. (2004). Finding and evaluating community structure in networks. *Phys. Rev. E*, 69(2):026113. [Cited on page 56]

[120] Newman, M. E. J., Watts, D. J., and Strogatz, S. H. (2002). Random graph models of social networks. *Proc. Natl. Acad. Sci. U.S.A.*, 99(suppl_1):2566–2572. [Cited on pages 14 and 47]

[121] Noh, J. D. and Park, H.-C. (2009). Phase transitions and critical behavior in networked sociophysical systems. *Phys. Rev. E*, 79(5):056115. [Cited on page 23]

[122] Olfati-Saber, R. (2006). Flocking for multi-agent dynamic systems: algorithms and theory. *IEEE Trans. Automat. Contr.l*, 51(3):401–420. [Cited on page 73]

[123] Olle Häggström (2002). Zero-temperature dynamics for the ferromagnetic Ising model on random graphs. *Physica A*, 310(3-4):275–284. [Cited on page 53]

[124] Paula, G. L. S. and Figueiredo, W. (1997). The glauber and metropolis transition rates on the stationary states of the ising model. *Modern Physics Letters B*, 11(13):565–570. [Cited on page 22]

[125] Payne, W. and BCcampus (2015). *An Introduction to Philosophy*. Bellevue College. [Cited on page 96]

[126] Penrose, M. (2003). *Random Geometric Graphs*. Oxford University Press. [Cited on page 15]

[127] Perinelli, A., Tabarelli, D., Miniussi, C., and Ricci, L. (2019). Dependence of connectivity on geometric distance in brain networks. *Scientific Reports*, 9(1). [Cited on page 15]

[128] Petter Törnberg (2018). Echo chambers and viral misinformation: Modeling fake news as complex contagion. *PLOS ONE*, 13(9):e0203958. [Cited on page 4]

[129] Pham, T. M., Korbel, J., Hanel, R., and Thurner, S. (2022). Empirical social triad statistics can be explained with dyadic homophylic interactions. *Proceedings of the National Academy of Sciences*, 119(6). [Cited on page 95]

[130] Potts, R. B. (1952). Some generalized order-disorder transformations. *Proc. Camb. Philos. Soc.*, 48:106–109. [Cited on page 23]

[131] Rao, R. P. and Sporns, O. (2014). Brain network dynamics and cognitive functions. *J. Cogn. Neurosci.*, 26(8):xxxx–xxxx. [Cited on page 7]

[132] Reichardt, J. and Bornholdt, S. (2004). Detecting fuzzy community structures in complex networks with a potts model. *Phys. Rev. Lett.*, 93:218701. [Cited on page 24]

[133] Reynolds, C. W. (1987). Flocks, herds and schools: A distributed behavioral model. *SIGGRAPH Comput. Graph.*, 21(4):25–34. [Cited on page 73]

[134] Richardson, L. F. (1949). *Arms and Insecurity*. Publisher Name. [Cited on page 5]

[135] Richardson, L. F. (1960). *Statistics of Deadly Quarrels*. Publisher Name. [Cited on page 5]

[136] Rodriguez, N., Bollen, J., and Ahn, Y.-Y. (2016). Collective dynamics of belief evolution under cognitive coherence and social conformity. *PLOS ONE*, 11(11):e0165910. [Cited on pages 97 and 99]

[137] Rutherford, A., Cebrian, M., Dsouza, S., Moro, E., Pentland, A., and Rahwan, I. (2013). Limits of social mobilization. *Proceedings of the National Academy of Sciences*, 110(16):6281–6286. [Cited on page 4]

[138] Sagarra, O., Szell, M., Santi, P., Díaz-Guilera, A., and Ratti, C. (2015). Supersampling and network reconstruction of urban mobility. *PLOS ONE*, 10(8):e0134508. [Cited on page 73]

[139] Sayama, H. (2017). Graph product multilayer networks: spectral properties and applications. *Journal of Complex Networks*, 6(3):430–447. [Cited on pages 16 and 98]

[140] Schelling, T. C. (1971). Dynamic models of segregation. *Journal of Mathematical Sociology*, 1(2):143–186. [Cited on pages 5 and 25]

[141] Schieber, T. A., Carpi, L., Díaz-Guilera, A., Pardalos, P. M., Masoller, C., and Ravetti, M. G. (2017). Quantification of network structural dissimilarities. *Nat. Commun.*, 8(1). [Cited on pages 15 and 75]

[142] SCHULZE, C. (2005). Potts-like model for ghetto formation in multicultural societies. *International Journal of Modern Physics C*, 16(03):351–355. [Cited on page 24]

[143] Schweitzer, F., Krivachy, T., and Garcia, D. (2020). An agent-based model of opinion polarization driven by emotions. *Complexity*, 2020:1–11. [Cited on page 129]

[144] Sen, P. and Chakrabarti, B. K. (2014). *Sociophysics: an introduction*. OUP Oxford. [Cited on page 19]

[145] Shekatkar, S. M. (2019). Do zealots increase or decrease the polarization of social networks? *J. Complex Netw.*, 8(4):473–493. [Cited on page 18]

[146] Silva, S. D. and Matsushita, R. (2022). Editorial: Granularity in econophysics and macroeconomics. *Front. Phys.*, 10. [Cited on page 7]

[147] Sinclair, A. and Stauffer, A. (2010). Mobile geometric graphs, and detection and communication problems in mobile wireless networks. [Cited on page 15]

[148] Sire, C. and Majumdar, S. N. (1995). Coarsening in the q-state potts model and the ising model with globally conserved magnetization. *Phys. Rev. E*, 52(1):244–254. [Cited on page 23]

[149] Son, S.-W., Jeong, H., and Noh, J. (2005). Random field ising model and community structure in complex networks. *European Physical Journal B*, 50. [Cited on page 56]

[150] Sood, V. and Redner, S. (2005). Voter model on heterogeneous graphs. *Physical Review Letters*, 94(17):178701. [Cited on page 47]

[151] Souma, W., Fujiwara, Y., and Aoyama, H. (2003). Complex networks and economics. *Physica A*, 324(1-2):396–401. [Cited on page 7]

[152] Sporns, O., Tononi, G., and Kötter, R. (2005). The human connectome: A structural description of the human brain. *PLoS Comput. Biol.*, 1(4):e42. [Cited on page 96]

[153] Starnini, M., Frasca, M., and Baronchelli, A. (2016). Emergence of metapopulations and echo chambers in mobile agents. *Sci. Rep.*, 6(1). [Cited on pages 4 and 92]

[154] Stewart, A. J., Mosleh, M., Diakonova, M., Arechar, A. A., Rand, D. G., and Plotkin, J. B. (2019). Information gerrymandering and undemocratic desicions. *Nature*, 573(7772):117–121. [Cited on page 19]

[155] Su, R., Xiao, J., McBride, E. C., and Goulias, K. G. (2021). Understanding senior's daily mobility patterns in California using human mobility motifs. *J. Transp. Geogr.*, 94:103117. [Cited on page 73]

[156] Suchecki, K., Eguíluz, V. M., and Miguel, M. (2005). Voter model dynamics in complex networks: Role of dimensionality, disorder, and degree distribution. *Phys. Rev. E*, 72(3):036132. [Cited on page 20]

[157] Svenkeson, A. and Swami, A. (2015a). Reaching consensus by allowing moments of indecision. *Sci. Rep.*, 5(1):14839. [Cited on page 25]

[158] Svenkeson, A. and Swami, A. (2015b). Reaching consensus by allowing moments of indecision. *Sci. Rep.*, 5(1):14839. [Cited on pages 45 and 68]

[159] Sznajd-Weron, K. and Sznajd, J. (2000). Opinion evolution in closed community. *Int. J. Mod. Phys. C*, 11(06):1157–1165. [Cited on page 5]

[160] Tapias, D., Paprotzki, E., and Sollich, P. (2020). From entropic to energetic barriers in glassy dynamics: the barrat–mézard trap model on sparse networks. *Journal of Statistical Mechanics: Theory and Experiment*, 2020(9):093302. [Cited on page 120]

[161] van der Maas, H. L. J., Dalege, J., and Waldorp, L. (2020). The polarization within and across individuals: the hierarchical ising opinion model. *J Complex Networks*, 8(2). [Cited on page 97]

[162] Vazquez, F., Krapivsky, P. L., and Redner, S. (2003). Constrained opinion dynamics: freezing and slow evolution. *J. Phys. A*, 36(3):L61–L68. [Cited on pages 24 and 25]

[163] Vazquez, F. and Redner, S. (2004a). Ultimate fate of constrained voters. *J. Phys. A*, 37(35):8479–8494. [Cited on page 25]

[164] Vazquez, F. and Redner, S. (2004b). Ultimate fate of constrained voters. *J. Phys. A*, 37(35):8479–8494. [Cited on page 45]

[165] Vicsek, T., Czirók, A., Ben-Jacob, E., Cohen, I., and Shochet, O. (1995). Novel type of phase transition in a system of self-driven particles. *Phys. Rev. Lett.*, 75:1226–1229. [Cited on page 73]

[166] Vlasceanu, M., Dyckovsky, A. M., and Coman, A. (2023). A network approach to investigate the dynamics of individual and collective beliefs: Advances and applications of the bending model. *Perspectives on Psychological Science*, 19(2):444–453. [Cited on page 96]

[167] Wang, X., Sirianni, A. D., Tang, S., Zheng, Z., and Fu, F. (2020). Public discourse and social network echo chambers driven by socio-cognitive biases. *Phys. Rev. X*, 10(4):041042. [Cited on page 4]

[168] Watts, D. J. and Strogatz, S. H. (1998). Collective dynamics of 'small-world' networks. *Nature*, 393(6684):440–442. [Cited on pages 5, 9, and 14]

[169] Weidlich, W. (1971). The statistical description of polarization phenomena in society†. *Br J Math Stat Psychol*, 24(2):251–266. [Cited on page 20]

[170] Weisbuch, G. (2004). Bounded confidence and social networks. *Eur. Phys. J. B*, 38(2):339–343. [Cited on pages 6 and 129]

[171] Wilson, K. G. (1971). Renormalization group and critical phenomena. i. renormalization group and the kadanoff scaling picture. *Phys. Rev. B*, 4(9):3174–3183. [Cited on page 21]

[172] Witoelar, A. and Roudi, Y. (2011). Neural network reconstruction using kinetic ising models with memory. *BMC Neurosci.*, 12. [Cited on page 7]

[173] Wu, F. Y. (1982). The potts model. *Rev. Mod. Phys.*, 54(1):235–268. [Cited on page 23]

[174] Wu, M. and Huang, Q. (2022). Human movement patterns of different racial-ethnic and economic groups in U.S. top 50 populated cities: What can social media tell us about isolation? *Ann. GIS*, 28(2):161–183. [Cited on page 73]

[175] Xie, J., Sreenivasan, S., Korniss, G., Zhang, W., Lim, C., and Szymanski, B. K. (2011). Social consensus through the influence of committed minorities. *Phys. Rev. E*, 84:011130. [Cited on page 47]

[176] Yang, V. C., Abrams, D. M., Kernell, G., and Motter, A. E. (2020). Why are U.S. parties so polarized? a "satisficing" dynamical model. *SIAM Rev. Soc. Ind. Appl. Math.*, 62(3):646–657. [Cited on page 18]

[177] Yang, Y.-H. (2010). Blume–emery–griffiths dynamics in social networks. *Physics Procedia*, 3(5):1839–1844. The International Conference on Complexity and Interdisciplinary Sciences. The 3rd China-Europe Summer School on Complexity Sciences. [Cited on pages 24 and 25]

[178] Yildiz, E., Acemoglu, D., Ozdaglar, A., Saberi, A., and Scaglione, A. (2013). Binary opinion dynamics with stubborn agents. *ACM Trans. Econ. Comput.*, 1(4):Article 19. [Cited on page 20]

[179] Zhang, J., Li, C., and Wang, J. (2023). A stochastic block ising model for multi-layer networks with inter-layer dependence. *Biometrics*, 79(4):3564–3573. [Cited on page 116]

[180] Zhao, F., Ye, M., and Huang, S.-L. (2021). Exact recovery of stochastic block model by ising model. *Entropy*, 23(1). [Cited on page 56]

[181] Zitnik, M. and Leskovec, J. (2017). Predicting multicellular function through multi-layer tissue networks. *Bioinformatics*, 33(14):i190–i198. [Cited on page 96]